Representation and Modulation of Mechanical Information in the Lateral Line of Larval Zebrafish

Paul Pichler

Submitted for the degree of Doctor of Philosophy

University of Sussex

January, 2018

DECLARATION

The thesis conforms to an 'article format' in which the middle chapters consist of discrete articles written in a style that is appropriate for publication in peer-reviewed journals in the field. The first and final chapters present synthetic overviews and discussions of the field and the research undertaken.

Chapter 2 is written in the style of an article appropriate for Methods Cell Biology.

Methods for Imaging Calcium Influx and Glutamate Release in Hair Cells and Afferent Neurons of the Lateral Line

Paul Pichler and Leon Lagnado

Chapter 3 is written in the style of an article appropriate for Neuron.

The Heterogeneous Transfer Characteristics of Hair Cells Encoding Mechanical Stimuli in the Lateral Line of Zebrafish

Paul Pichler and Leon Lagnado

Chapter 4 is written in the style of an article appropriate for Neuron.

Selective Suppression of Re-Afferent Information in the Lateral Line of Zebrafish Larvae

Paul Pichler and Leon Lagnado

In all 'article format' chapters the author contributions are as follows: PP was responsible for all aspects of data collection, data analysis, writing of the manuscript; LL was responsible for providing feedback on study design, corrections to the manuscript. PP and LL were collectively responsible for initial conception of the research

---

I hereby declare that this thesis has not been and will not be, submitted in whole or in part to another University for the award of any other degree.

Signature:……

Summary

The lateral line organ in fish and amphibians transforms fluid motion in the animal's surroundings into a representation of its hydrodynamic environment. This sense is involved in complex behaviors, ranging from rheotaxis to schooling. The primary sensory neurons are hair cells, each of which can tonically transmit a graded 'analog' signal to afferent neurons, via highly specialized 'ribbon' synapses. Many questions about this first step in sensory coding remain to be answered. For example: What is the relationship between the biologically relevant stimulus and hair cell output? How do the synaptic properties of different hair cells contribute to the signal that is sent to the brain? And how are these signals modulated by top-down (efferent) projections? The first chapter of this thesis describes a newly established preparation including an overview of transgenic fish lines, some of which were newly generated, to study the processing of mechanical information in larval zebrafish at various stages, from the periphery to the hindbrain. The second chapter contains a detailed characterization of the relationship between cupula deflection and hair-cell glutamate release. We show that the population of hair cells in the lateral line is highly heterogeneous in terms of their sensitivity, dynamic range and adaptive properties and that this heterogeneity has functional implications for downstream processing. These results are unique because of how well the biophysical, anatomical and physiological context of the actual sensory transduction is maintained. The third chapter describes the effects of (fictive) locomotion on the processing of mechanical information. We show that an efferent signal, which is highly correlated with motor neuron activity, is present in the neuromast and leads to a strong suppression of mechanically induced activity of afferent neurons. This efference copy appears to selectively reduce the gain to hair cells sensitive to posterior cupula deflections.

Acknowledgements

I would like to thank Leon, for his supervision and trust and for taking me into his lab and giving me the opportunity to learn so many exciting new things – with almost no prior experience. I would like to thank Sofie for everything she has done for me and all the ways in which she has helped me. I would like to thank Richard and Siân for sharing their office with me. I would like to thank Jamie for initial help and critical debates. I would like to thank Tristan for teaching me surprisingly much about the Cortex. I would like to thank Hazel for taking good care of our fish. I would like to thank all the members of the Lagnado lab who helped me along the way. I would like to thank the extended Susses Neuroscience community and the members of the reading group for an exciting and diverse research environment. I would like to thank all my friends at Sussex and in Brighton. I would like to thank João and Eva. I would like to thank my family, my parents, sisters and aunt for constant support from home. Most of all I would like to thank my partner Hanna. For being there. For always supporting me during this episode of our lives, which was not always easy.

Table of Contents

List of Figures and Tables

Chapter 1

General Introduction

Just one week after hatching, larval zebrafish are equipped with functional visual, olfactory, vestibular, auditory and somatosensory systems (Moorman 2001; Friedrich et al 2010). In addition to these classic modalities, zebrafish possess another sensory system unique to fish and aquatic amphibians called the lateral line. Signals in the lateral line originate in mechanosensitive hair cells on the surface of the body that detect local water motion in the animal's surroundings and has therefore been referred to as 'Ferntastsinn' or 'touch-at-a-distance' (Dijkgraaf 1963).

Although the lateral line system in larval zebrafish is extremely simple compared to that of other, larger fish (Metcalfe et al 1985), it contains all the basic building blocks and is already involved in behaviors such as rheotaxis and predator avoidance (McHenry et al 2009; Suli et al 2012; Stewart et al 2013; Oteiza et al 2017). As such, it is a model suited to study not only the physiology of hair cells, but also higher order principles of sensory encoding and modulation, which can only be addressed in an in vivo system.

The first main aim of this thesis is therefore to establish the necessary tools to fully utilise the advantages that zebrafish offer as a model organism, such as genetic tractability and optical transparency, for the investigation of sensory encoding in the lateral line system. Building on this, the second main aim is to employ these tools to provide a new perspective into the encoding of mechanical information by lateral line hair cells. In particular, I aim to directly describe the relationship between mechanical stimulation and neurotransmitter release, which fundamentally constitute the input and output of all hair cells, and have not previously been experimentally accessible. The third aim is to functionally describe the effects of efferent modulation on the encoding of mechanical information in the lateral line, in vivo, in the intact system.

Organization of the Lateral Line System

The lateral line system is composed of three major components, afferent neurons, which transmit sensory information from the periphery to higher brain areas, efferent neurons, which project from higher brain areas into the periphery to modulate sensory transduction and neuromasts, which constitute the functional unit of the transduction process. Neuromasts are distributed across the surface of the fish and consist of mechanosensitive hair cells whose apical hair bundles are embedded into a gelatinous structure called cupula. Each neuromast is sensitive to mechanical stimulation in opposite directions along a single axis, and information about deflections in the respective direction is signaled by separate afferent neurons. This planar sensitivity of

a single neuromast is the result of the specific arrangement and innervation of functionally polarized hair cells, which in turn is the result of its unique and highly specialized morphology.

Afferent Neurons of the Posterior Lateral Line

The central representation of flow information in the lateral line system depends on the position, orientation and innervation of individual neuromasts, which are distributed across the entire body of the fish. The lateral line system can be coarsely sub-divided into the anterior lateral line (ALL), consisting of cranial neuromasts and posterior lateral line (PLL) consisting of trunk neuromasts (Metcalfe et al 1985; Raible & Kruse 2000). The morphological and functional architecture of the PLL is fundamentally governed by developmental principles (Pujol-Martí & López-Schier 2013; Liao 2014). All neuromasts and lateral line afferents derive from two placodes just posterior of the otic vesicle (Sarrazin et al 2006). Within 1 day post fertilization (dpf), the first primordium (primI) forms from placode 1 and migrates posteriorly along the midline of the fish. After about 20 hours it reaches the tip of the tail and on its way deposits 5 neuromasts along the trunk and 3 ‘terminal’ neuromasts in close proximity on the tail of the fish (red dots in Fig. 1.1). A few hours after primI started its migration, the second placode forms and gives rise to two more primordia primII and primD, respectively. The former follows primI migrating posteriorly along the midline, while the latter also migrates posteriorly but towards the dorsal side of the fish. By 7 dpf, the PLL consists of 14 neuromasts, 8 primary neuromasts, derived from primI and 6 secondary neuromasts, derived from primII and primD (Fig. 1.1) (Metcalfe et al 1985; Kimmel et al 1995; Sarrazin et al 2010; Pujol-Martí & López-Schier 2013). All primary neuromasts are sensitive to deflections along the anterior posterior axis of the fish (parallel neuromasts), while all secondary neuromasts are sensitive to dorso-ventral (perpendicular) deflections of the cupula (except for the first neuromast of primD, which is also parallel) (López-Schier et al 2004).

Bipolar afferent neurons transmit flow information from the periphery to the hindbrain. Their cell bodies reside in the PLL ganglion (orange circle in Fig. 1.1), just posterior of the otic vesicle and their central axons project to the ipsilateral medial octavolateralis nucleus (MON) in the hindbrain. Their distal axons run along the midline of the fish and innervate the individual neuromasts. Each neuromast is innervated by at least two afferent neurons, each exclusively forming synapses onto hair cells with the same functional polarity (Nagiel et al 2008; Faucherre et al 2009). This innervation

pattern ensures that the output of any neuromast consists of two distinct channels with opposite directional sensitivity along the same axis and is strictly maintained during development, when both the number of neuromasts as well as the number of afferents innervating a given neuromast increase (Haehnel et al 2012).

In the MON, each afferent neuron bifurcates to form an anterior and a posterior arm and in total forms ~60 synaptic contacts with downstream targets (Pujol-Martí et al 2012). The MON receives input not only from the PLL but also from the ALL and the inner ear. It is somatotopically organized in respect to lateral line inputs, with afferent neurons from the ALL projecting more ventrally and those from the PLL projecting more dorsally (Alexandre & Ghysen 1999). This general rule also applies to afferent neurons within the PLL, although the picture is slightly more complicated. The central axons of primary afferents (derived from the first placode) that innervate posterior neuromasts, project to dorsomedial areas of the MON, and primary afferents that innervate more anterior neuromasts project to ventrolateral areas in the MON (Alexandre & Ghysen 1999; Pujol-Martí et al 2010). However, the central axons of secondary afferent neurons (derived from the second placodes) that innervate secondary neuromasts (and also very anterior primary neuromasts) always project more ventrally, irrespective of the position of the neuromast they innervate (Pujol-Martí et al 2012).

Primary and secondary afferents further differ in their morphology, physiology and downstream targets. Primary afferents, innervating more posterior neuromasts tend to have larger cell bodies, are more likely to innervate multiple neuromasts (mostly the terminal ones), and display lower spontaneous firing rates when compared to secondary afferents. Furthermore, only primary afferents directly innervate the Mauthner neuron, a large central reticulospinal neuron that elicits fast reflex escape behaviors (Metcalfe et al 1985; Korn & Faber 2005; McHenry et al 2009; Pujol-Martí et al 2012; Haehnel-Taguchi et al 2014; Troconis et al 2017). This has led to the proposition that the posterior lateral line system is functionally (and morphologically) dimorphic (Pujol-Martí et al 2012). Primary afferents are responsible for detecting strong stimuli such as a predator for instance, (McHenry et al 2009) with low spatial resolution (as they can innervate more than one neuromast) and directly trigger fast escape responses, circumventing higher brain areas. In contrast, secondary afferents have a higher spatial resolution and are involved in more sophisticated behaviors such as rheotaxis and prey tracking, which are not mediated by the Mauthner but rather by higher order premotor neurons (Liao 2010; Pujol-Martí et al 2012; Pujol-Martí & López-

Schier 2013; Liao 2014; Haehnel-Taguchi et al 2014). Indeed, one of the main targets of second order projection neurons, which further transmit sensory information from the MON, is the nucleus of the Medial Longitudinal Fascicle (nMLF), a cluster of cells in the midbrain which is involved in the regulation of swim posture and speed (Orger et al 2008; Sankrithi & O'Malley 2010; Thiele et al 2014; Severi et al 2014; Wang & McLean 2014). Other targets of second order projection neurons include the contralateral MON, the Torus Semicircularis (TS, homologue of the inferior colliculus in mammals) and the OculoMotor-Trochlear Complex (Fame et al 2006).

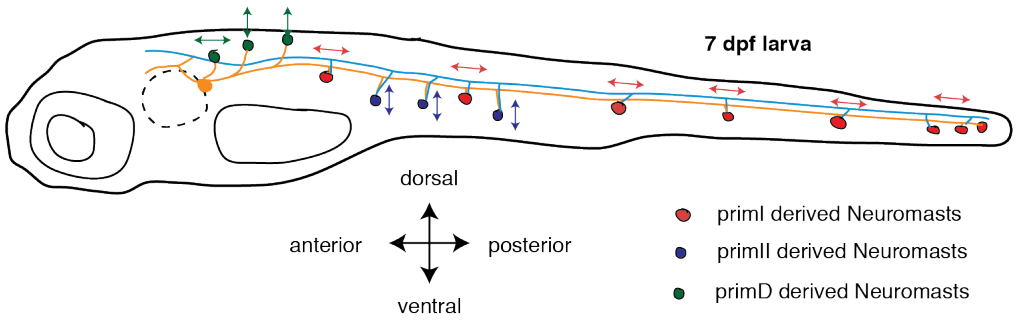

Figure 1.1. The Posterior Lateral Line System of larval Zebrafish
7 days post fertilization (dpf) the posterior lateral line (PLL) of larval zebrafish consists of 14 neuromasts that are positioned roughly along the midline of the trunk of the larvae. (All components of the anterior lateral line system are omitted for clarity.) Neuromasts derive from three migrating primordia and are polarized either along the anterior-posterior axis (parallel) or the dorsal-ventral axis (perpendicular). The axis of sensitivity, in all but the first neuromast of PrimD, is determined by the primordium that the neuromast originated from (colored arrows). Every neuromast is innervated by at least two afferent neurons (yellow), each of which selectively forms synapses with hair cells of the same polarity. Cell bodies of afferents constitute the PLL ganglion (yellow circle), which is positioned just posterior of the otic vesicle (dashed circle). The central projections of the afferents terminate in the medial octavolateralis nucleus (MON) in the hindbrain, where they bifurcate to form an anterior and a posterior arm. This area also receives input from anterior lateral line as well as from the inner ear and is in close proximity to reticulospinal neurons such as the large Mauthner neuron. Efferent neurons (blue) also innervate neuromasts of the PLL and stem from the diencephalon and the hindbrain.

On a behavioral level, the posterior lateral line system has been implicated in fast Mauthner mediated escape responses that can be triggered by stimulating a single neuromast and most likely involve primary afferents (Liao 2010; Haehnel-Taguchi et al 2014; Monesson-Olson et al 2014; Troconis et al 2017) as well as more sophisticated behaviors such as rheotaxis or avoiding a suction source, which are more likely to involve secondary afferents and higher order brain regions (Suli et al 2012; Olszewski et al 2012; Stewart et al 2013; Oteiza et al 2017).

Taken together, the position, directional selectivity and innervation patterns of neuromasts in 7dpf zebrafish larvae are highly stereotyped and their output is readily embedded in sensory motor transformations.

Efferent Neurons

Like the vestibular and auditory systems, the lateral line system is innervated by efferent neurons, which modulate the transmission of mechanical information at the very first synapse. Efferent neurons are a very heterogeneous population (Köppl 2011; Mathews et al 2017). In the larval zebrafish, efferent neurons are born very early and their axons migrate along with the primordia that give rise to afferents and neuromasts. In contrast to afferents, one efferent neuron is very likely to innervate multiple neuromasts (Sapède et al 2005). Their cell bodies are clustered in three nuclei; the caudal efferent nucleus (CEN) and the rostral efferent nucleus (REN) reside in the hindbrain, while the 'diencephalic efferent to the lateral line' (DELL) resides in the midbrain (Metcalfe et al 1985; Bricaud et al 2001). All three nuclei consist of only a handful of neurons and project their peripheral axons ipsilaterally along the PLL nerve.

DELL neurons are dopaminergic and innervate neuromasts without directly contacting hair cells or afferents, but rather releasing dopamine in a paracrine fashion. They have an excitatory effect by increasing presynaptic calcium influx at the hair cell ribbon synapse and thus increase afferent spiking (Toro et al 2015). Subsets of diencephalic dopaminergic neurons respond to tactile stimulation, visual stimulation and motor activity. However, only the ones sensitive to tactile stimulation projects into the trunk of the fish and they respond after stimulus application, in line with a potential feedback control function in adjusting the gain of the lateral line system (Reinig et al 2017).

Cell bodies of the CEN and REN lie in very close proximity to the Mauthner neuron and other reticular spinal neurons in the hindbrain (Metcalfe et al 1985; Bricaud et al 2001) and have been demonstrated to convey motor related signals (Russell 1971; Roberts & Russell 1972; Chagnaud et al 2015). They innervate hair cells in a presumably unspecific manner (Faucherre et al 2009) and release the neurotransmitter acetylcholine (ACh) (Flock & Lam 1974). Their effect is inhibitory and is probably mediated via α9/α10 nicotinic receptors, which are indeed expressed in the lateral line hair cells of larval zebrafish (Erickson & Nicolson 2015).

Taken together, it seems that the PLL, at least in larger fish, receives at least two types of efferent modulation. Firstly, excitatory feedback gain control, mediated via dopaminergic neurons in the midbrain and secondly feed-forward inhibition via cholinergic neurons in the hindbrain. The former might be involved in adjusting the sensitivity of the lateral line system, while the latter appears to convey an efference

copy signal that prevents the system from adapting to self generated sensory information. To what extent efferent innervation is specific to the orientation of a hair cell or if primary or secondary neuromasts are preferentially innervated remains unknown.

Neuromasts - The Receptor Unit

The functional building blocks of the lateral line system are the neuromasts (NM, Fig. 1.2 A). As in the auditory and vestibular system, the anatomical context of hair cells determines which physical property is being transduced. In the vestibular system for example, inertia of otoconia, positioned on top of a hair cell epithelium facilitates the sensation of linear acceleration. In the auditory system, the intricate mechanics of the inner ear translate air pressure waves into a shearing motion between the basilar and tectorial membranes, which in turn deflects the hair bundles. NM in the lateral line system facilitate the detection of water flow by conveying local fluid motion into the coherent activation of a distinctly organized population of hair cells.

Two aspects of neuromasts are particularly crucial in shaping the information that is represented by this modality. The first is the tightly regulated anatomical organization of hair cells in respect to their intrinsic polarity, which restricts the overall sensitivity of the neuromast to a single axis (Fig. 1.2 A). The second is the presence of the cupula, which mechanically constrains the hair bundles (in particular the much larger kinocilia) so that all individual hair cells of the NM are subjected to exactly the same stimulus. The cupula furthermore constitutes a mechanical filter, thereby shaping the information that the sensory system receives.

Two types of NM exist. Canal NM are embedded in bony canals underneath the scales of the fish, they consist of several hundred hair cells and are sensitive to flow acceleration (van Netten 2006). Superficial NM, in contrast, reside on the surface of the animal, are directly exposed to the surroundings and are sensitive to flow velocity (van Netten & McHenry 2014). While adult zebrafish possess canal and superficial NM, their larvae possess only the latter (Ghysen & Dambly-Chaudière 2007).

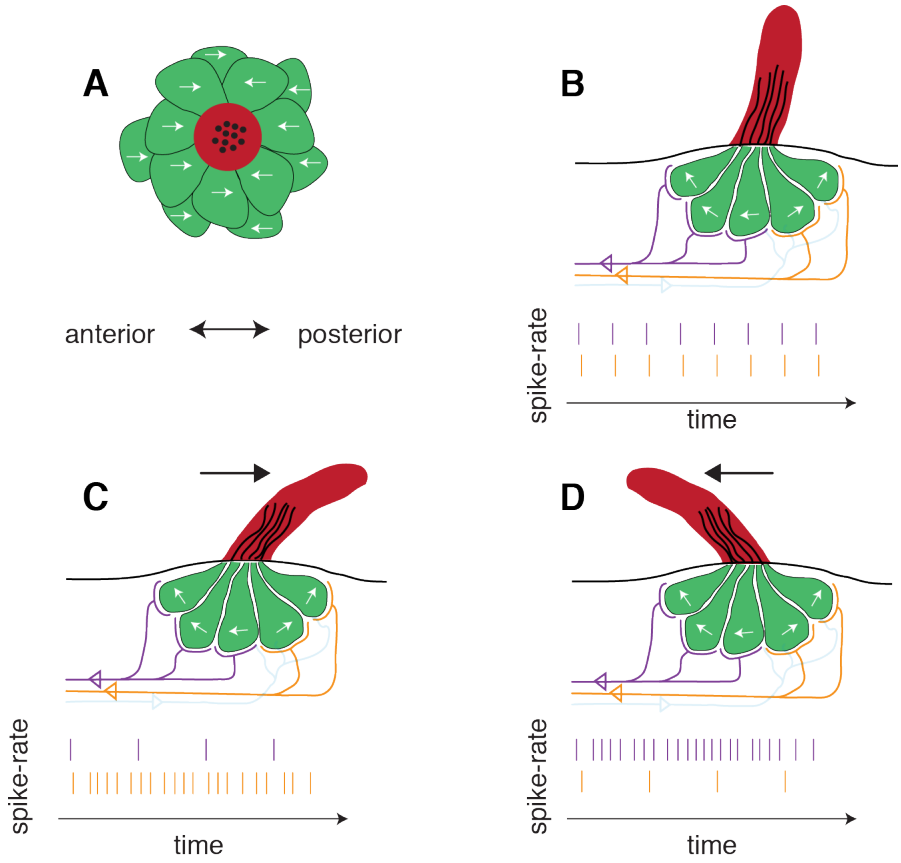

Figure 1.2. Functional Polarization of Superficial Neuromasts
(**A**) The functional polarization of neuromasts is a result of the parallel, but opposite arrangement of the hair cells that constitute it. Each neuromast contains between 10 and 20 hair cells, which can be separated into two populations of equal size, based on their orientation. Hair cells are surrounded by support cells, which can differentiate into hair cells and mantle cells (not shown), which generate the cupula. (**B**) The hair bundles of all hair cells are constrained by the gelatinous cupula (red), which projects ~20-50µm into the surroundings of the fish. Lateral line hair cells possess relatively long kinocilia, that extend approximately half way into the cupula (black lines in cupula), and which relay the cupula deflection to the much shorter stereocilia hair bundle (not shown). The two hair cell populations are specifically innervated by at least two afferent neurons, so that the deflection of the cupula along its axis of sensitivity is encoded by two separate channels. At rest, all afferents fire spontaneously at rates of up to 50Hz. (**C** and **D**) Upon deflection of the cupula, half the hair cells get depolarized and induce spiking in the afferent neuron innervating them (orange in C). The other population of hair cells gets hyperpolarized by the same stimulus, which leads to a decrease of firing rate in the other afferent neuron (purple in C).

Each superficial NM consists of 10-20 hair cells that are surrounded by ~30 support cells (López-Schier & Hudspeth 2006). Hair cells within a NM can be divided into two populations that are oppositely oriented in respect to their functional polarity (Flock & Wersäll 1962; Kindt et al 2012). 'Sibling' hair cells (with opposite polarity) are generated by the mitotic proliferation of support cells (López-Schier & Hudspeth 2006). As a result, both populations contain an equal number of cells. This is striking because hair cells in fish are able to regenerate throughout life and appropriately integrate into the NM (López-Schier et al 2004). Organization of cells in this manner

not only retains the intrinsic polarity of each hair cell at the level of the NM but by 'inverting' half of the hair cells also generates bidirectional sensitivity along a single axis (Fig. 1.2 A). Consequently, deflection of the cupula along its axis of sensitivity in one direction depolarizes one half of the hair cells and hyperpolarizes the other (although to a much lesser degree) and vice versa. These two populations of hair cells are specifically innervated by afferent neurons, thereby maintaining the two channels of opposing directional sensitivity (Faucherre et al 2009). As a result of this selective innervation, and because hair cells release glutamate at rest (Trapani & Nicolson 2011), any given deflection of the cupula along its axis of sensitivity leads to an increase of the firing rate in one afferent and a decrease of firing rate in the other (Fig. 1.2 B-D).

Hair cells and support cells are surrounded by mantle cells, which produce the elongated and gelatinous cupula (Fig. 1.2), composed of glycosaminoglycan (McHenry & van Netten 2007). Cupulae in larval zebrafish have an average base diameter of 10 – 15 µm and extend between 20 and 50 µm into the surrounding water (Van Trump & McHenry 2008). A hydrodynamic stimulus such as a uniform water current, for example, or turbulences due to an approaching predator, get heavily filtered before they induce hair bundle deflection and trigger a response. The two major components of this filtering are the boundary layer around the animal and the interaction between the local flow and the cupula mechanics. Boundary layers occur because of viscous properties of fluids. As water flows past an object (or vice versa), viscous forces slow down the water layer directly surrounding the object, thereby creating a velocity gradient between the 'free stream' velocity and the layers directly around the object. The thickness of this boundary layer depends on the speed of the liquid and the size of the objects. In the case of zebrafish larvae, the superficial neuromasts are predicted to fall well within this boundary layer. By attenuating low frequencies, it acts as a high pass filter for oscillating stimulus sources (Windsor & McHenry 2009; Levi et al 2014). The second component that contributes to the filtering of flow is the interaction between the local flow (within the boundary layer) and the cupula itself. The cupula itself is highly compliant, so that 80% of its stiffness can be attributed to the hair cell's kinocilia which extend approximately 20 µm into the cupula (McHenry & van Netten 2007). This region of the cupula can thus be modelled as a stiff lever, pivoting around its base (McHenry & van Netten 2007). The main determinants of the fluid-cupula interaction are the size of the cupula and its stiffness, i.e. number of kinocilia. These interactions attenuate low frequency stimuli and together these two components

constitute a band pass filter (McHenry et al 2008). Cupula size in zebrafish larvae varies strongly between NM, suggesting a high degree of heterogeneity in the responses profiles of these NM (Van Trump & McHenry 2008). The neuromasts including the cupula provide the anatomical context of mechanotransduction in the lateral line. The strict parallel but opposite arrangement of hair cells functionally maintains their intrinsic polarization and determines the directional sensitivity of the whole functional receptor unit. By mechanically coupling all kinocilia and interacting with the local hydrodynamic environment, the cupula furthermore constitutes a filter whose properties shape the transformation of local flow velocities to angular deflection of the hair bundle.

Mechanosensory Hair Cells

Hair cells constitute the cellular basis of mechanoreception across the vertebrate kingdom and beyond (Burighel et al 2011). They transform mechanical deflections into neuronal activity. As previously mentioned, depending on the anatomical context they are embedded in, these mechanical deflections can be the result of air pressure waves in the auditory system, inertial forces in the vestibular system or local water currents in the lateral line system. Hair cell morphology and physiology varies greatly between sensory system, organism and even developmental stage, however their basic operating principle remains the same. All hair cells are characterized by two highly specialized structures, the hair bundle on their apical and synaptic ribbons on the basal surface. The former facilitates the transduction of mechanical stimulus into graded electrical signals and the latter ensures sustained and temporally precise release of synaptic vesicles (Fig. 1.3 A).

Mechanoelectrical Transduction

The stereocilia comprising the hair bundle vary in their number, size and arrangement between hair cells in the auditory, vestibular and lateral line systems, but they are always arranged in rows of increasing height, producing a staircase like appearance. In vestibular and lateral line hair cells, there is also a non-motile kinocilium, consisting of the classical 9+2 arrangement of microtubules next to the highest stereocilium (Furness & Hackney 2006). The properties of the mechanoelectrical transduction process are a direct result of the morphological and mechanical properties of the hair bundle.

Lateral line hair cells of the larval zebrafish, for example, contain several dozen stereocilia, the tallest one about 5 µm high, that are arranged in a hexagonal array, and a single kinocilium, about 30 µm high (Flock & Wersäll 1962; Van Trump & McHenry 2008; Kindt et al 2012). In contrast to the kinocilium, stereocilia consist of tightly packed and cross-linked actin filaments (Flock & Cheung 1977; Tilney et al 1980; Shin et al 2013). At their base they taper and form a rootlet, which is anchored in a dense actin meshwork, called the cuticular plate (Kitajiri et al 2010). Because of extensive crosslinking between the stereocilia and the relatively stiff kinocilium (Fig. 1.3 B) (Goodyear & Richardson 2003; Goodyear et al 2005; Kozlov et al 2007; Nayak et al 2007; Karavitaki & Corey 2010; Spoon & Grant 2011), force exerted at the tip of the kinocilium leads to all stereocilia pivoting in parallel at their tapered bases. Tip links connect the tip of stereocilia to the shaft of their taller neighbors (Pickles et al 1984). It is this asymmetrical architecture that underlies the functional polarization of hair cells (Flock et al 1962) and ultimately of the whole neuromast. When the hair bundle gets deflected towards the kinocilium, tension in the tip links leads to the opening of the mechanoelectrical transduction channels that depolarizes the membrane potential (Fig. 1.3 B).

The molecular components of the mechanotransduction machinery have largely been identified but the picture is still not complete (reviewed by: Peng et al 2011; Zhao & Müller 2015; Fettiplace 2017). The tip links consists of two connected homodimers, Cadherin 23 and Protocadherin 15, respectively (Kazmierczak et al 2007). At their upper end, Cadherin 23 is associated with the actin filaments via the motor protein myosin (the isoforms 1c, Holt et al 2002 and 7a Kros et al 2002a), which maintains tip link tension at rest and plays an important role in adaptation. At the bottom end of the tip link Protocadherin 15 is connected to a large protein complex, sitting at the tip of the stereocilium, which contains the actual transduction channel (Hudspeth 1982; Lumpkin & Hudspeth 1995; Beurg et al 2009) (Fig. 1.3 B, inset). The complex consists of TMIE (transmembrane inner ear), LHFPL5 (lipoma HMGIC fusion partner-like 5) and TMC1 and 2 (transmembrane channel-like proteins), the latter being the most likely candidates to form the actual channel, although this is still under debate (Corey & Holt 2016; Wu & Müller 2016).

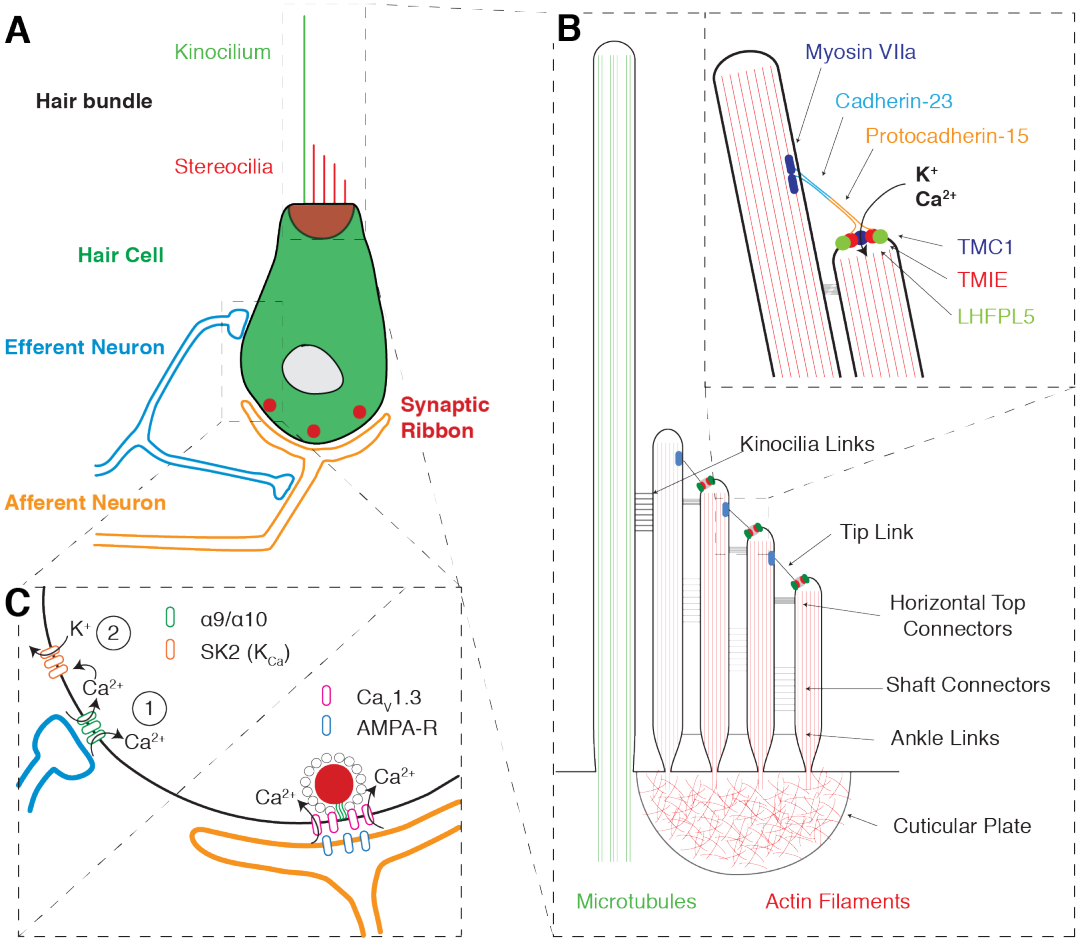

Figure 1.3. Molecular Components of Hair Cell Transduction and Transmission
(**A**) Hair cells contain two highly specialized structures: the hair bundle on their apical surface and the synaptic ribbon on their basal surface that govern the transduction and transmission of mechanical information, respectively. The hair bundle of lateral line hair cells consists of a single kinocilium (green, ~25μm tall) and several dozen stereocilia (red, ~5μm tall). Hair cells are furthermore innervated by afferent neurons (orange) that transmit mechanical information to the brain and efferent neurons (blue) that modulate the transmission process. (**B**) The hair bundle of lateral line hair cells consists of a few dozens of actin filled stereocilia and a large non-motile kinocilium, composed of microtubules. Stereocilia increase in height towards the kinocilium and are organized in a hexagonal fashion. They taper at their bases and are anchored via rootlets (not shown) in the cuticular plate, a dense actin meshwork. Stereocilia are heavily cross-linked to each other via ankle links, shaft connectors and horizontal top connectors. The largest row of stereocilia is also linked to the much larger kinocilium via kinocilia links. Together, these cross-links render the hair bundle a rigid structure that pivots around its base rather than bends upon mechanical stimulation. Tip links connect the top of one stereocilium with the shaft of their next tallest neighbor and are involved in the opening of the mechanotransduction channel. They are composed of Cadherin-23 towards the top and Protocadherin-15 towards the bottom. The mechanotransduction complex resides at the tip of the stereocilium and consists of TMIE, LHFPL5 and the non-selective cation channel, composed of TMC1/2. At the top, the tip link is anchored to a protein complex containing an unconventional myosin motor protein (myo 1c or myo 7a), which is crucial for resetting the mechanical tension in the tip links and thereby facilitates adaptation. (**C**) Hair cells contain synaptic ribbons, which facilitate the accurate transmission of the receptor potential to the afferent neurons. Synaptic ribbons (red sphere) are composed of the protein ribeye and are anchored to the basal membrane via the proteins bassoon and piccolo (green filaments below ribbon). Ribbons are surrounded by a halo of tethered vesicles and are involved in vesicle recruitment as well as clustering of the voltage dependent calcium channel ($Ca_V1.3$). →

Independent of its molecular identity, the mechanoelectrical transduction (MET) channel and its associated ionic currents have been thoroughly investigated. It is a non-selective cation channel (Ohmori 1985; Beurg et al 2006) with a relatively large pore diameter, which allows even large molecules such as the styryl dye FM1-43 to enter (Gale et al 2001). The current is predominantly carried by K^+ influx however Ca^{2+} influx plays a central role in adaptation (Eatock et al 1987; Assad et al 1989; Crawford et al 1989). Displacement of the hair bundle and concomitant tension in the tip links exerts a pulling force via a gating spring (Howard & Hudspeth 1987; Howard & Hudspeth 1988) on the MET channel that increases its open probability. The relationship between the peak current and hair bundle displacement can be described by a Boltzmann function (Holton & Hudspeth 1986; Crawford et al 1989; Hudspeth 1989). Because the open probability of the channel at rest is not zero, deflections in the negative direction, towards the smallest stereocilia, can further decrease the open probability (Fig. 1.4 B, Shepherd & Corey 1994). The sensitivity of hair cells, described by the working range (the deflection that changes the open probability from 10% to 90%) of the transduction process varies profoundly, ranging from 50 nm to several hundred nanometers (reviewed by: Fettiplace & Kim 2014) and depends not only on the type of hair cell but also on the means of stimulation (Vollrath & Eatock 2003). Activation kinetics of the MET channel are extremely fast, in the sub-millisecond range (Corey & Hudspeth 1979; Corey & Hudspeth 1983), and therefore oftentimes masked by the mechanical filtering of hair bundle stimulation.

A very important property of mechanoelectrical transduction is adaptation. As in other sensory systems, it resets the dynamic range of the sensor in response to sustained stimulation (Fig. 1.4 A), thereby re-establishing sensitivity to subsequent stimulations. Adaptation of the MET current to a step stimulation, can be explained by two distinct mechanisms. Both have been shown to depend on calcium (Wu et al 1999; Holt & Corey 2000; Vollrath & Eatock 2003) but occur in different time frames. Fast adaptation, operating in sub-millisecond to millisecond time frames, has been suggested to depend on calcium acting directly on the MET channel (Kennedy et al 2003). Slow adaptation, in contrast, operates in the time frame of several tens of

---

Upon vesicle fusion, glutamate is released into the synaptic cleft where it binds postsynaptic AMPA receptors. Additionally, most hair cells receive input from efferent neurons, which induces an inhibitory postsynaptic potential via the release of acetylcholine (ACh). This is mediated via α9/α10 nicotinic ACh receptors and calcium dependent potassium (SK2) channels. Calcium that enters the cell via the α9/α10 subunits activates the SK2 channels which leads to potassium efflux and hence hyperpolarises the hair cell.

milliseconds and is based on the mechanical relaxation of the hair bundle (Howard & Hudspeth 1987). This very elegant model, suggests that tension in the tip links is released by the calcium dependent motor activity of myosin 1c or VIIa (Holt et al 2002; Kros et al 2002b; Stauffer et al 2005), which upon calcium influx, slides down the larger stereocilium (Fig. 1.4 A), to re-establish the mechanical set point and thus the dynamic range of the hair cell (Howard & Hudspeth 1987; Hacohen et al 1989; Assad & Corey 1992). The myosin based mechanical resetting of the tension is also responsible for the hair cells ability to adapt to, and subsequently respond to the release of negative deflections (Holt et al 2002) Fig. 1.4 B).

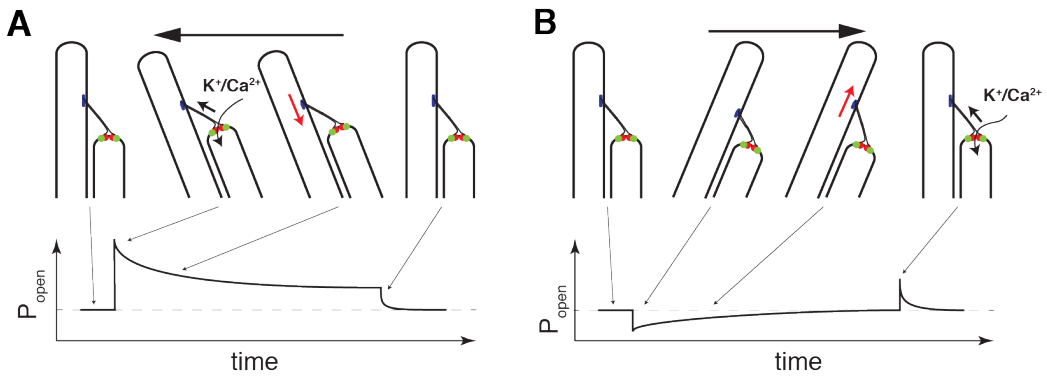

Figure 1.4. Adaptation to Positive and Negative Hair Bundle Deflections
(**A**) Stimulation of the hair bundle in its preferred direction leads to the stereocilia pivoting in parallel towards the tallest stereocilium. This induces tension in the tip links (small black arrow) connecting adjacent stereocilia and increases the open probability (P_{open}) of the mechanotransduction channel as a function of deflection. Over time, the channel adapts to the new bundle position and P_{open} decreases again. This process is mediated by the motor protein myosin, which moves downwards along the shaft of the taller stereocilium (red arrow) to mechanically release the tension on the tip link. (**B**) Stimulation of the hair cell towards the shortest stereocilium slightly reduces P_{open} of the mechanotransduction channel. Tip link tension is then re-established by the myosin motor activity (red arrow), so that the return to the initial resting position leads to a transient response.

The hair bundle transforms mechanical stimuli into constrained angular deflection of stereocilia. The stimulus is projected onto a morphologically defined plane of polarity, with deflection towards the tallest stereocilium increasing and deflection away from it decreasing the open probability of the MET channel. This leads to a sigmoid relationship between deflection and MET current, which can be rapidly shifted in a calcium dependent manner. The resulting graded change in membrane potential drives exocytosis of glutamate filled vesicles at a specialized sensory synapse, which facilitates the transmission of mechanical information with high fidelity.

Exocytosis at the Ribbon Synapse

Ribbon synapses are highly specialized synapses present in hair cells, in photoreceptors and bipolar cells in the retina, as well as in the pineal gland (Matthews & Fuchs 2010). These sensory synapses have at least two functional commonalities. They have to be able to tonically release large amounts of neurotransmitter to facilitate the continuous transmission of sensory information and exocytosis is driven by a graded change of membrane potential, in contrast to 'regular' synapses, where exocytosis is triggered by action potentials.

The morphological structure after which these synapses are named and which is believed to facilitate the continuous and graded release of synaptic vesicles is the synaptic ribbon (Fig. 1.3 C). In photoreceptors and bipolar cells in the retina ribbons are indeed elongated ribbon-like structures, whereas in hair cells they are spherical in shape and also referred to as dense bodies, after their electron dense appearance under the electron microscope. In all cases, ribbons are localized directly above the active zone and surrounded by a halo of glutamatergic vesicles. Within hair cells, the number and size of ribbons varies strongly between different types (Nouvian et al 2006). In the lateral line of larval zebrafish, there are between 2 and 3 ribbons per hair cell (Lv et al 2016; Sheets et al 2017), with an average diameter of 500 nm (Lv et al 2016; Sheets et al 2017).

The main structural component of synaptic ribbons is the protein ribeye, constituting two thirds of all proteins and responsible for the electron-dense appearance (Schmitz et al 2000; Zenisek et al 2004; Lv et al 2016). It appears to be anchored to the presynaptic membrane by two large scaffolding proteins piccolo and bassoon (Dick et al 2001; Khimich et al 2005) and plays a critical role in the spatial organization of the exocytosis machinery, as overexpression as well as knock down of *ribeye* leads to diminished calcium channel clustering in larval zebrafish (Sheets et al 2011; Sheets et al 2017). Unexpectedly, a complete knock out of *ribeye* resulted in a loss of the electron dense appearance and calcium channel clustering but not vesicle tethering, and even enhanced exocytosis (Lv et al 2016).

In principle, exocytosis at ribbon synapses follows the same steps as in any other synapse; calcium influx via voltage dependent calcium channels activates a calcium sensor that triggers the fusion of docked vesicles, usually via SNARE proteins. At ribbon synapses, however different functional components appear to take over these roles (Nouvian et al 2011). Hair cells in the inner ear and lateral line employ the unusual L-type voltage-dependent calcium channel CaV1.3 (Platzer et al 2000;

Spassova et al 2001; Sidi et al 2004). This channel is characterized by very fast gating and little to no inactivation (Platzer et al 2000; Johnson & Marcotti 2008), features that are crucial for a synapse that has to tonically transmit temporally precise signals. The molecular identities of the calcium sensor and fusion machinery are still subject to debate, as many components of the conventional SNARE complex are not expressed in hair cells. Currently, the most prominent candidate for the calcium sensor is otoferlin (Roux et al 2006; Dulon et al 2009; Beurg et al 2010). However, it appears to also be involved in other synaptic processes such as the replenishment of synaptic vesicles (Pangrsic et al 2010).

The tight spatial coupling and tethering of large vesicle pools at the ribbon synapse has several important functional consequences. The relationship between receptor potential and vesicle fusion, assessed by the change in membrane capacitance, follows a linear relationship (Johnson et al 2005; Schnee et al 2005). This was confirmed by performing very challenging double recordings of hair cells and afferent boutons (Keen & Hudspeth 2006; Goutman & Glowatzki 2007), postsynaptic to a single ribbon (active zone), which showed that the excitatory postsynaptic current is also a linear function of presynaptic calcium current. It was further demonstrated that establishment of this linear relationship correlated with hair cell maturation and that it is dependent on the tight spatial coupling of calcium channels and presynaptic vesicles (Johnson et al 2005; Wong et al 2014; Olt et al 2014). Opening of a few calcium channels leads to vesicle fusion (Brandt et al 2005) but whether activation of a single channel (nano-domain, Eggermann et al 2012) or several channels in close proximity (micro-domain, Bortolozzi et al 2008) is required, is still debated (although the latter seems more likely) (reviewed by: Wichmann & Moser 2015). The spatial coupling of calcium channels and site of vesicle fusion along with the resulting linear relationship between calcium current and exocytosis is crucial not only for reliable transmission of small stimuli but also for the temporal precision that is observed in the auditory system.

Another phenomenon observed in ribbon synapses, which strongly affects temporal precision, is multiquantal or multivesicular release (Glowatzki & Fuchs 2002; Goutman & Glowatzki 2007; Li et al 2009; Grant et al 2010). It was observed that excitatory postsynaptic currents in afferent neurons vary greatly in magnitude while being indistinguishable in their kinetics. These data implied that several vesicles, each constituting a single quantum, had to be released simultaneously (Glowatzki & Fuchs 2002; Keen & Hudspeth 2006; Li et al 2009). Just how this is achieved mechanistically

and what role the ribbon plays is not clear. The ribbon may provide a scaffold for the synchronous fusion of docked vesicles or facilitate the fusion of vesicles before they fuse with the plasma membrane (reviewed by: Matthews & Fuchs 2010). Irrespective of the mechanism, multivesicular release appears to play a crucial role in phase locking, the ability of a hair cell to follow the phase of a sinusoidal stimulation (Li et al 2014).

Besides their high temporal precision, ribbon synapses are characterized by their ability to maintain high rates of vesicle release over prolonged periods of time and are considered to be infatiguable (Schnee et al 2005; Schnee et al 2011). This implies that the vesicle turnover at these synapses has to be fast and efficient. Morphologically, vesicles can be divided into different pools based on their position relative to the ribbon and active zone, respectively. The first pool consists of vesicles that are tethered to the ribbon and primed at the active zone. The second pool contains all vesicles that are tethered to the ribbon but not in contact with the membrane and the third pool contains all vesicles that are freely floating around at the synapse (Nouvian et al 2006). The availability of synaptic vesicles and their replenishment can also be described functionally. This is possible by measuring the increase of overall membrane capacitance that results from the fusion of vesicles with the plasma membrane. At least two release components have been found, using this technique (Schnee et al 2005; Schnee et al 2011). A fast one, with a time constant of just a few milliseconds and a much slower one with a time constant of more than one hounded milliseconds (Nouvian et al 2006). The former is believed to correspond to the already docked vesicles and the latter to the ribbon tethered vesicles. While initially the replenishment of vesicles appears to be the rate limiting step, the ability of the ribbon to efficiently recruit new vesicles, reaches a rate that renders the fusion rate limiting after a steady state has been reached. Additionally it has been shown that vesicle replenishment itself is calcium dependent and enters a superlinear phase during prolonged stimulation (Schnee et al 2011).

It is important to note that the membrane potential of hair cells lies within the activation range of the CaV1.3 channel, which leads to spontaneous vesicle fusion. In lateral line hair cells of larval zebrafish, the resting membrane potential lies at around -68 mV (although variability was high), which overlaps with the recorded CaV1.3 channel activation potential of -70 mV (Olt et al 2014). This is partly due to the MET channels having a non-zero open probability at rest, but also to the expression of a hyperpolarization activated non-selective cation current (Ih) (Holt & Eatock 1995;

Trapani & Nicolson 2011). As a result, afferent neurons in the zebrafish lateral line spike spontaneously at rates ranging from <10 - 50 spikes per second (Liao 2010; Trapani & Nicolson 2011; Liao 2014; Haehnel-Taguchi et al 2014). In mutant fish that lack tip links, and hence do not display any MET current, the afferent spiking rate is reduced. However, only additional block of the Ih current completely abolished the spontaneous spike rate (Trapani & Nicolson 2011). Thus, the resting membrane potential is moved to fall within the dynamic range of exocytosis. This shift enables the ribbon synapse to transmit not only the depolarizing positive deflections, but also hyperpolarizing negative deflections of the hair bundle, thereby enabling the signalling of the entire dynamic range of mechanically induced currents. This property of hair cells - that they release vesicles at rest - is responsible for the spontaneous spike rate of afferent neurons and hence for their ability to encode deflections into the preferred as well as the opposite direction of the hair cell population they innervate.

Taken together, although the molecular components and their exact role are still not resolved, it is clear that the synaptic ribbon complex acts as a central organising unit at the hair cell afferent synapse, facilitating the high fidelity transmission of mechanical information.

Efferent Modulation of Hair Cells

Efferent neurons are present in the auditory, vestibular and lateral line systems. They can convey contextual information to adjust hair cell sensitivity, provide feedback inhibition to protect from damaging noise and feed forward inhibition to account for self-induced stimulation, and are involved in the functional maturation of hair cells. This functional heterogeneity is well reflected by the anatomical and physiological implementation. Depending on cell type and organism, efferent neurons form synapses directly onto hair cells or onto the postsynaptic boutons of afferent neurons, their modulation can be inhibitory or excitatory and is mediated via the release of different neurotransmitters, such as dopamine, ACh and gamma-Aminobutyric acid (GABA) (Ryugo et al 2011). Despite this heterogeneity, ACh appears to be the most abundant efferent neurotransmitter (Jordan et al 2013; Fuchs 2014; Mathews et al 2017).

Early experiments in the lateral line of frogs and fish reported inhibitory postsynaptic potentials in hair cells as a result of efferent activity and the effect was already attributed to the release of acetylcholine (Russell 1968; Flock & Russell 1973; Flock & Russell 1976a). Today it is known that in vestibular efferent neurons of turtles,

releasing ACh can act on hair cells and afferents via at least three distinct mechanisms (Jordan et al 2013). Firstly, afferent boutons expressing α4/β2 nicotinic receptors are depolarized upon ACh release (Holt et al 2015). Secondly, the excitability of afferent boutons is increased via muscarinic ACh receptor mediated suppression of the M-current (Holt et al 2017), and thirdly, as previously suggested, hair cells themselves can be acutely hyperpolarized (Glowatzki 2000; Holt et al 2006).

The inhibitory effect on hair cells is mediated by an unusual two-step mechanism (Fuchs 2014) (Fig. 1.3 C). In the first step, ACh released by the efferent neuron activates α9/α10 nicotinic receptors. These hair cell specific subunits possess very unusual pharmacological properties, they can be inhibited by both nicotinic and muscarinic antagonists and are highly permeable to calcium (Elgoyhen et al 1994; Verbitsky et al 2000; Baker et al 2004). In the second step, the calcium influx through the nicotinic receptors activates near-by small conductance calcium-activated potassium channels (SK2), which hyperpolarize the membrane potential (Glowatzki 2000; Dawkins et al 2005; Kong et al 2008). Via this mechanism, efferent neurons can modulate the graded membrane potential that leads to vesicle fusion and thereby decouple the mechanoelectrical transduction machinery in the hair bundle from the ribbon-mediated transmission of mechanical information.

Aims of this Thesis

This thesis has three main aims: The first is to establish the lateral line of larval zebrafish as a model to functionally investigate the encoding of mechanical information by hair cells as well as afferent neurons, using genetically encoded neuronal activity reporters such as calcium and glutamate indicators. While optical tools have been used to study the development, innervation and regeneration of hair cells, this approach was only recently extended to study the physiology of hair cells and afferent neurons, despite its great potential. The second aim is to use these tools to describe the relationship between cupula deflection and glutamate release, which fundamentally constitute the input and output of lateral line hair cells. As described above, the two major processes that shape hair cell function, namely mechanoelectrical transduction in the hair bundle and exocytosis at the ribbon synapse, have been investigated in great detail using electrophysiological techniques. By clamping the membrane potential and deflecting the hair bundle various aspects of the MET current were intimately studied. In contrast, to investigate exocytosis the

membrane potential was artificially depolarized and the change in capacitance was assayed. Each approach, therefore offered only a partial picture of hair cell physiology. Using the genetically encoded glutamate sensor iGluSnFR in lateral line hair cells of zebrafish larvae permits to measure the output of individual hair cells in the intact sensory unit and as a function of physiological stimulation, namely cupula deflection, without decoupling these two processes. The third aim is to describe how mechanical information in the lateral line system is modulated during (fictive) locomotion using optical and electrophysiological techniques. While efferent modulation of hair cells and afferent neurons has been investigated for a long time and in many different systems, little is known about its function in larval zebrafish, despite the experimental access this model organism grants.

In summary, we aim to exploit the exposed nature of lateral line hair cells and the genetic and imaging tools available in zebrafish larvae, to investigate the encoding and modulation of mechanical information in the most realistic biological context.

Chapter 2

Methods for Imaging Calcium Influx and Glutamate Release in Hair Cells and Afferent Neurons of the Lateral Line

Abstract

The zebrafish larva has been one of the most prominent model organisms for developmental biologist. In particular, the lateral line composed of superficial mechanosensory hair cells, was used as a system to study sensory development and the genetics of hearing and balance. However, relatively little advantage was taken of genetically encoded calcium indicators, which in contrast, are heavily used to study the visual and motor system. Here we describe a preparation for the optical investigation of mechanical information in zebrafish larvae. It includes a protocol to mount the larvae without compromising the integrity of neuromasts, an easily implemented method to measure the deflection of the cupula as a function of applied pressure, and an overview of transgenic lines and reporters that were tested. Together, these methods provide optical access to the first steps of the processing of mechanical information starting from the actual sensory stimulus and following the transmission of the signal to its output in the hindbrain of the fish.

Introduction

The zebrafish, Danio *rerio* is a well-established model system in the biological sciences. The small vertebrate is easy to maintain, has a relatively short generation time, is genetically tractable and produces large quantities of transparent larvae. These properties, together with constantly improving genetically encoded reporters of neuronal activity and fast advancing imaging techniques, have made it particularly attractive for systems neuroscience and resulted in numerous publications, the vast majority of which are focused on the brain structures and behaviors associated with the visual system (e.g.: Bianco et al 2011; Ahrens et al 2012; Ahrens et al 2013; Semmelhack et al 2014; Chen & Engert 2014; Kubo et al 2014; Bianco & Engert 2015; Temizer et al 2015; Barker & Baier 2015; Dunn et al 2016b; Dunn et al 2016a).

However, for the investigation of the vestibular and auditory system zebrafish larvae have yet another big advantage: like other fishes and amphibians, they possess a lateral line system that consists of superficial hair cells, the type of sensory cell that is usually localized in the inner ear and mediates hearing and balance in all vertebrates (Fritzsch & Straka 2014). The sensory units of the lateral line organ are neuromasts (NM) each consisting of up to 20 hair cells whose apical hair bundles are constrained by a gelatinous structure called the cupula, that projects into the fish's surrounding (Fig. 2. 1 A and B). NM are distributed over the surface of the fish and detect small

pressure changes and currents that contain information important for navigation, schooling and predator avoidance (McHenry et al 2009; Suli et al 2012; Stewart et al 2013; Coombs et al 2014; Oteiza et al 2017). At least two afferent neurons innervate each NM and signal deflections of the cupula to higher order brain regions or directly to command neurons that can initiate appropriate motor programs (Metcalfe et al 1985; Alexandre & Ghysen 1999; Ghysen & Dambly-Chaudière 2004; López-Schier & Hudspeth 2006; Faucherre et al 2009).

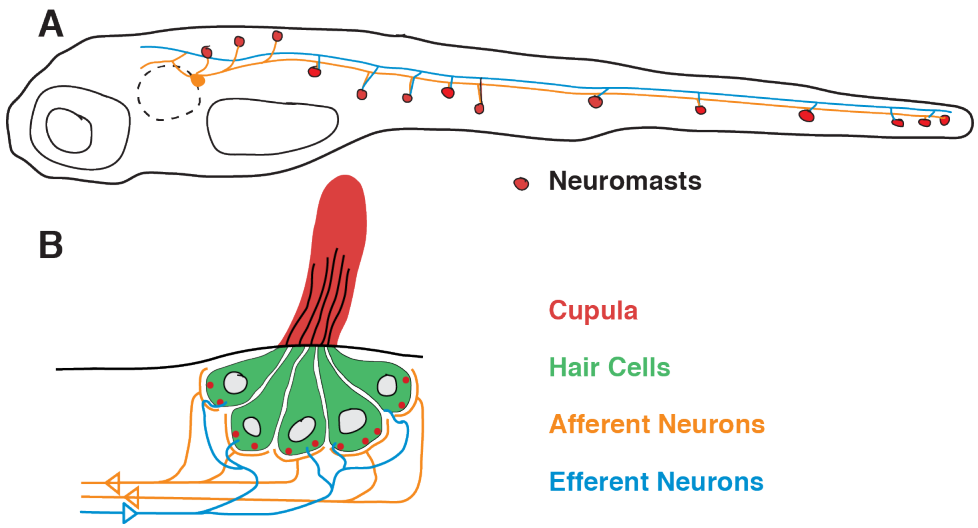

Figure 2.1. The Posterior Lateral Line of Zebrafish Larvae
(**A**) The posterior lateral line of larval zebrafish consists of approximately 14 neuromasts on each side of the fish (red dots). Each neuromast is innervated by at least two afferent neurons (yellow) transmitting information centrally to the hindbrain and an efferent neuron, projecting from the brain onto hair cells or afferent neurons. (**B**) Approximately 20 hair cells are present in every neuromast and all of them project their hair bundles into the gelatinous structure called the cupula, ensuring that all hair cells are deflected equally.

Their superficial localization makes lateral line hair cells readily accessible for mechanical stimulation, electrophysiology, live imaging and the application of drugs, in vivo, without the need for invasive procedures. Because of these advantages the zebrafish lateral line is being used very successfully as a model to study the development and genetics of hair cells and afferent neurons (Nicolson et al 1998; Sidi et al 2004; Nicolson 2005; Obholzer et al 2008; Trapani et al 2009; Sheets et al 2011; Trapani & Nicolson 2011; Sheets et al 2012) and more recently to screen for hair cell protective compounds (Ou et al 2010; Thomas et al 2015; Kruger et al 2016; Kirkwood et al 2017). For these studies hair cell functionality (viability) was rather coarsely assessed by either measuring the uptake of styryl dyes such as FM1-43, which enter the cell via the mechanoelectrical transducer (MET) channel (Gale et al 2001), or by

measuring microphonic potentials, the changes in the extracellular potential of the whole NM due to cation influx through the MET channels (Trapani & Nicolson 2010).

In contrast, the zebrafish lateral line was largely overlooked in respect to studying functional and physiological aspects of hair cells. Patch-clamp recordings from individual hair cells were only recently established (Ricci et al 2013; Olt et al 2014; Olt et al 2016) and remain technically challenging. Whole-cell recordings from individual afferent neurons, in contrast, provide the integrated response of several hair cells and are similarly challenging (Trapani & Nicolson 2010; Haehnel et al 2012; Liao & Haehnel 2012; Haehnel-Taguchi et al 2014; Levi et al 2014; Olt et al 2016).

As an alternative, synthetic and genetically encoded calcium indicators (GECIs) are increasingly used to optically study hair cell physiology. Despite lacking the temporal resolution of electrophysiological techniques they have the key advantage of introducing a spatial dimension. This allows the researcher to resolve calcium dynamics within different compartments of a cell or to measure the activity of different cells simultaneously. Synthetic dyes such as Fluo-4ff together with high-speed confocal imaging were used to simultaneously measure the local calcium influx through the MET channel in individual stereocilia of the hair bundle (Beurg et al 2009) or the calcium influx at individual synaptic ribbons of a hair cell (Ohn et al 2016), for example. Genetically encoded calcium indicators on the other hand, were used to image different hair cells within a NM. Because of their slower kinetics, compared to synthetic dyes, they generally report the cytosolic calcium concentration and hence provide a more qualitative assessment of hair cell activity. So far, both FRET based indicators (Chamelion D3) and single fluorophore indicators (GCaMP3, RGECO and GCaMP6s) have been used successfully in NM hair cells (Kindt et al 2012; Zhang et al 2016; Sebe et al 2017; Sheets et al 2017). However, they also come with limitations, some of which will be discussed below.

Another crucial parameter for the functional investigation of hair cells in lateral line NM is the direct measure of the sensory stimulus. This is complicated by the fact that the driving signal of the stimulating device (Piezo actuator or fluid jet, see below) and the cupula deflection do not necessarily follow a linear relationship. Although the biophysical and mechanical properties of the cupula are relatively well investigated, these measurements required sophisticated equipment and knowledge of the underlying mechanics (Dinklo et al 2007; McHenry & van Netten 2007; McHenry et al 2008; Van Trump & McHenry 2008). That is a potential reason why in most previous studies concerned with hair cell physiology, NM were assumed to be stimulated to

saturation and cupula motion was merely qualitatively confirmed by eye (Toro et al 2015; Zhang et al 2016; Sebe et al 2017; Sheets et al 2017 but see: Kindt et al 2012; Sheets et al 2012).

In this section we review the methodological requirements to optically investigate the lateral line system and present a relatively simple preparation, an easily implemented method to measure cupula deflection and an overview of some of the current genetically encoded reporters that we tested.

Results

A Non-Invasive and Mechanically Stable in vivo Preparation for Imaging

A successful in vivo imaging experiment heavily relies on a stable preparation as motion artefacts can render the most beautiful recordings unusable. Two aspects are crucial for achieving this, mechanical mounting of the fish and pharmacological immobilisation. The most commonly used way of mounting zebrafish is embedding them in low-melting point agarose. This method is unfortunately not applicable as it would embed the cupula and make any mechanical stimulation impossible. Even removing the agarose around the region of interest is not possible, as the cupula would be removed with it. A number of laboratories studying the lateral line are instead using thin tungsten pins to perforate the larva in the head and tail region and pinning it down onto a thin layer of PDMS (Sylgard 1-84: Dow Corning) (Trapani & Nicolson 2010; Olt et al 2016; Sheets et al 2017). Although this approach appears to work fine, there remains a risk of damaging the nervous system, which we wanted to avoid. Alternatively, dental floss (Lv et al 2016) or thin PDMS ‘flaps’ (Pirih et al 2014) can be used to hold down the larvae, however this appeared quite cumbersome so we came up with a different approach.

We used a coverslip coated with approximately 750µm of PDMS, from which we carefully carved out a ‘pit’ or cavity that roughly resembled the shape of a 7 day post fertilization (dpf) zebrafish larva lying on its side (Fig. 2.2 A). The PDMS-coated coverslip was placed in a Warner chamber (Warner Instruments LLC.), and could be reused multiple times, until the PDMS became physically damaged. To hold the larva in place during an experiment, we used a slice anchor or ‘harp’ (Warner Instruments LLC.) appropriate for the respective chamber. When properly positioned the strings of the harp pushed the larva into the pit (Fig. 2B and C) without damaging tissue or obstructing blood flow, which could easily be monitored through a standard

dissecting microscope. Once a suitable configuration was found, it was easily reproducible because the position of the strings relative to the chamber was fixed. It was furthermore possible to carve out two or more pits next to each other to mount several fish at the same time.

The second component of a stable preparation is the immobilisation of the fish, either by anaesthetizing or paralyzing. During the process described above, larvae were anaesthetized by immersion into 0.016% Tricaine (MS-222, Sigma Aldrich). Tricaine itself has been shown to reduce activity of lateral line afferent neurons in the toadfish and block the MET channels (Palmer & Mensinger 2004; Trapani & Nicolson 2010). The most abundantly used paralysis agents are alpha-Bungarotoxin (α-BTX) (Nikolaev et al 2013; Dunn et al 2016a; Knafo et al 2017) and tubocurarine (dTC) (Lv et al 2016; Thompson et al 2016), both of which act as antagonists of the nicotinic acetylcholine receptors (nAChR) in skeletal muscles. It should be noted that both of these agents are also potent inhibitors of the α9/α10 nAChR subunits, which are specifically expressed in hair cells and are involved in efferent inhibition (Verbitsky et al 2000; Holt et al 2006).

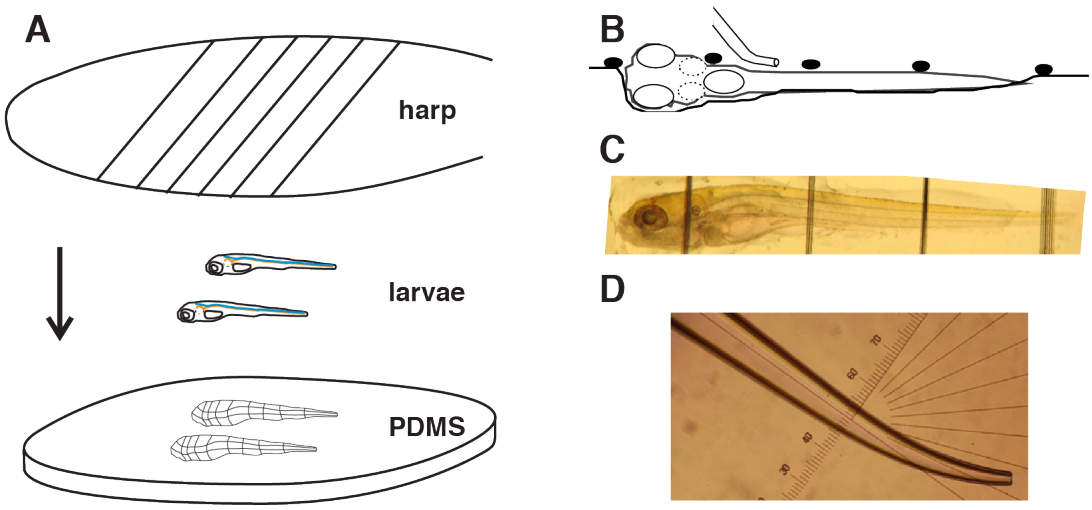

Figure 2.2. Mounting the Larvae
(**A**) We prepared a coverslip with a thin layer of PDMS, in a roughly oval shape, so it would fit into the Warner chamber and underneath the harp. Two 'larva-shaped' pits were carved into the PDMS at the center of the oval. To mount the larvae they were anaesthetized with Tricaine and placed above the pits in as little liquid as possible. Once properly positioned (with a fine tungsten wire or an eye lash), the harp was carefully placed on top of the coverslip and slowly pushed down to hold the larvae in place (**B** and **C**). The tension between the harp and the surrounding Warner chamber was sufficient to keep the harp in place over the course of an experiment. Blood circulation was carefully monitored to ensure that the strings of the harp were not too tight. After the larvae were in place, they were injected with α-Bungarotoxin and the Tricaine was replaced with E2 solution. (The strings of the harp were 1 mm apart). (**D**) To stimulate neuromasts, we used a narrow glass pipette, connected to a HSPC-1 pressure clamp. We bent the tip of the pipette in order to facilitate access to the neuromasts.

This might be of importance when studying efferent modulation of hair cells. Furthermore, it has recently been shown that dTC acts as a permeant MET channel blocker (Kirkwood et al 2017) and is therefore best avoided when studying hair cell function.

To paralyze the larvae, we used 2 mg/ml α-BTX (Tocris, Bio-Techne Ltd.) injected into the heart. After a few minutes Tricaine was washed out with standard E2 medium (Brand et al 2002) and the success of the paralysis was tested by stroking the head of the fish with an eyelash, which would usually induce twitching in the larvae.

During the entire mounting procedure, great care should be taken not to damage the fragile cupula by avoiding any unnecessary contact with the to-be-exposed lateral surface of the fish. Staining the cupula (see next section) revealed that it is indeed very easy to render it either bent, stuck to the surface of the fish or partly removed (Fig. 2.3.). Although cupula morphology varies 'naturally' after hatching (Van Trump & McHenry 2008), altering or damaging the cupula during mounting will further impact the sensitivity of the NM and should be considered when interpreting the data.

Stimulating an Individual Neuromast

At least three factors should be considered when deciding on a means to stimulate a lateral line NM: the ecological plausibility of the stimulus, its controllability and the ease of implementation. Two main strategies have been employed, each having distinct advantages and disadvantages (thoroughly reviewed by: Pirih et al 2014).

The first is to use a glass pipette (with a tip-diameter of 1-20 μm), mounted to a piezoelectric stimulator, which can be driven by an analog voltage signal. The pipette is then positioned to directly contact the cupula of the NM and to push it along its axis of sensitivity (for example used by: Levi et al 2014; Haehnel-Taguchi et al 2014; Lv et al 2016). An advantage of this method is that the distance of cupula displacement is equal to the stimulus distance and hence very easily controllable (assuming the tip is properly positioned and the stiffness of the tip exceeds that of the cupula). Another potential advantage is that stimulation is relatively direct and fast circumventing most filtering properties that are introduced by fluid jets. The latter could however also be regarded as a disadvantage as any stimulus the NM would naturally encounter is filtered by the properties of the fluid surrounding it. Another disadvantage is that stimulation can only be applied in one direction, away from the resting position (although it should be possible to change that fairly easily).

The second general means of stimulation is to move the cupula by fluid currents, as in the real world. These currents are usually applied via pipettes (tip diameters of 30-40 µm) that are positioned in a reasonable distance (50-200µm) from the cupula and controlled by either a piezo-jet (Kros et al 1992; Dinklo et al 2007) or a commercially available pressure clamp (HSPC-1, ALA-science) (Trapani & Nicolson 2011; Kindt et al 2012; Olt et al 2016; Sheets et al 2017). The pressure clamp has the advantage of being able to supply sustained positive and negative pressures and is equipped with a feedback control system. As previously mentioned, this way of stimulating NM is preferable in the respect that it is less artificial and subjects the cupula to the physical forces that would also move it in a natural environment.

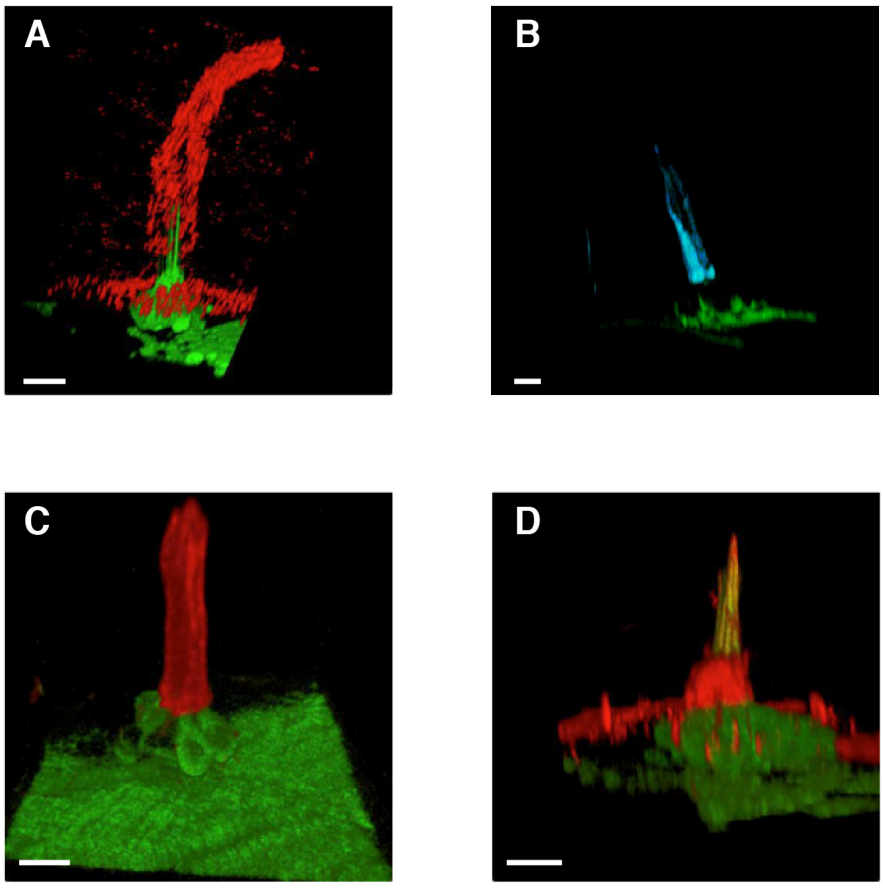

Figure 2.3. Cupula Staining and Morphological Heterogeneity
(**A-D**) Four examples of decorated cupulae. (**A**) This cupula of a 7dpf zebrafish larva expressing membrane targeted EGFP in lateral line hair cells (Tg[Rib::mem-EGFP]) is decorated using fluorescent poly-styrene beads with a diameter of 500 nm and clearly bent in the absence of any stimulation. Kinocilia are nicely visible underneath the beads. (**B**) The cupula of a larvae expressing iGluSnFR in lateral line afferents (Tg[Sill, UAS::iGluSNFR]) and incompletely stained with Alexa350-WGA. (**C**) The completely intact cupula of Tg[Rib::mem-EGFP] larvae nicely stained with Alexa594-WGA. (**D**) This is an example of a NM from which the cupula was almost completely removed and only the kinocilia remain visible. Although not always as extreme, heterogeneity in cupula shape and size was regularly observed and should be considered when interpreting functional data. (Scale bars indicate 10µm)

However, this advantage comes at the cost that the signal driving the pressure changes gets heavily filtered, not only by the water itself, but also by the components of the experimental set up, such as the pipette-tip (Dinklo et al 2007). The filter properties can change from experiment to experiment, making it hard to predict the forces that the cupula actually experiences as a result of a given stimulation protocol. Consequently, it becomes necessary to also monitor the *actual* cupula deflection as a function of stimulus magnitude during every experiment.

It should also be mentioned that zebrafish NM have successfully been stimulated optically by expressing Channelrhodopsin-2 specifically in hair cells (Monesson-Olson et al 2014). While this approach is well suited to study the central effects of mechanical information, e.g. in eliciting a behavior (Troconis et al 2017), it bypasses too much of the hair cell physiology to be relevant for the current project.

In the light of the above-mentioned considerations, we decided to use the HSPC-1 pressure clamp for our experiments. We added a slight modification to previous protocols by bending the tip of the pipette (Fig. 2.2 D). This enabled us to approach the specimen at a steeper angle while maintaining a relatively shallow angle to stimulate the cupula. The tip of the pipette was positioned approximately 100µm away from the NM, at the height of the kinocilia. As the signal that drives the pressure clamp is filtered and might vary between experiments the next important step is to monitor the cupula deflection.

Directly Quantifying Stimulation of Hair Cells

While a number of approaches have been used to visualise the cupula and measure its displacement to a stimulus, most of them require special optics and would be cumbersome to implement into a multiphoton microscope (reviewed by: Pirih et al 2014). We therefore took advantage of the fact that we are already using (two-photon) fluorescence microscopy to image neuronal activity of hair cells and afferent neurons and looked for a way to fluorescently decorate the cupula. Fluorescently labelled polystyrene beads adhere to the cupula (McHenry & van Netten 2007) (Fig. 2.3 A), however the degree of adhesion varied a lot in our experience and beads detached over the course of an experiment, making them too unreliable for our purposes. We therefor turned to fluorescently coupled wheat germ agglutinin (AlexaFluor-350 or 594-WGA, LifeTechnologies), a lectin that specifically binds the glycosaminoglycan on the surface of the cupula (Hung et al 2013) (Fig.3 B-D). The staining step was readily

implemented in the mounting procedure by incubating the paralyzed larvae in a 1:500 dilution of 1 mg/ml WGA for 3-5 minutes, before thoroughly washing it out with E2 medium.

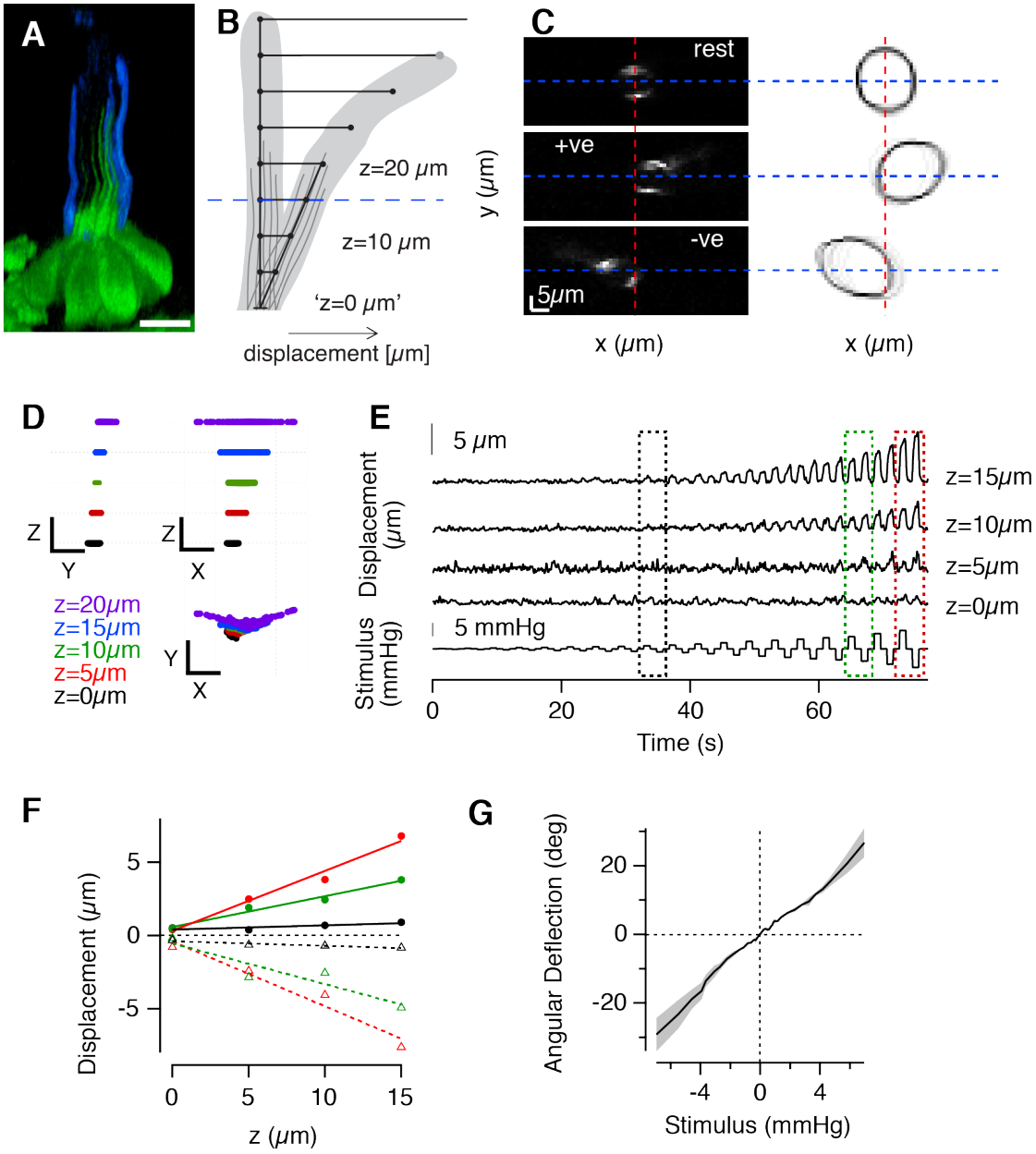

Figure 2.4. Controlling the Mechanical Stimulus
(**A**) Side view of a NM of a 7dpf larva, expressing GFP in hair cells (Tg[Rib::mem-EGFP]). The cupula is stained with Alexa350-WGA. Notice how the kinocilia extend roughly half way across the cupula height (scale bar represents 10 μm). (**B**) Schematic of the rationale for obtaining the angular deflection; the translational deflection (in μm) was measured in several planes above the 'base', within the proximal, rigid region, and was then used to calculate the (pivoting) angle of deflection in degrees (°). (**C**) Three representative frames of the stained cupula (left) and fitted ellipses (right), 15 μm above the base (blue in D), at rest and deflected by a positive and negative pressure step. The center of mass of the staining was used to obtain the positional information within each plane. (**D**) Cupula motion in space over the course of the entire experiment can be extracted from these data. →

With a fluorescently stained cupula at hand we sought to best describe the 'stimulus pressure – cupula deflection' relationship. Our approach is based on the model that the proximal region of the cupula, containing the kinocilia, acts as a rigid beam that pivots around its base (McHenry & van Netten 2007). To describe this pivoting motion, we recorded the translational displacement of the cupula at various heights above its base (Fig. 2.4 B), while it was subjected to different positive and negative pressure steps. Using the 'ImageAnalyzeParticles' function in Igor Pro (WaveMetrics Inc.), the cupula position within each optical section was automatically tracked over time by fitting its perimeter with an ellipse, whose center of mass was extracted (Fig. 2.4 C). This enabled us to reconstruct the stimulus-induced pivoting motion of the cupula in space (Fig. 2.4 D) and time (Fig. 2.4 E). Figure 2.4 F shows that the displacement induced by different pressure steps and measured at four heights, indeed follows a linear relationship, confirming the pivoting motion of the cupula. This implied that we could average the angular deflection measurements from the 'rigid zone' at different heights and plot them as a function of stimulus strength (Fig. 2.4 G). Establishing this relationship is important for several reasons. As mentioned above, variation may be introduced experimentally, by using a different pipette with a slightly different tip diameter, or by positioning the pipette tip at a slightly different angle or distance to the cupula, for example. However, there is also biological variability between individual NM, mainly due to two factors - the size of the cupula (Fig. 2.3) and the number of hair cells that project their kinocilia into the cupula (McHenry & van Netten 2007; McHenry et al 2008; Van Trump & McHenry 2008). Figure 2.3 shows some examples of cupulae that vary significantly from each other. So even under perfectly reproducible conditions the relationship between applied pressure and angular deflection would vary.

The cupula was stimulated along the x-axis (parallel to the fish), leading to stronger translational displacements further towards the tip of the cupula and hardly induced motion along the y-axis (scale bars indicate 10 µm in x and y and 5 µm in z.) (**E**) Positional information measurements were converted to distance (in µm) from the resting position and plotted over time for different cupula heights. The bottom trace depicts the stimulus protocol, consisting of 1 sec intervals of positive and negative pressure. (**F**) The proximal region of the cupula, defined by the presence of the kinocilia (~15-20 µm) behaves like a rigid lever, pivoting around its base. The displacement to three pressure steps of increasing magnitude (colors corresponding to dotted boxes in D), measured at 0, 5, and 15 µm fall onto a line, whose slope represents the angular deflection of the cupula. (F) The overall angular deflection of the cupula was calculated by taking the average of the measurements taken from within this rigid region and plotted as a function of stimulus strength. (Grey shading represents the standard error of means.)

Taken together, visualising the cupula and establishing the relationship between applied pressure and cupula deflection is key to interpreting the functional data. Given the delicate nature of the preparation, in particular of the cupula, the deflection data should be very carefully analyzed. Table 2.1 lists a number of potential artefacts that might get introduced by this approach. However, if care is taken to avoid them, these procedures yield reliable results.

Artefact:	**Potential Reason:**	**Bias:**
Cupula is not perpendicular to anterior-posterior axis of fish.	damaged or bent Cupula.	underestimate
Cupula is not perpendicular to imaging plane (dorso-ventral).	Fish is mounted crooked.	underestimate
Base moves.	Pipette is too low / too close to base.	misinterpret
Pipette not parallel to anterior-posterior axis.	Pipette (or fish) not positioned properly.	overestimate
Cupula bends into imaging plane.	Large floppy region.	overestimate
Noise in detectiion appears as deflection.	Cupula is represented by too few pixels.	overestimate
Diameter of pipette-opening varies.		misinterpret
Segments of Cupula are not trackable.	uneven WGA staining.	misinterpret

Table 2.1. Possible Artefacts and the systematic bias each would introduce when Assessing Cupula Deflection

Imaging Fluorescent Reporter Proteins

Functional imaging of neuronal activity has emerged as an indispensable tool for neuroscientists. One of its biggest advantages is that the activity of large populations of neurons can be imaged simultaneously, *in vivo*; in combination with Single Plane Illumination Microscopy (SPIM) even the whole zebrafish brain (Ahrens et al 2013; Vladimirov et al 2014; Keller & Ahrens 2015). The most widely used class of reporters are genetically encoded calcium indicators (GECIs), which have the additional advantage that expression can be targeted to genetically identified subsets of neurons, and maintained over long periods of time. GECIs change their fluorescence as a function of the intracellular calcium concentration, which in turn is a function of neuronal activity. Most commonly, the action potential induced calcium influx at the soma of the neuron is used as a proxy of the activity of a neuron. However, the fluorescent signal that can be detected is influenced by a number of factors that

should be kept in mind when designing an experiment and interpreting its results (next section). Additionally, another type of genetically encoded reporter iGluSnFR will be introduced.

The type of microscope has implications not only for the type of experiment that can be performed but also for the quality of the data that is being collected. While most imaging studies in the lateral line of larval zebrafish are using either upright (Kindt et al 2012) or confocal (Castellano-Muñoz & Ricci 2014; Beurg et al 2016) microscopes, we took advantage of two-photon (2P) excitation microscopy (Denk et al 1990). The advantages of 2P microscopy are that it causes less unspecific photo bleaching due to the spatially restricted excitation volume, less scattering because of higher excitation wavelength, therefore improved image quality at deeper imaging depths and a broader excitation range, allowing for the simultaneous excitation of multiple fluorophores. The deeper penetration capability would not be necessary when imaging the superficial NM but is very beneficial when imaging the output of lateral line afferent neurons, which project into the medial parts of the hindbrain.

Our experimental set up was custom built (Fig. 2.5 A) around a Chamelion Ultra II (Coherent Inc.) mode-locked Titanium::Sapphire laser which emitted 100 fs pulses at 80 MHz. The actual laser power, as measured out of the objective, was in the tens of mW range, and rarely exceeded 80 mW. Two galvo-mirrors controlling the scanning motion of the laser, as well as all other image acquisition parameters were controlled via ScanImage 3.8 (Vidrio technologies). The objective for most imaging experiments is to maximise temporal and spatial resolution without photo-bleaching the reporter or even damaging the tissue, the latter being of particular importance when using 2P excitation. The most crucial parameters in finding the right compromise are the laser power, the field of view (zoom), and the pixel dwell-time (the time that the laser excites a given position of the sample), which in turn depends on the spatial resolution (number of pixels that the image consists of) and the temporal resolution (acquisition- or frame rate).

At a given laser power, resolution, and frame rate, increasing the zoom will increase photo bleaching because the energy from the laser is focused on a smaller area. Zooming out, however, will either decrease the spatial resolution (if the number of pixels is the same) or the temporal resolution if the number of pixels is increased accordingly. It is therefore important to know what can be sacrificed in order to get the best results in the prioritized parameter.

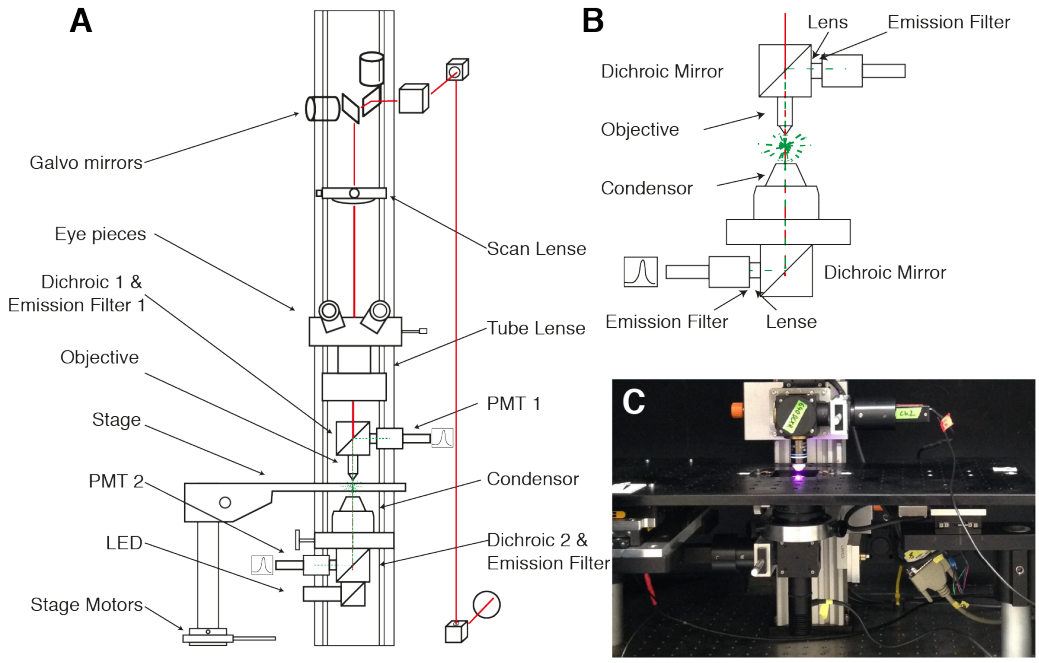

Figure 2.5. The Experimental Set Up
(**A**) A schematic of the excitation light path of the two-photon microscope, indicating the most important components. The laser is directed against a set of galvo-mirrors that scan the sample. The scan and tube lenses, together form one of two telescopes (the other is positioned right after the laser), which expand the diameter of the laser-beam so that it slightly overfills the back aperture of the objective, which focuses the beam onto the sample. (**B**) A schematic of the emission pathway. Photons are emitted from the sample in all directions but are only collected through the objective above and the condenser below. In both pathways, emitted light is passed through a dichroic mirror and subsequently through an emission filter, reflecting all but the desired wavelength, before it is focused onto a photon multiplier tube (PMT). If the same wavelength is collected through the objective and condenser then the currents from the two PMTs can be summed to increase the signal-to-noise ratio. If different colors are being collected simultaneously, then different emission filters are used and the currents are recorded separately. (**C**) An image corresponding to the components depicted in (B). The emission filters are mounted on a slider so they can be changed easily.

For example, when imaging a NM and two active zones are in the respective optical section, then it might be sufficient to resolve each active zone with just a few pixels, while imaging faster, thus sacrificing spatial for temporal resolution. In contrast, in case of an overview image or stack, when spatial resolution is prioritised, temporal resolution can be decreased. In practice, we imaged at a frame rate of 10-100 Hz and a spatial resolution of 256x100 to 128x10 px, respectively, to capture several hair cells in one frame. Before doing so however, a high-resolution overview stack of the whole NM was also acquired, for future reference. The quality and even feasibility of image registration (see later section) also depends on the number of pixels, which is why using less than 20 lines per image is generally not recommended should motion be a potential problem.

The choice of wavelength influences the efficiency with which fluorophores get excited. Common GCaMPs are maximally excited at 915-940 nm. When imaging two colors simultaneously, the excitation wavelength has to be adjusted to maximally excite both fluorophores. In the case of GCaMP6f and mCherry, for example, this would be at 1010-1030 nm (Drobizhev et al 2011; Akerboom et al 2013).

The limiting factor that underlies all of the above considerations is the efficiency with which emitted photons are collected. The more efficient this process the better the signal-to-noise ratio (SNR) for a given set of excitation parameters. This means that the laser power can be lowered, leading to a reduced likelihood of bleaching and tissue damage. In our set-up, we aimed to maximise the SNR of the images by collecting emitted photons through the objective above, as well as through a condenser below the sample (Fig. 2.5 B and C). The numerical aperture (NA) of the oil condenser (NA=1.4) is higher than the water-immesion objective (NA=0.8) so addition of the condenser more than doubled the efficiency of photon collection.

Choice of Reporter Protein

Potentially the most important factor determining the results of an imaging experiment is the choice of calcium reporter. GECIs can be characterized by their baseline fluorescence, the rate-constant with which they bind and release calcium, and their linearity with respect to increased calcium concentrations.

The cytoplasmic calcium concentration of hair cells is estimated to be in the 100 nM range at rest, but upon stimulation can increase to several μM (Lumpkin & Hudspeth 1998; Bortolozzi et al 2008; Zhang et al 2016). Figure 2.6 A shows the relative fluorescence (F/F_{max}) of several GECIs of the GCaMP and RCaMP family (Chen et al 2013) as a function of varying calcium concentrations. The shape of this function is determined by the calcium affinity of the reporter and the cooperativity of the calcium binding sites, described by the Hill-Coefficient. It is immediately apparent that a change from 50 nM to 100 nM, for example, would lead to a strong response in a GCaMP6s expressing cell but would most likely be unnoticed in a GCaMP6f expressing cell. In hair cells the situation is even more complicated because, unlike in most other neurons, calcium influx and the respective change in bulk calcium concentration is not the result of action potentials.

There are two distinct processes that mediate calcium influx in hair cells. Ca^{2+} ions enter through the cation-permeable MET channel on the tips of the stereocilia as well as through voltage gated calcium channels (CaV1.3) at the ribbon synapse. As a

result, the calcium concentration and rate of influx will greatly vary across the cell, which will heavily influence the fluorescent signal that can be measured in different areas. Consequently, pre-defining the subcellular localization of the reporter can determine which process is being imaged. One approach that has been used for whole-brain imaging in zebrafish larvae has been to target the GECI to the nucleus in order to facilitate segmentation of the images, but this comes at the expense of losing temporal resolution (Vladimirov et al 2014; Dunn et al 2016b). Similarly, tethering the reporter to the synaptically localized protein synaptophysin (Sy-GCaMP2/6) has been demonstrated to not only aid in identifying active zones, but also to increase the linear range of the reporter (Dreosti et al 2009; Nikolaev et al 2013). This is because the reporter is not detecting the changes in bulk calcium concentration, but rather the transient changes, more representative of the voltage gated influx.

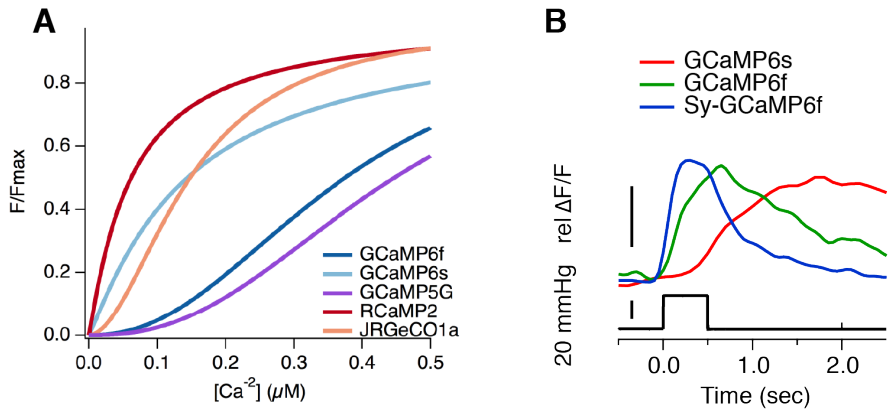

Figure 2.6. Comparing Genetically Encoded Calcium Indicators
(**A**) The sensitivity of five different GECIs is depicted as a function of calcium concentration (Data taken from (Rose et al 2014) and compiled by S. Seibel and J. Johnston). The shape of these curves is determined by the calcium affinity and the hill coefficient, describing the cooperativity of calcium biding. When deciding upon a GECI, it is important to have an approximate idea about the range of calcium concentrations that it will be detecting, in order to reach an approximately linear relationship between changes in calcium concentration and change in fluorescence. (**B**) An example of three different GECIs (GCaMP6f, GCaMP6s and synaptically targeted SyGCaMP6f), all expressed under the *ribeye* promoter in lateral line hair cells and their responses to a 500 ms saturating cupula deflection. The amplitudes of the responses are normalized to the maximum ΔF/F (scale bar represents 50% max). The synaptically localized Sy-GCaMP6f rises and decays the fastest. While the cytosolic GCaMP6f rises slightly slower, it decays significantly slower as compared to the synaptic SyGCaMP6f. The most striking difference is the GCaMP6s, which starts rising only after the 500ms stimulus. This is not a mistake but consistently occurred when increasing the stimulus duration. The decay times were also significantly slower compared to both the GCaMP6f and the Sy-GCaMP6f.

A second advantage of SyGCaMP is the improved temporal characteristics of the signal. Although hair cells do not endogenously express synaptophysin, SyGCaMP6 still greatly improved the kinetics as compared to GCaMP6f, driven by the same

promoter (Fig. 2.6 B). (This was more elegantly demonstrated, however, by adding a membrane CAAX-tag to GCaMP6s (Sheets et al 2017).)

Yet another factor that influences, the SNR as well as the kinetic properties of the calcium indicator is the expression level in the cell. Intuitively, if there is too little expression, the cells will not be visible. Under strong expression conditions, however, the large buffering effect of the reporter will lead to smaller relative changes in fluorescence. The expression level of a reporter depends not only on the promoter itself but can be influenced by using a binary expression system such as Gal4-UAS (Brand & Perrimon 1993) or trpA-tUAS (Suli et al 2014) and is also subject to insertion effects that vary from one stable fish-line to another. To make matters even worse, expression levels can vary over time, both within an animal as well across generations. For that reason every combination of promoter and reporter has to be empirically tested. To date *myo6b* (Kindt et al 2012; Sheets et al 2017), *brn3c* (Xiao et al 2005), *ppv3b4* (McDermott et al 2010) and *rib* (Odermatt et al 2012) have been successfully used to drive the expression of transgenes in lateral line hair cells.

Imaging Glutamate Release from Ribbon Synapses

Much more recently a new type of sensor, called iGluSnFR, was established (Marvin et al 2013). It was bio-engineered from the E.coli periplasmic Glutamate binding protein GltI, which was inserted into a circular permutated GFP (cpGFP) and fused to an extracellular membrane anchor and was successfully used in the retina to detect the glutamate release of bipolar cells (Borghuis et al 2013; Franke et al 2017). In this system, it has furthermore been shown that the relationship between receptor current and change in fluorescence (ΔF/F) is linearly related (Borghuis et al 2013). As the sensor detects the glutamate that is released into the synaptic cleft it can be expressed either pre-, or postsynaptically.

As with GECIs, the results that can be obtained with iGluSnFR are strongly affected by its expression level. While iGluSnFR driven by the *ribeye* promoter directly, did not yield sufficient expression levels to be detected, employing the Gal4-UAS system increased expression but responses were very weak (despite yielding beautiful results in the retina of the same fish). The best results were obtained when expressing the iGluSnFR postsynaptically in the afferent neurons. But even within the same cell type, using the Sill promoter (Pujol-Martí et al 2012) to drive expression of lateral line afferent neurons resulted in significantly nicer responses as compared to the *isl2b* promoter, although both were used in combination with the Gal4-UAS system.

Cell type:	Location:	Reports:	Construct(s):	Comment:	
Hair Cells	Neuromast	Calcium Influx	**Rib::SyGCaMP6f**	very dim expression, very few responding cells	stable line
			Rib::GCaMP6f	strong expression, many responding cells	stable line
			Rib::SyGCaMP2	very dim expression, very few responding cells	stable line
			Rib::jRGECO1a	no expression	injected and stable
			Rib::Gal4 / UAS::GCaMP6s	Mosaic expression, many responding cells	injected GCaMP6s
			Rib::Gal4 / UAS::SyGCaMP3.5	mosaic expression, no responses	stable line
			brn3c::SyGCaMP6f	very dim expression, no responses	injected and stable
			brn3c::Gal4 / UAS::SyGCaMP3.5	very dim expression, no responses	stable line
		Glutamate Release	Rib:trpA / tUAS::iGluSnFR	mosaic expression, weak responses	co-injected
			Rib::Gal4 / UAS::iGluSnFR	mosaic expression, very weak responses	stable line
			Rib::iGluSnFR	No expression	injected
			Sill::Gal4 / UAS::iGluSnFR	mosaic expression, good responses	injected and stable
			Sill::trpA / tUAS::iGluSnFR(-SF)	mosaic expression, good responses	injected
			isl2b::Gal4 / UAS::iGluSnFR	mosaic expression, good responses (not specific *)	stable line
Afferent Neuron	Neuromast	Calcium Influx	Sill::GCaMP6f	dim expression, weak responses	injected and stable
			HuC::GCaMP6f	strong expression, good responses (not specific *)	stable line
	PLL Gnaglion	Calcium Influx	**Sill::GCaMP6f**	dim expression, weak responses	injected and stable
			HuC::GCaMP6f	strong expression, good responses (not specific *)	stable line
	MON	Calcium Influx	Sill::Gal4 / UAS::SyGCaMP3.5	good expression, good responses	stable line
			Sill::GCaMP6f	dim expression, weak responses	injected and stable
		Glutamate Release	**Sill::Gal4 / UAS::iGluSnFR**	mosaic expression, good responses	injected and stable
			Sill::trpA / tUAS::iGluSnFR	mosaic expression, good responses	injected
Efferent Neuron	NM	Calcium Influx	**HuC::GCaMP6f**	strong expression, good responses (not specific *)	stable line

* expression is not restricted to a specific cell type.

Table 2.2. List of Tested Constructs to Access Calcium Influx and Glutamate Release in the Lateral Line System

Our observations on the usage of different promoter systems to drive expression of different GECIs and iGluSnFR in hair cells and afferent neurons are summarized in Table 2.2. As previously mentioned, the specific insertion site of the transgene as well as the number of insertions can strongly influence the functionality of a reporter. This also explains why we regularly observed large differences between acutely injected larvae when compared to the stable line. Figure 2.7 summarizes the sites and physiological processes that we could observe using different reporters in the lateral line system of larval zebrafish.

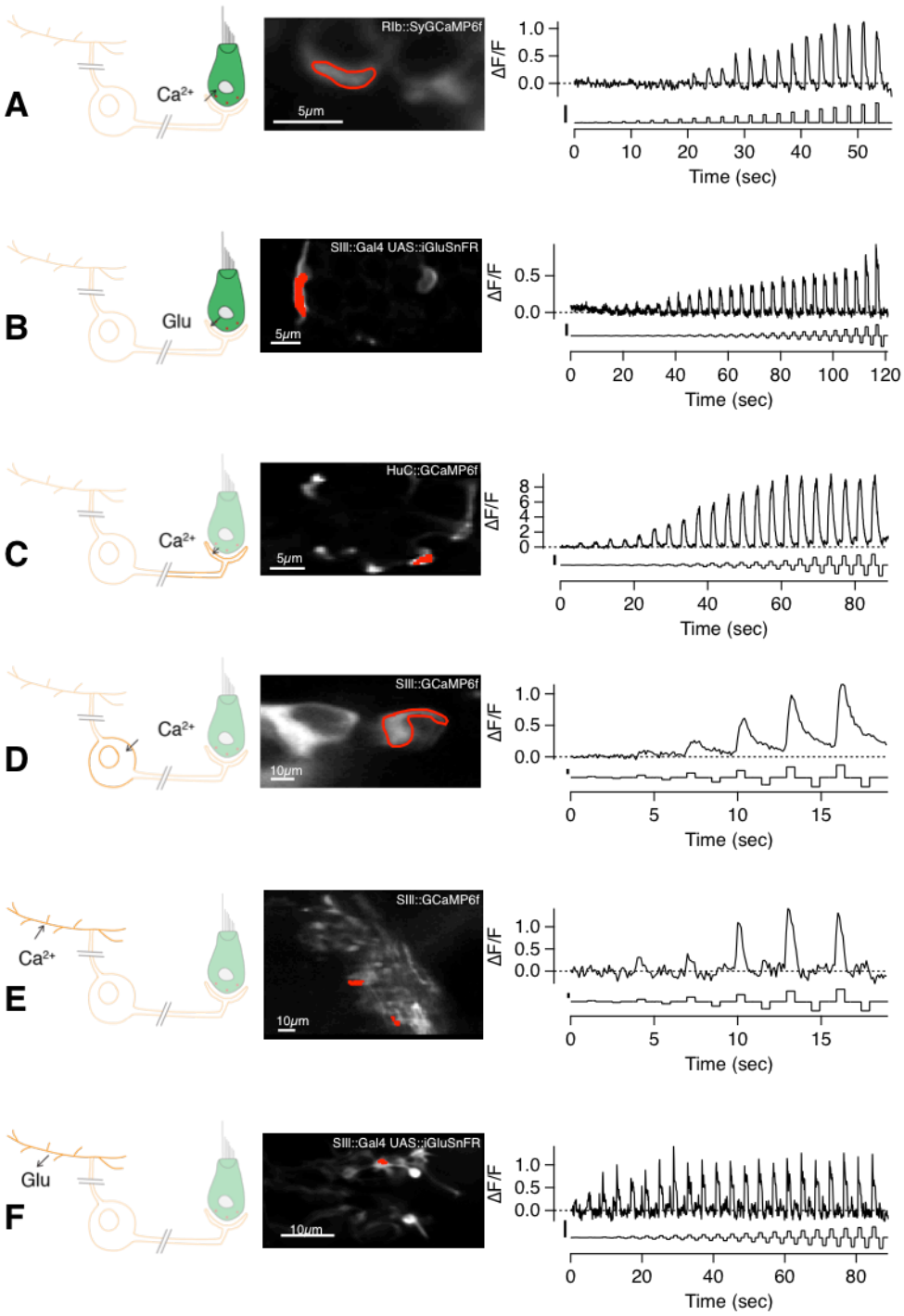

Figure 2.7. Summary of Glutamate and Calcium Reporters in Hair Cells and Afferent Neurons of the Zebrafish Lateral Line

The first steps in the transmission of mechanical information can be optically investigated using calcium and glutamate reporters (GCaMP6f and iGluSnFR, respectively). The first column depicts a cartoon of the location and physiological process monitored (from right to left: green hair cell, spherical cell body in the PLL ganglion and bifurcating central projection in the hindbrain). The second column depicts average projections of the respective movies, indicating the region of interest and the reporter line used and the third column contains example traces of responses to a stimulus of increasing pressure steps. (**A**) SyGCaMP6f is expressed in hair cells, monitoring calcium influx at the basal side of the cell, close to the synaptic ribbons. (**B**) iGluSnFR, expressed in lateral line afferents (under the Sill promoter) detects the glutamate that is released by the hair cells. (**C**) Glutamate binding to AMPA →

Although every result should be interpreted with the abovementioned constraints in mind, it still allows unprecedented access to this sensory modality.

Image Analysis

The image stacks (or movies) that are acquired during an experiment usually contain the desired information, such as the activity of a hair cell, hidden as a localized change in fluorescence within a noisy background. The sample may drift a little during the acquisition period, other cells or pigments usually surround the hair cell, and within a hair cell the signal might be strongest at one location and gradually decline, without a clear border. Furthermore, different cells might display different levels of baseline fluorescence, which have to be accounted for when interpreting the responses. To analyze the movies, we extracted the change in fluorescence from a spatially confined region of interest (ROI) over time. This required a few basic processing steps, such as registration, segmentation and calculation of the relative change of fluorescence (ΔF/F). We used IgorPro7 (WaveMetrics Inc.) for all of our analysis, although free image processing tools such as FIJI (Schindelin et al 2012), provide a number of very useful features.

The first step of image analysis is usually registration of the movie. This process enables the automatic correction of small motion artefacts such as drift in the X/Y dimension. It cannot account for large or sudden displacements and maybe most importantly it cannot account for displacements in the z dimension. Every movie should therefore be looked at by eye first to prevent the procedure from introducing artefacts. Although registration algorithms differ somewhat, all follow the same basic idea of aligning the respective image of the stack to either the previous image or a reference image by applying some sort of transformation, such as translation, rotation or warping. These algorithms require a certain spatial resolution, so that small changes between frames do not affect their overall similarity.

---

receptors on afferent nerve endings leads to postsynaptic calcium influx, which can be detected by expressing GCaMP6f in afferent neurons, in this example, under the pan-neuronal *HuC* (*elavl3*) promoter. (**D**) Exclusively expressing GCaMP6f in afferents facilitates the identification of the posterior lateral line ganglion. The calcium influx detected in the cell body is a result of action potentials. (**E**) The presynaptic calcium influx in the central projections of the afferents in the hindbrain (medial octavolateralis nucleus, MON) can be measured by, expressing GCaMP6f in all afferents (as in D). (**F**) Finally, the glutamate release in the hindbrain, that leads to the activation of secondary projection neurons can be imaged using the same line as in (B), expressing iGluSnFR exclusively in afferents.

If the resolution is too low, the change in fluorescence of a few pixels can yield the whole movie un-registerable. Once the movie is registered, the next crucial step is to define appropriate ROIs. If the signal is confined in space, for example by localising the reporter in the nucleus or tethering it to the synapse, the boundaries of the ROI are predetermined and defining individual ROIs becomes easier. On the other hand, if the fluorescent reporter is expressed in the whole cytosol, then defining the ROI becomes significantly more difficult as the signal changes continuously without clear demarcations. In these cases it might be best to draw the ROI manually by using either morphological criteria or another marker, such as mCherry tethered to synaptic ribbons for example (see next chapter). Alternatively, different algorithms exist that automatically define ROIs and extract the time series data from them. These algorithms use either spatial features such as edges (Dorostkar et al 2010), or spatio-temporal correlations (Portugues et al 2014). In our experience, the appropriate segmentation method depends largely on the type of movie and empirically testing several different algorithms to see which one works best is worthwhile.

The segmentation yields the absolute change in brightness of the respective ROI. This value depends not only on microscope settings such as the dynamic range of the detector or the gain of the amplifier, but also on the laser power, reporter brightness and expression levels. To compare different ROIs and different experiments, the change in fluorescence has to be expressed as the relative change normalized by the baseline fluorescence or $\Delta F/F$. The baseline fluorescence is usually defined as the first few seconds of acquisition, in the absence of any stimulation.

Only after all these steps are performed can the traces, representing for example the changes of calcium concentration of glutamate release of a cell, be further analyzed. These processing steps form the foundation of any further and more sophisticated analysis and should therefore be undertaken carefully.

Conclusion

Here we described a fast and non-invasive method to mount zebrafish larvae without damaging their lateral line organ, we introduce an approach to measure cupula deflection that is very easily integrated into a fluorescent microscope and we reviewed some considerations that should be kept in mind when using genetically encoded calcium and glutamate reporters to study the encoding of mechanical information in the lateral line system. Functional imaging techniques have the main advantage that multiple cells can be observed simultaneously. Within the NM this allows one to

assess the contribution of individual hair cells to the net output at the level of the afferent neuron, for example. However, this advantage becomes even more powerful when investigating the output of the afferent neurons in the Medial Octavolateralis Nucleus (MON) in the hindbrain, where each individual afferent neuron forms around 60 synaptic contacts to second order neurons (Pujol-Martí et al 2012). Given the continuous development of new reporters including red and blue-shifted GECIs (Akerboom et al 2013; Dana et al 2016), and voltage indicators (Jin et al 2012; St-Pierre et al 2014; Storace et al 2016) the prospect of simultaneously imaging pre- and postsynaptic calcium or glutamate release as well as calcium influx of the same neuron are within arm reach. In combination with two-photon imaging, this could lead to important insights in the central representation of mechanical information.

Chapter 3

The Heterogeneous Transfer Characteristics of Hair Cells Encoding Mechanical Stimuli in the Lateral Line of Zebrafish

Abstract

Ribbon synapses of hair cells transmit mechanical information but the transfer characteristics relating deflection of the hair bundle to glutamate release have not been assessed directly. Here we have imaged glutamate to investigate how hair cells encode information in the lateral line of zebrafish. About 50% of hair cells signaled motion in either direction from rest, achieving maximum sensitivity for deflections of up to ~100 nm in the preferred direction. The remainder rectified completely and were less sensitive, extending the operating range of the neuromast beyond 1 μm. Adaptation was also heterogeneous, with some hair cells generating sustained outputs and others transient ones. A unique signal encoded a return to rest: a transient output from hair cells unresponsive to the initial stimulus. A mixed population of hair cells with these various transfer characteristics will allow a neuromast to signal weak stimuli while maintaining the ability to encode the amplitude and duration of stronger deflections.

Introduction

An increasingly important context for the study of mechanotransduction is the lateral line of larval zebrafish (Ricci et al 2013; Olt et al 2014; Olt et al 2016; Graydon et al 2017; Oteiza et al 2017; Sheets et al 2017; Erickson et al 2017; Maeda et al 2017; Troconis et al 2017). This sensory system enables the animal to detect vibrations and pressure gradients in its hydrodynamic environment and is implicated in social behaviors (Butler & Maruska 2016), predator avoidance (McHenry et al 2009; Stewart et al 2013) and the maintenance of position against a current (rheotaxis) (Suli et al 2012; Olive et al 2016; Oteiza et al 2017). The functional units of the lateral line, called neuromasts, are distributed over the head and body of the zebrafish, each being composed of 10-20 hair cells (Metcalfe et al 1985; Ghysen & Dambly-Chaudière 2007; Pujol-Martí & López-Schier 2013). As in the auditory and vestibular systems, the hair cells within a neuromast convert small displacements of the hair bundle into changes in the rate of glutamate release from ribbon-type synapses (Marcotti & Masetto 2010; Nicolson 2012). Understanding the transfer characteristics of these synapses is therefore fundamental to understanding how mechanical information is encoded within the lateral line.

All the hair cells within a neuromast act as a population to encode a single mechanical stimulus – the deflection of the cupula into which they all project. The

direction of deflection is encoded by a 'push-pull' system in which half the hair cells are maximally depolarized by motion in one direction and the other half by motion in the opposite, with segregation of these two populations onto separate afferent fibers (Faucherre et al 2009). A number of fundamental questions about signalling in the lateral line of larval zebrafish remain unanswered. How sensitive are individual hair cells to deflection of the cupula? What is the dynamic range over which the ribbon synapse operates? How does the output adapt? And how do the hair cells within a neuromast act as a population?

Direct answers to these questions require assaying the release of glutamate from individual hair cells while deflecting the hair bundle by known amounts. The output of hair cells has been studied by measuring capacitance changes (Beutner et al 2001; Brandt et al 2005; Ricci et al 2013; Olt et al 2014) or by recording synaptic currents in the afferent fiber (Keen & Hudspeth 2006; Li et al 2009; Weisz et al 2012), but both these techniques require the synapse to be activated by direct injection of current, which bypasses the normal process of mechanotransduction (but see: Rabbitt et al 2005). We therefore developed an all-optical approach in which deflections of the cupula and release of glutamate from multiple hair cells were imaged in the same neuromast. Monitoring synaptic transmission using the glutamate sensor iGluSnFR (Marvin et al 2013) allowed us to investigate the transfer characteristics of both individual hair cells and the population within a neuromast.

Here we show that the output of a neuromast is determined by two basic types of hair cells. About 40% signal deflections of the hair bundle less than 150 nm, while the remainder are less sensitive and extend the dynamic range of the neuromast to encode deflections beyond 1 μm. These heterogeneous transfer characteristics extend to the dynamics of adaptation generating a population code that reliably signals weak stimuli while maintaining the ability to encode the amplitude and duration of stronger deflections.

Results

An all-optical Approach to Measuring the Transfer Characteristics of Hair Cell Ribbon Synapses in vivo

Although the lateral line system has been studied for decades, the input-output relation of hair cells within neuromasts is still unclear. To observe the output we used the Sill promoter to drive expression of the fluorescent glutamate sensor iGluSnFR in

the surface membrane of primary afferents postsynaptic to hair cell ribbons (Pujol-Martí et al 2012; Marvin et al 2013). Neuromasts in the posterior lateral line of larval zebrafish were stimulated using a narrow pipette that applied positive and negative pressure steps of varying amplitude (Fig. 3.1 B). Although iGluSnFR was distributed over the whole surface of the afferent fibers (Fig. 3.1 C), signals were generated at distinct hotspots (Fig. 3.1 E-G). To test if these hotspots coincided with presynaptic ribbons we used fish co-expressing iGluSnFR with Ribeye-mCherry (Odermatt et al 2012). Figs. 3.1 E and F home in on four varicosities from two afferents: two of the ROIs were contacted by one ribbon (amber and blue ROIs) while the other two were not (red and green ROI). iGluSnFR signals were only observed in areas that were in close apposition to a ribbon synapse (Fig. 3.1 G), and this was the rule in all three neuromasts in which this test was made. This example also demonstrates how synapses of opposite polarity could be monitored simultaneously: while the blue ROI was activated by positive deflections towards the head, the amber ROI was activated by negative deflections towards the tail.

To directly observe the mechanical input to the hair cells, deflections of the cupula were visualized by staining polysaccharides on the surface blue or red with Alexa-350/594 coupled Wheat Germ Agglutinin (Fig. 3.1 H-K; detailed in Experimental Procedures and Chapter 2). The rotational deflection of the cupula was calculated based on the idea that the proximal region, containing the kinocilia, acts as a rigid lever pivoting on a plane at the apical surface of the hair cells (Fig. 3.1 I, McHenry & van Netten 2007). We tested this model by imposing a variety of pressure steps and tracking the translational motion of the cupula through planes at four different distances from the apical surface of the hair cell (Figure 2.4 F). Fig. 3.1 J shows images of the cupula at z = 15 µm, from which the x translation was estimated from the movement of the center of mass of the fluorescence. Figure 2.4 E plots the x displacement as a function of time from four such movies at z distances between zero and 15 µm. At any single pressure, the x translations at different z gave consistent estimates of the angle of rotation, confirming that the lower part of the cupula behaves as a beam pivoting around its base. We were therefore able to calibrate the relation between applied pressure and rotation of the cupula for each experiment, which in turn allowed us to control for variables such as pipette diameter and location (Fig. 3.1 K & Fig. 2.4 G).

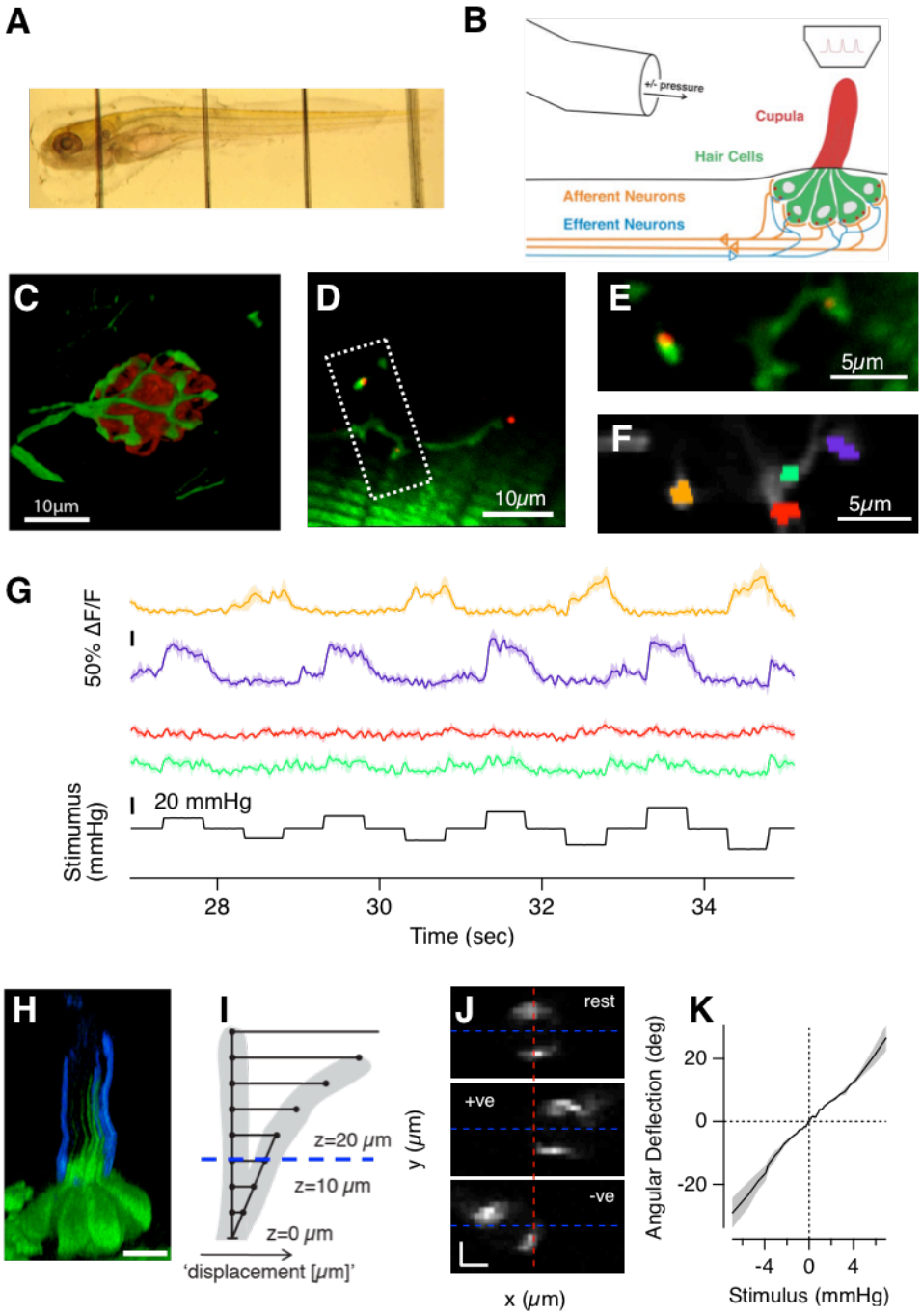

Figure 3.1. Imaging the Input and Output from Hair Cells in a Neuromast
(**A**) Lateral view of a paralyzed larva, lying in a custom made sylguard 'pit' and held down by nylon strings. (Spacing between strings: 1 mm) (**B**) The NM was stimulated with positive and negative pressure steps applied through a bent pipette while being imaged through a two-photon microscope. (**C**) iGluSnFR was expressed over the surface of afferent neurons (green) which form a basket like structure around hair cells, here counterstained in red using FM4-64. (**D**) Image of a NM in a 7 dpf larva (Tg[Sill2, UAS::iGluSnFR, Rib::Rib-mCherry]) showing varicosities of afferent neurons (green) as well as synaptic ribbons (red). (**E**) Close-up of the boxed area in D. Of the four visible varicosities, two did not coincide with presynaptic ribbons. (**F**) Regions of interest (ROIs) used for analysis. (**G**) The responses of the four ROIs in F. The amber and blue ROIs, postsynaptic to ribbons responded to positive and negative pressure steps, respectively. The red and green ROIs not apposed to ribbons did not respond. (**H**) Side view of a NM expressing GFP in hair cells with the surface of the cupula stained with →

Ribbon Synapses in the Lateral Line can Signal Deflections less than 100 nm

What is the mechanical sensitivity of hair cells in the lateral line? Relating spikes in the afferent nerve to estimates of cupula deflection, Haehnel-Taguchi et al (2014) report that deflections below 8 µm cannot be encoded. In contrast, calcium imaging in the hair cells themselves indicates that robust responses can be elicited by deflections of about 2-3 µm (Sheets et al 2012; Kindt et al 2012; Zhang et al 2016). Imaging glutamate release using iGluSnFR, we found that many hair cells signaled deflections less than 150 nm.

The traces in Fig. 3.2 A show iGluSnFR signals from two nearby hair cells in response to positive and negative pressure steps of increasing amplitude, each lasting 1 s. It can immediately be seen that hair cell 1 (black trace) was more sensitive to small deflections from rest, generating changes in glutamate release at stimulus strengths that did not elicit glutamate release from hair cell 2 (red trace). The mechanical tuning of these receptors was characterized as the peak amplitude of the iGluSnFR signal (R) as a function of angular rotation of the cupula (X), as plotted in Fig. 3.2 B. A good description of this relation was provided by a two-state Boltzmann equation of the form:

$$R = R_{min} + R_{max}/\{1+\exp[(X_{1/2} - X)/ X_S]\} \quad (1)$$

Where R_{max} is the saturating response in the preferred direction, R_{min} is the maximum change in the null direction, $X_{1/2}$ is the rotation that half-activates and X_S is the slope factor. Notably, this equation also provides a good description of the relation between hair bundle displacement and mechanotransducer current in hair cells of a number of species, where it has been interpreted as reflecting the transition of the mechanotransducer channel between an open and a closed state (Holton & Hudspeth 1986; Crawford et al 1989).

Alexa-350-WGA. Notice how the kinocilia extend roughly half way up the cupula (scale bar 10 µm). (**I**) Schematic of the model used to calculate angular deflections of the cupula from a pivot at its base. The translational deflection for a given stimulus pressure was measured at several distances z above the apical surface of the hair cell. (**J**) Three representative frames of the stained cupula at z = 15 µm at rest and deflected by a positive and negative pressure step. The angular deflection was calculated as $\tan^{-1}(\Delta x/z)$, where (Δx) was the translation in the center of mass of the staining. (**K**) Example of a calibration curve relating the stimulus pressure to the angular deflection. These relations were generally linear.

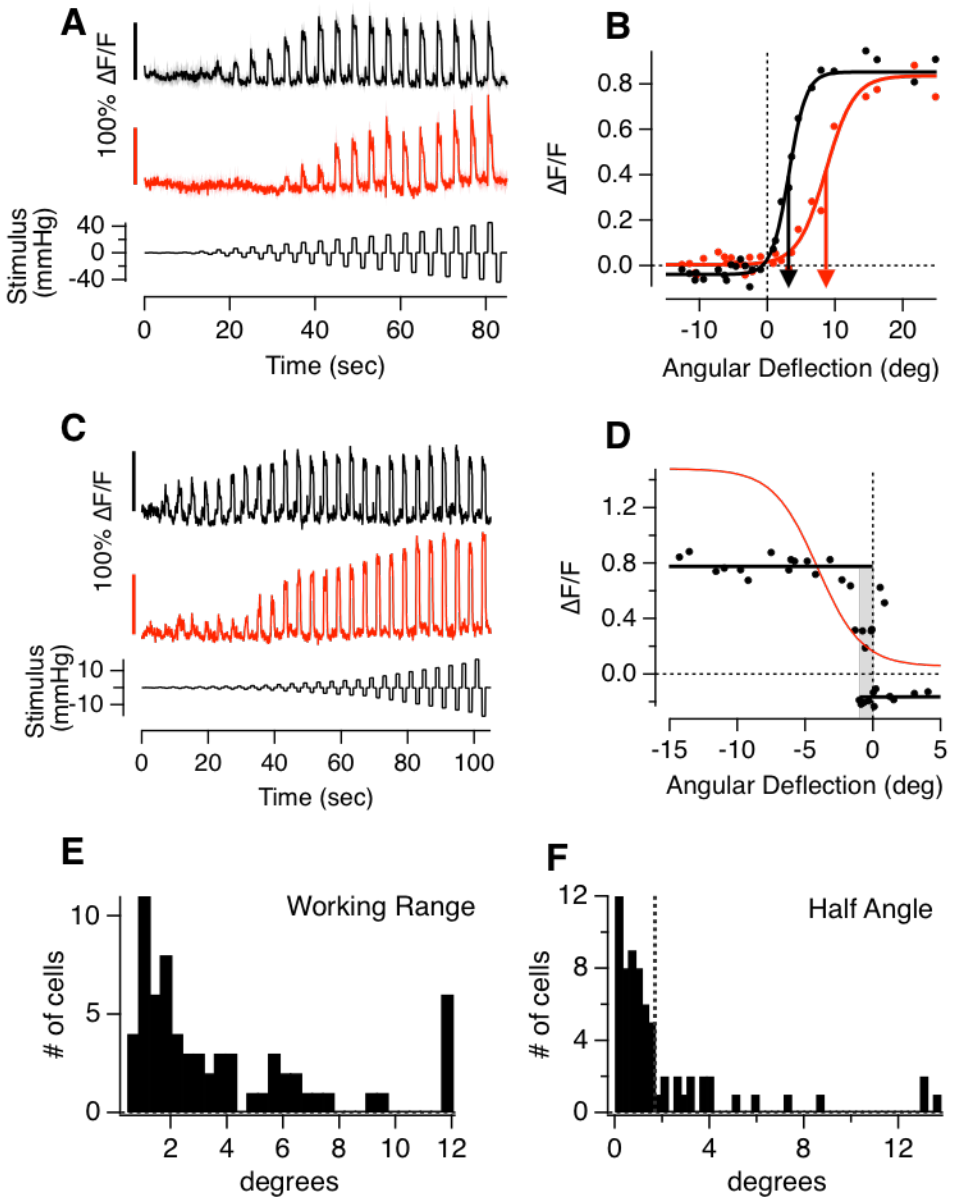

Figure 3.2. Sensitivity of Lateral Line Hair Cells

(**A**) Responses of two hair cells recorded in the same neuromast, both responding to positive pressure steps. The upper hair cell (black) responds to smaller deflections than the bottom (red). (**B**) Peak iGluSnFR signals (R) from A plotted as a function of the angular deflection of the cupula (X). These stimulus-response relations could be described by a two-state Boltzmann function (equation 1), with parameters R_{max}, R_{min}, $X_{1/2}$ and X_s.: $R_{max(1)}$= 0.89 ± 0.02, $R_{min(1)}$= -0.04 ± 0.01, $X_{1/2(1)}$= 3.19 ± 0.15° and $X_{s(1)}$= 1.28 ± 0.15, $R_{max(2)}$= 0.83 ± 0.02, $R_{min(2)}$= 0.00 ± 0.01, $X_{1/2(2)}$= 8.65 ± 0.34° and $X_{s(2)}$= 2.07 ± 0.3. (**C**) Responses of two hair cells from another neuromast that differ more significantly in their working range. (**D**) Stimulus-response relations of the cells in C. The cell depicted in red had a working range of 7°, and the one in black < 1° (grey bar). (**E**) A histogram of working ranges measured in 67 hair cells. About 30% of the cells have working ranges within 1.5°. The last bin contains all cells above 12°. (**F**) Histogram of the $X_{1/2}$ values in 67 hair cells. The majority (75%) had $X_{1/2}$ < 2° (dashed line).

The two synapses in Fig. 3.2 B differed most significantly in $X_{1/2}$ (arrowed), which is the point at which the gradient of the input-output relation is at its steepest and the sensitivity of the receptor at its maximum (Butts & Goldman 2006). The distribution of half-angles across 67 hair cells is shown by the histogram in Fig. 2F. 70% of synapses had half-angles below 2°, corresponding to deflections less than 180 nm at the top of the ~5 µm tall hair bundle (McHenry et al 2008; Maeda et al 2017). The majority of hair cells in the lateral line therefore have a mechanical sensitivity significantly higher than previously suspected and comparable to auditory hair cells in mice and other species, which have working ranges estimated to be between 20 nm and 300 nm (reviewed by: Fettiplace & Kim 2014).

Heterogeneous Transfer Characteristics of Hair Cells within Individual Neuromasts

The input-output relation of hair cells within a neuromast varied significantly, both in terms of half-angle and slope factor (equation 1). The slope factor reflects the range of deflections over which the output is most strongly modulated, which can be described more intuitively as the working range (WR) - the deflection required to increase the response from 10% to 90% of maximum (WR = 4.4 * X_S , Markin & Hudspeth 1995). Estimates of the working range have been made in auditory and vestibular hair cells in a number of species and have varied between ~20 nm and 400 nm (Fettiplace & Kim 2014), corresponding to angular deflections of 0.23° to 4.6°. The hair cells in the lateral line featured in Fig. 3.2 A and B operated over working ranges of 5.6° and 9.1° but other hair cells operated with working ranges of ~1°, corresponding to a translation of just 80-90 nm at the tip of the hair bundle. Responses from such a high-sensitivity hair cell are shown by the black trace in Fig. 3.2 C and the plot in Fig. 3.2 D demonstrates that the response was complete with deflections of ~1° (shaded area). Another cell in the same neuromast signaled deflections within a WR of 7.2° (red traces in Fig. 3.2 C and D), again indicating the co-existence of receptors with different working ranges.

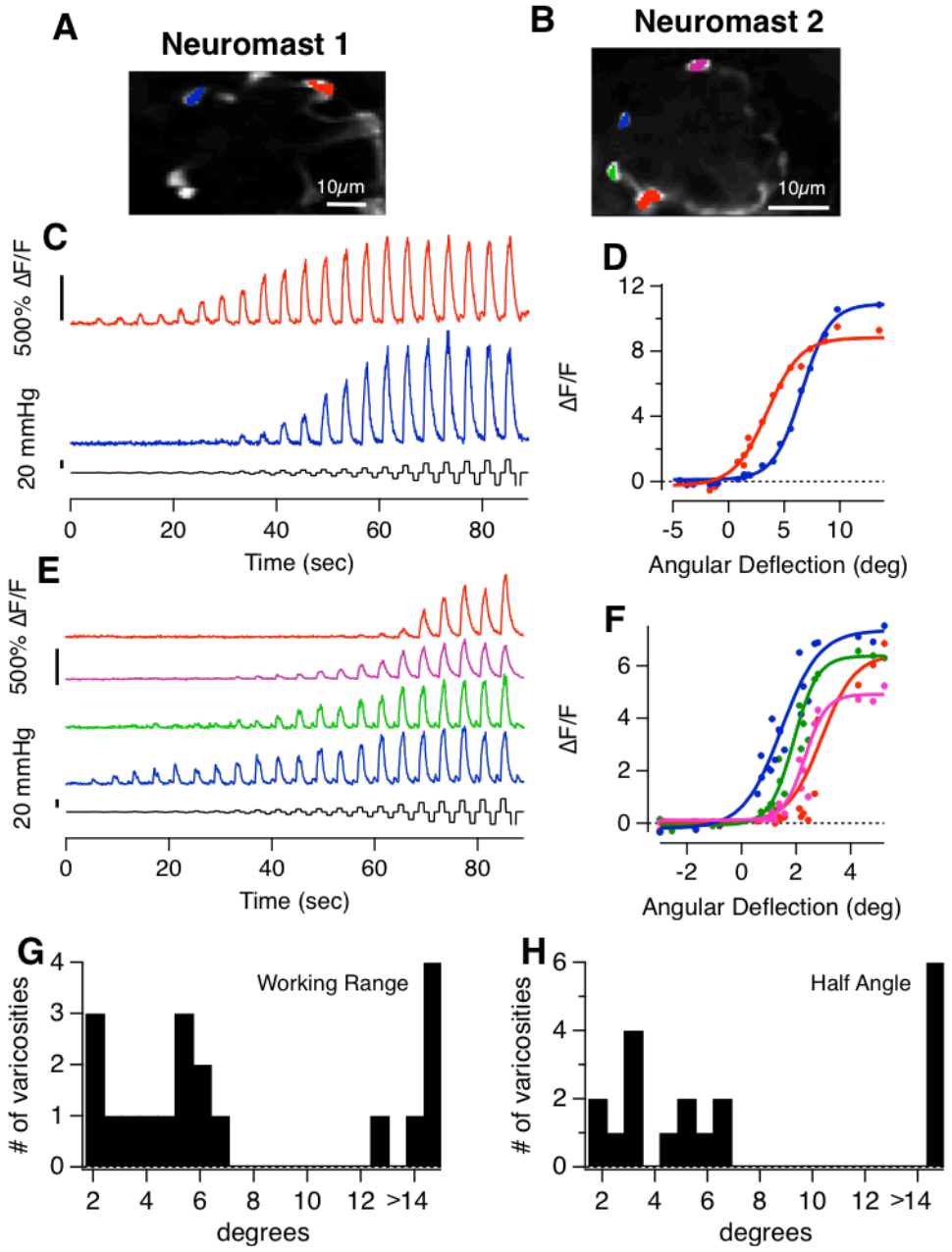

Figure 3.3. Heterogeneous Transfer Characteristics of Hair Cells Revealed by Measuring Calcium Signals in Afferent Neurons

(**A,B**) The Tg[HuC::GCaMP6f] line expresses the calcium indicator GCaMP6f in afferent neurons of the posterior lateral line but not in hair cells. (**A,C,D** and **B,D,F**) show the variety of stimulus response relations from hair cells in two neuromasts. In Neuromast 1 the red and blue traces in (B and C) have an $X_{1/2}$ of 3.5° and 6.6° and a working range of 6.6° and 5.5°, respectively. In neuromast 2 (D-F) $X_{1/2}$ ranges from 1.4° to 3° and the working range spans from 1.7° to 3°. (**G** and **H**) The distribution of working ranges and half-angles in 19 postsynaptic varicosities.

The distribution of working ranges across 67 synapses is shown by the histogram in Fig. 3.2 E. The initial peak is centered at ~1.5° (equivalent to deflections of 150 nm) and contains about half the synapses while the remainder had a wide variety of working ranges up to ~30°. The variety of input-output relations measured using iGluSnFR was not expected and we wondered if it might reflect the use of this reporter.We therefore also assessed the signal transmitted from hair cells by imaging the calcium signal in the post-synaptic afferent using GCaMP6f under the pan-neuronal *HuC* (*elavl3*) promoter (Experimental Procedures). Fig. 3.3 A,C,D show responses in two ROIs within one neuromast and Fig. 3.3 B,E,F show the responses in four ROIs of a second. Equation 1 also provided a good description of the input-output relation measured as a post-synaptic calcium signal and the half-angles and working ranges again varied significantly between different synaptic contacts (Fig. 3.3 G and H). We conclude that the neuromast encodes deflections of the cupula through a heterogeneous population of receptors operating over different ranges.

Individual Hair Cells can Encode Opposing Directions of Motion

Neuromasts encode mechanical information using a 'push-pull' system in which half the hair cells are depolarized by a deflection of the cupula in one direction and the other half by a deflection in the opposite direction, with each of these two groups segregating to different afferent fibers (Flock & Wersäll 1962; Ghysen & Dambly-Chaudière 2007). It is less clear whether individual hair cells also encode opposing directions of motion. Afferents leaving the neuromast spike spontaneously and this has been shown to depend on the release of glutamate from hair cells at rest, which is in turn dependent on the activity of the mechanotransducer channel (Trapani & Nicolson 2011). To which extent can this activity be reduced by deflection in the non-preferred direction? The red trace in Fig. 3.4 A shows an example where this is indeed the case: deflections of the cupula in the non-preferred direction caused a decrease in glutamate release. The input-output relation in Fig. 3.4 B shows that this synapse used 40% of its dynamic range to signal motion in the null direction. In contrast, another hair cell in the same neuromast was completely rectifying, only modulating release in the preferred direction (black trace in Fig. 3.4 A).

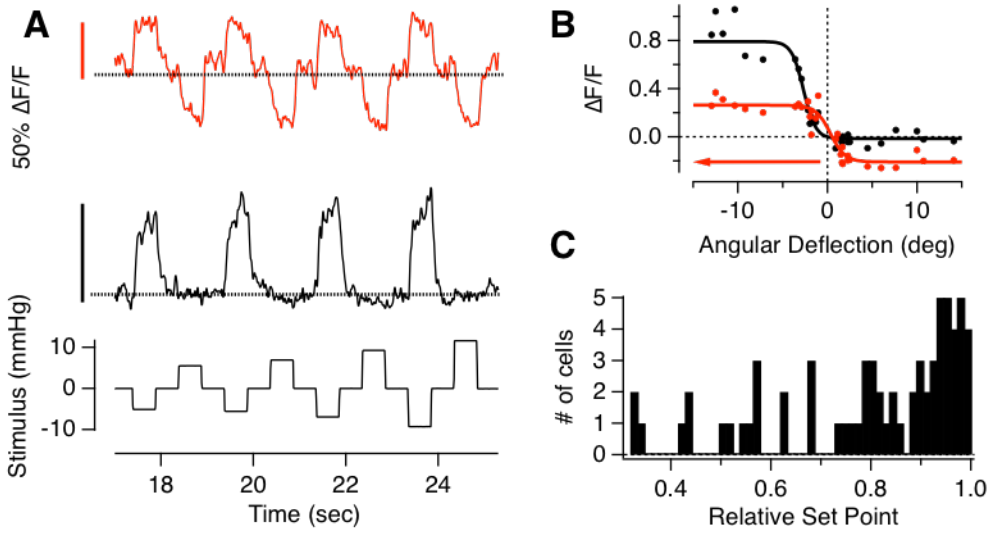

Figure 3.4. Push-pull Signalling in Individual Hair Cells
(**A**) Glutamate release from two hair cells in the same neuromast, both polarized in the negative direction. The cell depicted in black was completely rectifying but the cell in red could also clearly signal deflections in the positive direction as a decrease in glutamate release. (**B**) Stimulus-response relations of the hair cells in A. $R_{max(1)}$= 0.81 ± 0.04, $R_{min(1)}$= -0.02 ± 0.07, $X_{1/2(1)}$= -2.68 ± 0.18° and $X_{s(1)}$= 0.67 ± 0.16, $R_{max(2)}$= 0.47 ± 0.03, $R_{min(2)}$= -0.21 ± 0.05, $X_{1/2(2)}$= 0.32 ± 0.36° and $X_{s(2)}$= 0.83 ± 0.22. (Axis is reversed to represent the sensitivity to negative deflections.) The relative set points of the black and red relations were 1 and 0.4, respectively. (**C**) Distribution of the relative set points from 67 hair cells. Although the majority were strongly rectifying with relative set points close to 1, there was a large degree of variability.

The ability of individual hair cells to signal opposite directions of motion was quantified as the 'relative set point' for glutamate release - the fraction of the total dynamic range of the synapse modulated by deflections from rest in the preferred direction. The distribution of relative set point across a sample of 67 hair cells is shown by the histogram in Fig. 3.4 C. In 42% of synapses this fraction was greater than 0.9, i.e. deflections in the null direction reduced glutamate release by less than 10% of the dynamic range. However, in 7 synapses 50% or more of the dynamic range was used to encode deflections in the null direction as a decrease in the rate of glutamate release. These results demonstrate that while the output from most hair cells rectifies strongly, the large majority can encode both positive and negative deflections of the cupula. This property will allow for push-pull signalling within the lateral line, whereby a deflection in one direction increases the spike rate in one afferent while simultaneously decreasing the rate in the second to *below* the spontaneous rate in the absence of a stimulus.

A Mixed Population of High- and Low-Sensitivity Hair Cells

How do hair cells with different mechanical sensitivities act as a population to encode a deflection of the cupula? To obtain an overall picture of how the neuromast operates we estimated the total input to a single afferent by averaging the stimulus-response relation from 67 hair cells, as shown in Fig. 5 A. This average could be described as the sum of two sigmoid functions with significantly different slope factors and half-angles ($X_{S(1)}$= 0.4 ± 0.1, $X_{S(2)}$ = 1.9 ± 0.9, $X_{1/2(1)}$ =0.6 ± 0.09° and $X_{1/2(2)}$ = 6.1 ± 1.1°). The distribution of half-angles shown in Fig. 3.2 F also indicated two basic populations of hair cells, separable either side of $X_{1/2}$ = 2°. We therefore also averaged the stimulus-response relations for hair cells above and below this threshold, as shown in Fig. 3.5 B. The slope factors and half-angles describing the transfer function of these two populations were $X_{S(<2°)}$= 0.5 ± 0.04, and $X_{1/2(<2°)}$ = 0.7 ± 0.04° (red trace) and $X_{S(>2°)}$= 1.8 ± 0.3, and $X_{1/2(>2°)}$ =5.0 ± 0° (blue trace). Separating these populations according to $X_{1/2}$ revealed another important functional difference: hair cells of low sensitivity were completely rectifying with a relative set point of 1 while cells of high sensitivity had a relative set point of 0.8.

The sensitivity of a sensory neuron can be calculated as the first derivative of the stimulus-response relation (Dayan & Abbott 2001) and the dashed line in Fig. 3.5 C shows this function for the average output of all 67 hair cells. The sensitivity of the neuromast as a whole is at a maximum at deflections of 0.5° but, because of the negative set point of the high-sensitivity population of hair cells, small deviations around zero are also signaled with a sensitivity about 70% of maximum, either as an increase or a decrease in glutamate release. This population is saturated at deflections greater than about 3° (Fig. 3.5 B) but the dynamic range of the neuromast is extended up to about 12° by the low-sensitivity population of completely rectifying hair cells which generate a second peak in the sensitivity function around 6°. Acting together, these two populations of hair cells will make the neuromast very sensitive to small deflections of the cupula while maintaining a large dynamic range. This coding strategy can be compared with the visual system, where the trade-off between sensitivity and dynamic range is dealt with using high-sensitivity rods and low-sensitivity cones (Masland 2012).

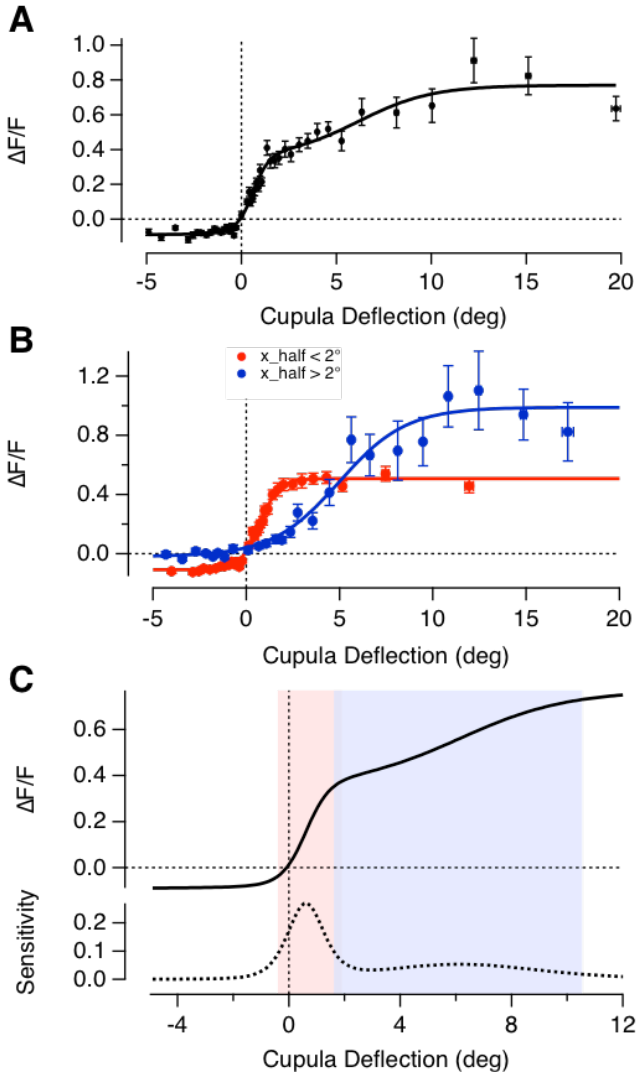

Figure 3.5. The Average Transfer Characteristics of Hair Cells in a Neuromast
(**A**) 2800 paired measurements of cupula deflection and peak glutamate release, recorded from 67 hair cells. All responses are plotted as a function of the magnitude of deflection, irrespective of direction. A good empirical description was provided by the sum of two Boltzmann relations (equation 1) as shown by the fitted curve (R_{min}= -0.1 ± 0.02, $R_{max(1)}$= 0.44 ± 0.09, $R_{max(2)}$= 0.42 ± 0.12, $X_{1/2(1)}$= 0.60 ± 0.1°, $X_{1/2(2)}$= 6.14 ± 1.17°, $X_{s(1)}$= 0.42 ± 0.12, $X_{s(2)}$= 1.95 ± 0.95). The working range of the whole population is 8.9°. (**B**) The average stimulus-response relation of hair cells separated into two groups based on half-angle with a threshold of 2°. The two subsets had average half-angles of 0.7° (red) and 5° (blue). The high- and low-sensitvity groups of hair cells also differed significantly in R_{min}, the maximum change in the null direction, with values of -0.11 ± 0.01 and -0.02 ± 0.02, respectively. The working ranges of these populations were 2.3° and 8° respectively, and overlapped between 1° and 1.9°. (**C**) The sensitivity of the whole population calculated as the derivative of the fit in (A). Small deflections (below 2°) are encoded with high sensitivity by the large population of hair cells whereas the second smaller population extends the dynamic range significantly to also capture larger cupula deflections, ranging beyond 10°.

Heterogeneous Adaptive Properties of Hair Cells within Individual Neuromasts

A second strategy by which sensory systems prevent saturation to maintain sensitivity is adaptation, a time-dependent change in gain that adjusts the working range in response to the recent history of stimulation (Wark et al 2007). In the lateral line, ramped deflections of the cupula cause the spike rates in the afferents to adapt strongly (Haehnel-Taguchi et al 2014) but the cellular mechanisms are not clear. In hair cells of the auditory and vestibular systems the two main loci of adaptation are the mechanoelectrical transducer (MET) in the hair bundle (Eatock et al 1987; Howard & Hudspeth 1987; Shepherd & Corey 1994; Kros et al 2002b; Vollrath & Eatock 2003; Corns et al 2014, reviewed by: Eatock 2000; Fettiplace & Ricci 2003; Ricci & Kachar 2007) and depression at the ribbon synapse (Schnee et al 2005; Schnee et al 2011; Goutman 2017 reviewed by: Nouvian et al 2006). Although these two processes have been studied in isolation, little is known about how they act together to adjust the input-output relation of the hair cell.

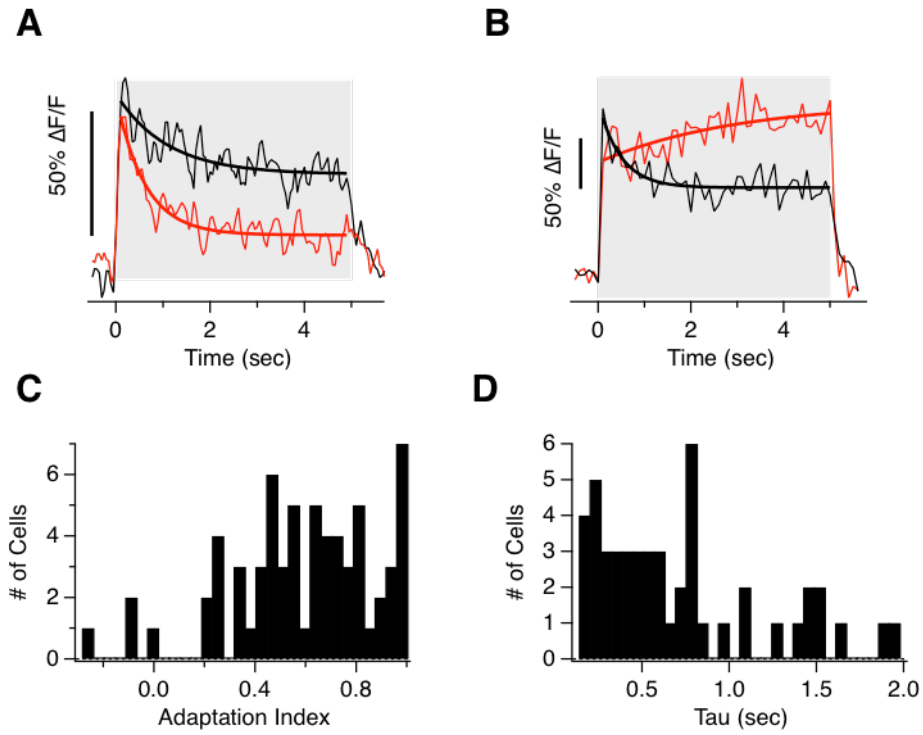

Figure 3.6. Heterogeneous Adaptive Properties of Hair Cells
(**A**) Two hair cells from the same neuromast adapt to different extents to a 5 s step deflection. The red cell adapted with a time-constant of 0.61 ± 0.09 s (solid line) with an adaptive index of 0.65. The black cell adapted with a time-constant of 1.09 ± 0.32 s with an adaptive index of 0.42. (**B**) The iGluSnFR signal from two hair cells of a second neuromast. Note that while one cell adapted (black, AI = 0.53) the second sensitized (AI = -0.13). (**C**) Distribution of adaptation index from 65 hair cells stimulated with a 5 s step. (**D**) Distribution of the decay time constants from the 55% of cells that could be fit with tau < 2 s. In the remainder of cells tau was greater than 2 s and could not be estimated.

To investigate the adaptive properties of the neuromast we applied saturating or near-saturating pressure steps of 2 s or more. In 61 of 65 hair cells adaptation was apparent as synaptic depression but there was a large degree of variability between hair cells within the same neuromast. For instance, Fig. 3.6 A shows an example in which glutamate release fell to about 40% of peak in one hair cell (red) but only to 60% of peak in another (black). We quantified the reduction in glutamate release as an adaptation index (AI), which varied from 1 (complete recovery of the iGluSnFR signal to baseline) through zero (no change) to negative values (reflecting an acceleration of glutamate release; Experimental Procedures). The distribution of AIs measured at the end of a saturating 5 s pressure step is shown in Fig. 3.6 C: the average was 0.6 but the variance (σ^2=0.084) was large. The speed of decay of the response could be described by a time-constant of 2 s or less and the distribution is shown in Fig. 3.6 D (slower decays could not be fit reliably from a trace of 5 s). The smallest time constant we observed was 130 ms and 39% of the cells had a decay constant below 500 ms.

These results demonstrate that hair cells of the lateral line apply different temporal filters: in some, a step stimulus generates a transient response that most strongly signals the onset of the deflection (e.g. red trace in Fig. 3.6 A) while in others the output is more sustained and effectively signals the duration (e.g. black trace in Fig. 3.6 B). An analogy can again be made with the transformation of signals in the retina, where the distinction between transient and sustained neurons has long been recognized (Masland 2012).

Hair Cells Sensitized by Small Deflections

Adaptation in sensory systems is usually thought of as a reduction in gain, which acts to prevent saturation (Wark et al 2007), but in 3 cells a strong deflection caused the rate of glutamate release to *increase* over periods of a few seconds, as shown by the red trace in Fig. 3.6 B. The ability of some hair cells to sensitize to a constant stimulus became more apparent when measuring responses to small deflections. For example, Fig. 3.7 A shows the iGluSnFR signal from a single hair cell in which relatively small deflections did not generate a significant output within the first 500 ms, after which glutamate release gradually accelerated for the remainder of the stimulus (black and red traces). A deflection of intermediate amplitude generated a response that gradually achieved a steady state (green) while larger deflections generated responses that reached a peak within ~200 ms and then depressed (blue and violet traces). The ability to sensitize to small deflections was also one that varied between different hair

cells within one neuromast, as shown by the two examples in Fig. 3.7 B. A shift from sensitization to depression with increasing stimulus strength was observed in 4 of 14 hair cells stimulated for 2 s and could be described by the AI plotted as a function of deflection angle, as shown in Fig. 3.7 B.

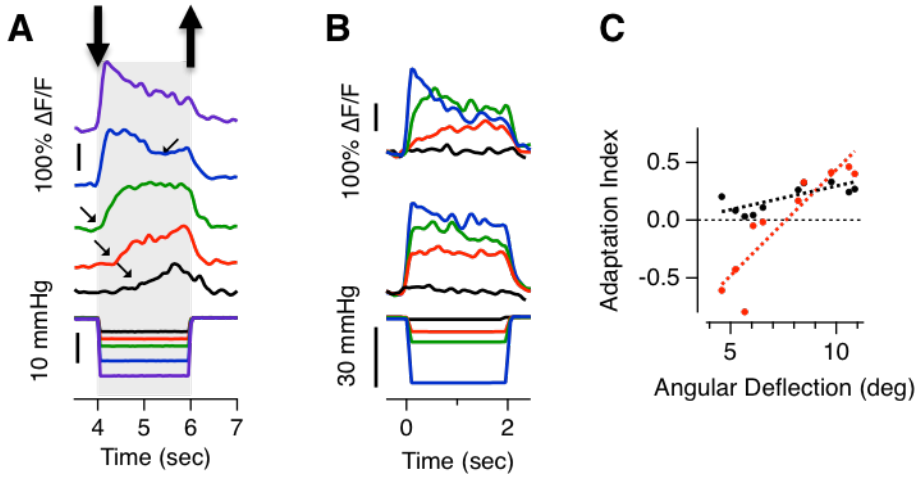

Figure 3.7 Sensitizing Responses to Weak Deflections
(**A**) A series of iGluSnFR signals from one hair cell. Large deflections cause glutamate release to rapidly reach a peak and then depress while small deflections do not generate a detectable signal for ~0.5 s after which glutamate release accelerates. (**B**) Two hair cells from the same neuromast responding to negative deflections. Cell 1 shows sensitization to small deflections but cell 2 does not. (**C**) The adaptation index as a function of deflection angle for cell 1 (red) and cell 2 (black) from B. Dashed lines are fits to the points.

A functional role for sensitization can be appreciated by asking when the offset of the stimuli in Fig. 3.7 A are signaled most clearly: the largest decrease in glutamate release occurred after *smaller* deflections that caused sensitization (red and green traces). A rapid sensitization of subsets of neurons has also been observed in the visual system. For instance, an increase in contrast causes some bipolar cells and ganglion cells in the retina to respond strongly and then depress, while others generate weak initial responses and then sensitize (Kastner & Baccus 2011; Nikolaev et al 2013; Kastner & Baccus 2013). Such a mixture of adaptive effects allows the retinal circuit as a whole to signal both increases and decreases in contrast more effectively than would be the case if all neurons simply reduced their gain when contrast increased (Kastner & Baccus 2011). An analogous mechanism appears to operate in the neuromast to allow the signaling of deflections both away from rest and back to rest.

Population Signaling of a Return to Rest

Here we have shown that push-pull signaling within a neuromast can occur not just through two populations of hair cells of opposite polarity but also within individual hair cells of high sensitivity (Fig. 3.4 A). A second and distinctive property of the population signal is shown by the pair of synapses in Fig. 3.8 A. These synapses were of opposite polarity and completely rectifying such that a deflection in the non-preferred direction did not generate a response. A return to rest from the non-preferred direction did, however, generate a strong and transient release of glutamate (black boxes). In other words, only one of the two hair cells signaled a deflection from rest (green boxes), while *both* signaled a recovery to rest with transient responses of opposite directions (black boxes). Such a 'reset' or 'rebound' signal was observed in 33 of 55 hair cells stimulated with steps of 1 s duration.

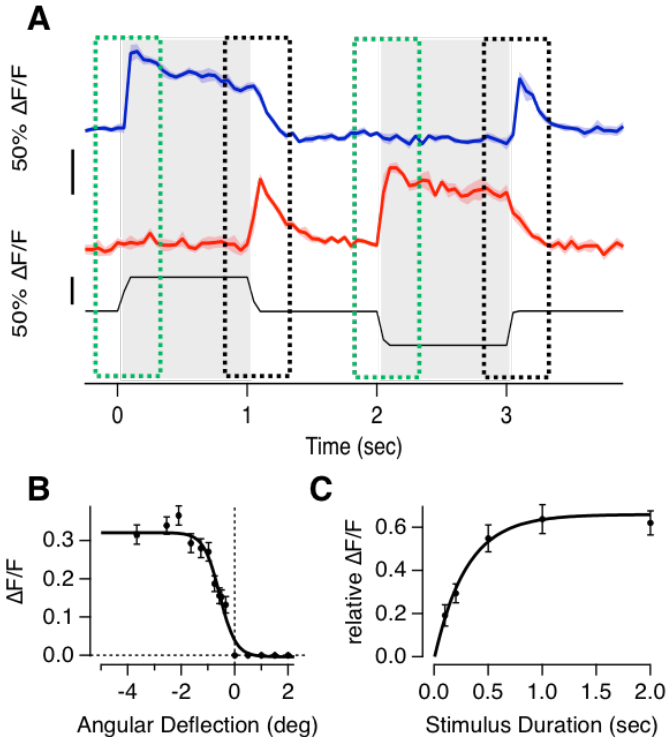

Figure 3.8. Hair Cells Signalling a Return to Rest
(**A**) Responses of two hair cells that generate a 'rebound-response' – a large and transient release of glutamate after the release of a deflection in the null direction. (**B**) The relationship between angular deflection in the null direction and amplitude of the rebound response. Data is averaged from 33 hair cells in which the largest rebound response exceeded 20% of the maximum response in the preferred direction (R_{max}= 0.32 ± 0.01, R_{min}= 0 ± 0.01, $X_{1/2}$= -0.56 ± 0.05° and X_s= 0.3 ± 0.05, axis is reversed to represent the sensitivity to negative deflections). (**C**) The relationship between duration of deflection in the null direction and the magnitude of the rebound response (as a fraction of the response to stimulation in the preferred direction). These experiments were performed with large deflections generating the maximum rebound. Results are described by an exponential that yields a time constant of 0.3 s for the development of the rebound response.

The amplitude of the reset signal depended on both the magnitude and duration of the deflection in the non-preferred direction. The peak response after a 1 s deflection to different angles could be described by a two-state Boltzmann equation, with a half-angle of -0.6° (Fig. 3.8 B) and during a large deflection the response developed with a time-constant of 0.3 s (Fig. 3.8 C). The reset signals transmitted through the hair cell synapse are qualitatively similar to the process of 'negative adaptation' described in the MET current of a variety of hair cells and is therefore likely driven by the same myosin1c (7a) dependent mechanism (Hacohen et al 1989; Holt et al 2002; Hirono et al 2004; Stauffer et al 2005). These results indicate that negative adaptation in the lateral line generates a population signal that can be reliably decoded as a cessation of a stimulus as would occur, for instance, at the end of a swimming bout (Palmer et al 2005; Ayali et al 2009) or an inter-bout interval, to integrate different flow gradients (Oteiza et al 2017).

Discussion

We present an in vivo system that permits the optical measurement of angular cupula deflection and hair cell glutamate release that constitute the direct input and output of hair cells in lateral line neuromasts. These measurements were performed in the intact sensory system, preserving the mechanical filter properties of the cupula, and without the decoupling of mechanoelectrical transduction from the exocytosis process (as electrophysiological approaches would).

With this at hand we demonstrate that lateral line hair cells are extremely sensitive and that they transform flow information in a number of different ways before it is transmitted centrally by afferent neurons. Fundamental features of the transfer characteristics of hair cells that varied within a single neuromast included sensitivity (Fig. 3.2, 3.3 and 3.5), set point (Fig. 3.4 and 3.5) and adaptation (Fig. 3.6 - 3.8). Below we discuss these results in terms of their underlying mechanism and the operation of the lateral line.

Sensitivity and Working Range

Previous studies have characterized the sensitivity of a single neuromast by measuring the spiking activity of the afferent neuron and varying the deflection distance and velocity (Haehnel-Taguchi et al 2014). They could show that a cupula displacement of 8 µm led to spiking activity exceeding spontaneous activity by 25%. Assuming the displacement was applied at the tip of the kinocilia, this would yield an

angle of 21°, which clearly exceeds our measurements of a dynamic range between 0° and 10° (which is much closer to the estimate of 6° – 8° in (Zhang et al 2016) or 5° – 10° in (Sheets et al 2012)). A significant fraction of hair cells in this study had half angles below 2° (Fig. 3.2 F), which corresponds to a displacement of 170 nm at the tip of the stereocilia (~5 µm). The most sensitive hair cells observed here saturated with a 1° deflection of the cupula, corresponding to only 80 – 90 nm deflection at the tip of the hair bundle. Such a high degree of sensitivity has been demonstrated in vestibular hair cells of the inner ear, which have been shown to have a threshold sensitivity of 500 picometers and saturate at deflection of about 4.7° (500 nm displacement at the tip of the stereocilia) (Hudspeth & Corey 1977; Eatock et al 1987).

One parameter that strongly influences the experimentally observed working range is the means of stimulation. Using a fluid jet to deflect inner ear hair bundles leads to shorter working ranges when compared to stimulation with a stiff probe (Fettiplace & Kim 2014). This difference can at least partly be attributed to the fluid jet equally deflecting all stereocilia leading to the synchronous opening of all MET channels, in contrast to the stiff probe, which sequentially deflects different stereocilia (depending on its shape), resulting in asynchronous MET channel opening and thus a broadening of the working range (Nam et al 2015). In our preparation, the mechanical coupling between fluid pressure and MET channel opening is embedded in its endogenous context and should therefore represent the physiological condition.

We observed profound variability (over a 10 fold range) in the half angle as well as the working range of hair cells (Fig. 3.2 E & F) and within the same neuromast. Because the hair bundle of all cells is constrained by the cupula, this heterogeneity cannot be explained by the stimulation technique but must rather stem from physiological factors. What could these be? One possible source is the transduction process itself. Functional heterogeneity has been reported for the ‘current – displacement’ (I/X) relationship, both in terms of working range and half angle, between different hair cells (vestibular and auditory) but under the same experimental conditions (Holt et al 1997; Stauffer & Holt 2007). A second possible source is the process of exocytosis. Even within a single hair cell, different active zones were reported to vary in terms of the voltage dependence and the number of calcium channels leading to heterogeneous release rates driven by the same receptor potential (Ohn et al 2016). The lateral line system is still developing at 7 dpf (Ghysen & Dambly-Chaudière 2004; Pujol-Martí & López-Schier 2013), and so are the hair cells. It was shown that both mature and immature hair cells coexisted within a neuromast and

that they differed by their basolateral K^+ current as well as by the efficiency of exocytosis (Olt et al 2014). It is thus likely that the heterogeneity that we observe among hair cells is at least in part a result of this maturation process, although we cannot exclude an additional role of the mechanoelectrical transduction process. Irrespective of the mechanism, variability in the 'Glutamate release – Cupula deflection' (Glu/α) relationship was also observed in the postsynaptic Ca^{2+} influx in afferent neurons (Fig. 3.3), suggesting functional relevance in the encoding of mechanical information.

What do heterogeneous transfer characteristics of individual lateral line hair cells mean for the transmission of mechanical information by the whole population? Figure 3.5 shows that external stimuli get decomposed by lateral line hair cells. Weak stimuli are encoded by a large number of high sensitivity hair cells and stronger stimuli are encoded by fewer low sensitivity hair cells with an extended dynamic range. The working range of the high sensitivity sub-population starts at negative deflections. This implies that not only are there more high sensitivity cells, small fluctuations around 0° are furthermore encoded by both plane polarized hair cell populations.

Set Point

The relative set point of a hair cell is defined as the fraction of its dynamic range that is used to encode deflections in its preferred direction (Fig. 3.4). The measurements of glutamate release that we have made are determined by the interaction of mechanoelectrical transduction and voltage-dependent exocytosis, so the open probability of the MET channel is not the direct driver of these signals. Push-pull modulation of glutamate within individual hair cells requires that the resting potential in the absence of cupula deflection sits in a range where CaV1.3 channels are activated sufficiently to drive vesicle fusion (Platzer et al 2000; Olt et al 2014). To prevent complete rectification of the relationship between deflection and glutamate release, there has to be significant 'overlap' of the voltage range where P_{open} of the MET channel varies and the activation potential of the CaV1.3 channels. P_{open} at rest has indeed been shown to vary between hair cells, and estimates range from 10-30% (Shepherd & Corey 1994; Eatock 2000; Hudspeth 2014). The voltage-dependence of CaV1.3 is also subject to modulation (Striessnig et al 2010). Further, it has been demonstrated that lateral line hair cells in zebrafish express an inward rectifier I_h current (Trapani & Nicolson 2011), which is responsible for depolarizing the membrane

and therefore contributes to setting the resting potential. Variations in the density of I_h channels might therefore be another factor that underlies the different set points.

Adaptation

Adaptation is a crucial aspect of sensory encoding which permits a system to maintain sensitivity by adjusting the working range in response to the recent stimulus history (Wark et al 2007). In the present study we find a large degree of variability in the adaptive properties of hair cells, tested by a simple 5 s stimulation step of saturating magnitude. While the average AI was 0.6, it ranged from AI=1 (full adaptation) to AI=0 (no adaptation) and in rare cases even took a negative value, indicating sensitization (see later). The time constants of decay displayed a large degree of heterogeneity as well, ranging from 130 ms to far beyond 2 s (after which it became impossible to extract it) with a population average > 0.7 s (Fig. 3.6 D). This degree of variability held true for hair cells within a single neuromast.

The various degrees and speeds of adaptation can be summarized in a more general way: while some hair cells generated sustained outputs in response to a step input, others were transient. A similar distinction between transient and sustained neurons has long been recognized in the retina (Masland 2012) and in afferents of the vestibular system (Rabbitt et al 2005). Such a mixture of response properties may make the population of hair cells within a neuromast signal both sustained stimuli, such as water flow (Voigt et al 2000), as well as sudden deviations, such as eddy currents or the approach of a predator (McHenry et al 2009).

What are the sources of adaptation in the input-output relation of hair cells? Adaptation of the MET current varies strongly between hair cells and depends on hair cell type as well as means of stimulation. It can generally be described by two time constants (τ_{fast} in sub ms – ms range, and τ_{slow} in the tens of ms range). While both depend on Ca^{2+} influx, the former is a property of the MET channel itself and the latter is mediated by the motor protein myosin 1c (7a) (Holt et al 2002; Kros et al 2002b; Stauffer et al 2005), which anchors the top of the tip link with the actin filaments in the shaft of the taller stereocilium. Upon hair bundle deflections in the preferred direction, it slides down the filament, thereby releasing the tension acting on the MET channel and resetting its P_{open} the top of the tip link to the actin filaments in the shaft of the taller stereocilium (Howard & Hudspeth 1987; Hacohen et al 1989; Assad & Corey 1992).

However, several lines of evidence suggest that adaptation of the MET current is not the primary determinant of adaptation in the synaptic output observed in our experiments. First, even the fastest decay time constants in the present study (~130 ms) are still too slow to be explained by the myosin dependent (motor) mechanism, not to mention the average of 700 ms. Second, because we are deflecting the cupula within the viscous boundary layer, our step stimulus is low pass filtered and might not even elicit the initial transient response (McHenry et al 2008). Third, even if MET adaptation took place, we would potentially not resolve it with our imaging approach (usually 50 ms frame intervals). Fourth, the extent of slow MET adaptation is a function of stimulus strength with weaker stimuli leading to less adaptation (Shepherd & Corey 1994; Holt et al 1997; Rabbitt et al 2005). Using physiological stimuli, we are very likely on the weak end of the spectrum when compared to in vitro studies (Rabbitt et al 2005). And finally, it has been shown that exocytosis in hair cells of the zebrafish lateral line, measured as the change of capacitance induced by a strong depolarization, decays with time constants around 500 milliseconds (Lv et al 2016; Eatock 2000), similar to the time-constants of decay of the iGluSnFR signal. It therefore seems likely that the time-course of adaptation measured at the output of the hair cell is dominated by depletion of releasable vesicles at the ribbon synapse. The degree of adaptation in the steady-state will likely reflect the balance between the rate of vesicle release and the rate of replenishment at the active zone. Indeed, the ribbon is thought to be a key feature that allows sensory synapses to maintain vesicle release for prolonged periods (Lagnado & Schmitz 2015).

An intriguing finding was that a small number of hair cells sensitized during weak stimulation by increasing the rate of glutamate release, but adapted during stronger stimuli (Fig. 3.7). This was not an artifact of stimulation, as a neighboring cell did not display the same behavior (Fig. 3.7 B). Mechanistically this might be due to synaptic glutamate accumulation or the recruitment of intracellular Ca^{2+}-dependent vesicle trafficking or Ca^{2+}-release (Schnee et al 2011; Castellano-Muñoz & Ricci 2014). Functionally, this has two potential consequences: firstly, the offset of sustained stimulation in the preferred direction gets signaled stronger than the onset and secondly, improved signaling of weak but continuous stimuli. The latter might play a role in behaviors such as rheotaxis, where constant but slow flow continually deflects the neuromasts, and deviations from this flow orientation triggers a righting (orientation) behavior (Oteiza et al 2017).

The finding that a return to rest is reliably signaled (Fig. 3.8) points towards an active role of negative adaptation (adaptation to hair bundle deflections away from the kinocilium) in the transduction of mechanical information. Mechanistically, this process is based on myosin 1c (7a) resetting the anchor point of the tip link away from the MET channel and thereby reestablishing tension during a deflection in the non-preferred direction. The rebound MET currents in hair cells of mouse and frog develop considerably faster, however, with time-constants in the order of 10 ms (Holt et al 2002; Hirono et al 2004; Stauffer et al 2005). This difference is likely to reflect the indirect mechanical coupling of stimulus and bundle deflection, which attenuates the deflection caused by shorter pressure steps. Nonetheless, our measurements of the glutamatergic output provide a more physiological measure of the way in which hair cells within a neuromast respond to changes in water currents, for instance.

Experimental Procedures

Fish husbandry

Adult zebrafish (Danio rerio) were maintained in fish water at 28.5°C under a 14:10 hour light:dark cycle under standard conditions (Brand et al 2002). Fish were bred naturally and fertilized eggs were collected, washed with distilled water and transferred into 50 ml of E2 medium (concentrations in mM: 0.05 Na2HPO4, 1 MgSO4 7H2O, 0.15 KH2PO4, 0.5 KCl, 15 NaCl, 1 CaCl2, 0.7 NaHCO3, pH7-7.5). At 24 hours post fertilization (hpf) 1-phenyl2-thiourea (pTU) was added to yield a final concentration of 0.2 mM to inhibit pigment formation. All procedures were in accordance with the UK Animal Act 1986 and were approved by the Home Office and the University of Sussex Ethical Review Committee.

Fish Lines

The Tg[HuC::GCaMP6f] line (kindly provided by Isaac Bianco) expresses GCaMP6f pan-neuronally (Park et al 2000), including in afferent neurons of the lateral line, but not in hair cells. The Tg[Sill2, UAS::iGluSnFR] line expresses iGluSnFR (Marvin et al 2013) exclusively in afferent neurons of the lateral line system (Pujol-Martí et al 2012). It was generated by injecting the Sill2 construct, containing the Sill enhancer driving expression of the Gal4-VP16 element (kindly provided by Hernan Lopez-Schier), into single-cell stage embryos expressing 10xUAS::iGluSnFR. Larvae were sorted for expression of iGluSnFR and reared to adulthood to identify fish with germ-line

transmission (founders). To generate the Tg[Sill2, UAS::iGluSnFR, Rib::Rib-mCherry], the Sill construct was injected into the embryos derived from an outcross between 10xUAS::iGluSnFR and Rib::Rib-mCherry (Odermatt et al 2012) adults and screened for the expression of iGluSnFR and mCherry. This line allowed us to image the iGluSnFR signal in afferent neurons while visualising synaptic ribbons in hair cells. All fish were maintained in a nacre mutant background (Lister et al 1999).

Mounting and Cupula Staining

All experiments were performed at room temperature (20°C – 25°C) using larvae at 7-10 days post fertilization (dpf). At 4 dpf, embryos were screened for the strongest expression of the appropriate transgene. Larvae were anaesthetized by immersion in 0.016% tricaine (MS-222), diluted in E2. They were then placed side-down into a 'fish-shaped' pit carved into a thin (~1 mm) layer of PDMS (Sylgard184, Dow Crowning) on a coverslip. Mechanical stability was provided by a 'harp' (Warner Instruments) placed on top of the larva. The pressure applied by the nylon strings was adjusted to allow normal blood flow while maintaining enough pressure to hold down the larvae. The larva was then paralyzed by injection of 0.25 mM alpha-Bungarotoxin (αBTX; Tocris) into the heart. To avoid damaging the cupula, special care was taken not to touch the upward-facing side of the fish during the mounting procedure. The cupula was then stained by incubating the fish in a 1:500 dilution of 1 mg/ml WGA AlexaFluor-594 or WGA AlexaFluor-350 (Life Technologies) for 2 minutes followed by thorough washing with E2. When counter-staining hair cells with FM4-64 (Synaptored, Biotium) larvae were incubated in a 1 μM solution for 1 minute and then washed with E2.

Mechanical Stimulation

Pressure steps were applied to a neuromast through a glass pipette attached to a high speed pressure clamp (HSPC-1, APA scientific) (Trapani et al 2009). The output pressure was controlled and recorded using mafPC software (courtesy of M. A. Xu-Friedman) running in IgorPro (WaveMetrics) and synchronized to image acquisition. The micropipette (GC150T-10, Harvard Apparatus) was pulled to a diameter of ~30 μm and the tip bent through ~30° using a micro forge (Narishige) to allow liquid flow parallel to the body of the larva. The tip was positioned ~20 μm above the body, ~100 μm from the neuromast. This study was confined to neuromasts of the posterior lateral line with an 'anterior-posterior' axis of sensitivity. The direction of the pipette (pointing

towards the tail or towards the head) was changed during the course of some experiments but did not affect measurements.

In Vivo Two-Photon Imaging

Fish were imaged on a custom built two-photon microscope driven by a mode-locked Titanium-sapphire laser (Chameleon 2, Coherent) tuned to 915 nm. Excitation was delivered through a 40x water immersion objective (Olympus, 40x LUMIPlanF, NA: 0.8) and emitted photons were collected both through this objective and an oil condenser (NA 1.4, Olympus) below the sample. Green and red fluorescence was separated by a 760dcxru dichroic and filtered through 525/70 nm and 620/60 emission filters before being focused onto GaAsP photodetectors (Hamamatsu). The microscope was controlled by ScanImage v3.8 (Vidrio Technologies) and image acquisition was synchronized with the stimulus. Movies were acquired at 10-50 Hz.

Measuring Deflections of the Cupula

The angular deflection of the stained cupula was assessed by measuring its translational displacement in multiphoton images in planes at different z distances from the surface of the hair cells. These measurements were made at a variety of stimulus pressures and repeated in 3-4 planes 5 μm increments. The central position of the cupula within each frame was extracted by first thresholding the image and then fitting an ellipse to estimate the center of mass. Next, the translational deflections induced by the applied pressure steps in each plane were calculated: these were consistent with the proximal regions of the cupula ($z < 15$-20 μm) behaving as a pivoting beam (McHenry & van Netten 2007). In this way, a calibration of the angular deflection of the cupula for each stimulus pressure was obtained for each experiment (Fig. 2.4). This calibration was repeated if, for instance, the pipette was moved.

Image Analysis

Images were analyzed in Igor Pro (Wavemetrics) using custom-written software including the SARFIA toolbox (Dorostkar et al 2010). Movies containing small drifts in the x-y dimension were registered but movies with large drifts, including potential z-motions, were discarded. Regions of Interest (ROIs) were determined using an algorithm that began by identifying pixels with both large signals and high degrees of

temporal correlation. Pixels surrounding the ROI 'seeds' were added to the ROI until the correlation value fell below a threshold. Background fluorescence was then subtracted and baseline fluorescence (F_o) was defined as the average fluorescence preceding the first stimulation interval. The change in fluorescence relative to baseline ($\Delta F/F_o$) was calculated and used for further analysis.

The adaptation index (AI) was calculated as:

$$AI = (R_{peak} - R_{sustained}) / R_{peak} \quad (1)$$

Where R_{peak} is the instantaneous peak response after stimulus onset, $R_{sustained}$ is the average response during the last 100 ms of stimulus presentation. Therefore, an AI close to 0 indicates no adaptation, an AI close to 1 indicates complete adaptation and a negative AI indicates sensitization.

The relative set point (SPr) was calculated as:

$$SPr = 1 - abs\{(R_{min} - R_{max})\} \quad (2)$$

Where R_{max} is the saturating response in the preferred direction of deflection and R_{min} is the maximum change in the opposite direction.

Chapter 4

Selective Suppression of Re-Afferent Information in the Lateral Line of Zebrafish Larvae

Abstract

Active locomotion can activate the same sensory channels as external events. One strategy to deal with this self-induced activation is to temporarily supress the activated sensory channel whenever the motor system is active. An example for this is the lateral line system in zebrafish. It senses small pressure changes in the fish's environment, which could be due to external events or self-induced, by locomotion. The lateral line consists of mechanosensory hair cells that are organized in small clusters, called neuromasts, each of which is innervated by at least two afferent neurons, which transmit information centrally and efferent neurons, which transmit information from the hindbrain by releasing acetylcholine. We are investigating how this system works in vivo by using two-photon microscopy in larval zebrafish expressing genetically encoded indicators of calcium (GCaMP6) and glutamate (iGluSnFR) in the three main elements of the neuromast: hair cells, afferents and efferents. We simultaneously perform extracellular recordings of the motor nerve to monitor the fictive swimming behavior of the paralyzed larvae and visual stimulation to induce it. Using this preparation, we could confirm that the activity of the efferent synapses in the neuromast is tightly correlated with fictive swimming. We find that efferent activity reduces the saturating signal from the neuromast by ~50%. This reduction could be observed at the level of the afferent output in the hindbrain as well as just postsynaptic to the hair cell, in the neuromast. This suggests that the effect of locomotion is at least partly present at the primary receptor. Initial experiments furthermore suggest that the effect is specific to afferent neurons that encode tail-wards deflections of the neuromast, however more data needs to be collected.

Introduction

Organisms have to differentiate sensory information caused by changes in their environment (ex-afferent) from sensory information that is caused by their own behavior within the environment (re-afferent). The same sensory stimulus, such as backwards-drifting visual surrounding for example could be the result of active forward locomotion or passive displacement in the same direction. This problem was first described by von Holst & Mittelstaedt, who proposed the idea that a copy of the motor command (efference copy, green arrow in Fig. 4.1) would be transmitted to the sensory apparatus to account for the (predictable) self-induced sensory information (re-afferent, red arrow in Fig. 4.1) (von Holst & Mittelstaedt 1950). Although initially

formulated more than half a century ago, the exact neuronal mechanisms underlying this process remain poorly understood and are still being investigated in both vertebrates and invertebrates (Chagnaud et al 2015; Kim et al 2015; Kim et al 2017). A special case, in which the distinction between ex-afferent and re-afferent sensory stimuli is fundamental, are behaviors that lead to re-afferent sensory signals which, by themselves, would trigger the behavior. Examples for this include reflexes and visual stabilisation behaviors such as the optomotor-responses (OMR) and the optokinetic response (OKR) (Brockerhoff et al 1995; Roeser & Baier 2003; Kim et al 2015; Orger 2016; Kim et al 2017).

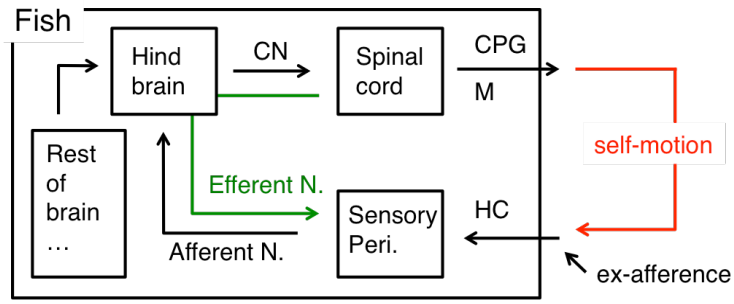

Figure 4.1. Schematic of von Holst and MIttelstaedt's Re-Afference Principle
Mechanosensitive hair cells (HC) on the surface of fish detect small hydrodynamic stimuli in its vicinity, indicating, for example an approaching predator. The information about this ex-afferent stimulus is sent via afferent neurons from the sensory periphery to the hindbrain, where it is able to directly activate command neurons (CN) that initiate an appropriate motor program (for example an escape response) by activating central pattern generators (CPGs) and motor neurons (M) in the spinal cord. During swimming, the displacement of the fish relative to its environment generates currents across the fish's body surface, which have the potential to trigger the same circuit described above. To prevent this from happening, von Holst and Mittelstaedt proposed that a copy of the motor signal (efference copy, green) is sent to the sensory periphery to account for this self-induced and predictable (re-afferent, red) component of the sensory information. Any locomotion initiated in the rest of the brain would lead to the same scenario.

A non-visual modality that is also facing this problem is the lateral line system of amphibians and fish. This sensory organ senses small pressure changes and currents in the animal's environment (ex-afferent stimuli) and is involved in a number of behaviors, such as obstacle and prey avoidance and rheotaxis (McHenry et al 2009; Stewart et al 2013; Oteiza et al 2017). Some stimuli acting on the lateral line directly trigger a locomotor reflex, such as the mechanically triggered startle or escape responses (Burgess & Granato 2007; Haehnel-Taguchi et al 2014; Troconis et al 2017). Whenever the animal is swimming, however, it produces currents in respect to its own body that will activate the lateral line system (re-afferent stimuli), and potentially,

again, lead to a locomotor behavior (Palmer et al 2005; Ayali et al 2009) (full circle in Fig. 4.1). How exactly this sensory system is prevented from triggering a reflex every time the larva voluntarily starts swimming is not understood.

The lateral line system in zebrafish larvae consists of clusters of about 20 mechanosensory hair cells (HC) called neuromasts (NM) that are distributed across the surface of the fish. Every HC is functionally polarized, so that deflection of its hair bundle towards the kinocilium leads to depolarization, and away from the kinocilium to hyperpolarization of the receptor potential. Within a NM of the posterior later line, half of the HCs are sensitive to posterior deflections (towards the tail) and the other half to anterior deflections (towards the head). At least two lateral line afferent neurons innervate each NM and selectively synapse onto HCs of one directional sensitivity, thereby maintaining the functional polarization (Nagiel et al 2008; Faucherre et al 2009). Centrally, afferent neurons of the lateral line (and inner ear) project to the medial octavolateralis nucleus (MON) in the hindbrain, where a subset directly innervates the Mauthner neurons that govern an escape reflex (Pujol-Martí et al 2012).

The transmission of mechanical information in the auditory and vestibular system is extensively modulated by descending efferent neurons that act on hair cells as well as afferent neurons. These efferents predominantly release dopamine and acetylcholine and can have both inhibitory and excitatory effects (reviewed by: Ryugo et al 2011; Mathews et al 2017). NM in the larval zebrafish are also innervated by efferent neurons that originate from three different nuclei in the hindbrain and diencephalon (Metcalfe et al 1985; Bricaud et al 2001). Diencephalic efferents have recently been shown to release dopamine in a paracrine fashion, leading to an increase of HC neurotransmission (Toro et al 2015). There is evidence from other aquatic species that cholinergic efferents indeed transmit a copy of the motor command to the NM, which leads to a decrease in afferent firing rate, probably via the activation of α9/α10 nicotinic receptors in hair cells (Russell 1968; Russell 1971; Flock & Russell 1973; Flock & Russell 1976b; Verbitsky et al 2000; Baker et al 2004). However, little is known about the role of efferent neurons in zebrafish larvae, despite its increasing importance as a model organism in systems neuroscience.

The lateral line system of larval zebrafish has several advantages for addressing the question of how sensory systems deal with self-induced, re-afferent stimuli. (1) The lateral line receives strong re-afferent stimulation during locomotor behavior (Ayali et al 2009). (2) It is accessible for controllable mechanical stimulation. (3) Fictive swimming can be induced visually and monitored. (4) The input (NM) as well as the

output (MON) of the afferent neuron are optically accessible with two-photon microscopy.

We show that mechanical information from the posterior lateral line organ is modulated by fictive locomotion, that this modulation is inhibitory and most likely due to the activity of efferent neurons that transmit a precise copy of the motor commands directly to the NMs. Notably, the inhibitory effect of locomotion appears to be restricted to afferent neurons sensitive to posterior deflections of the hair bundle, putatively, the afferent that would be most strongly stimulated during swimming, while leaving sensitivity of the other afferent unaffected. These data highlight the importance of understanding (mechano-) sensation as an actively modulated and embedded process.

Results

Using the Optomotor Response to Induce Fictive Swimming while Observing Glutamate Release in the MON

To study the effects of efferent modulation of the representation of mechanical information in the larval zebrafish, we took advantage of its genetic tractability and transparency. The output of the lateral line system in larval zebrafish was previously characterized by measuring the spiking activity of the primary afferent neurons (Obholzer et al 2008; Trapani & Nicolson 2010; Liao 2010; Liao & Haehnel 2012). These studies generally ignored the potential influence of efferent activity and locomotion (but see (Toro et al 2015)), even though effects of efferent neurons on the encoding of mechanical information have been demonstrated in a number of aquatic species, mostly in isolated or semi-isolated preparations (Russell 1968; Flock & Russell 1973; Flock & Russell 1976a).

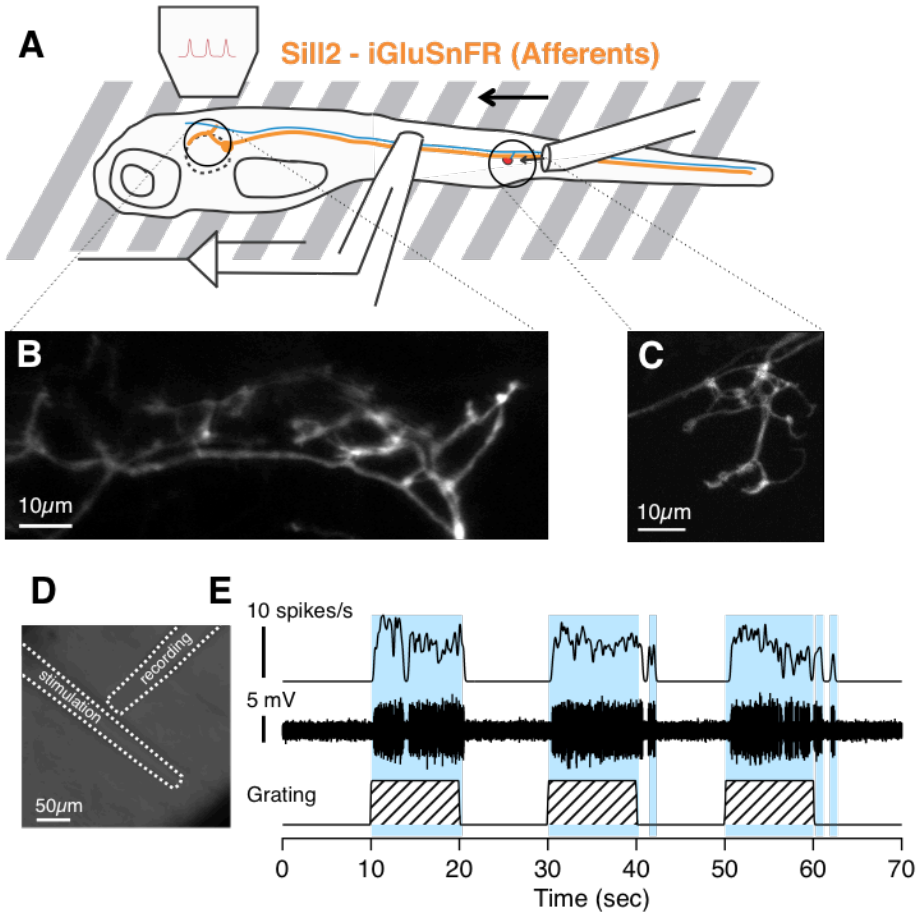

Figure 4.2. A Preparation to Investigate the Modulation of Lateral Line Afferent Neurons during Fictive Swimming
(**A**) A diagram of the experimental set-up: The glutamate release of the afferent neurons in the hindbrain was monitored with a two-photon microscope while mechanically stimulating a NM, measuring the motor neuron activity and inducing fictive swimming with a grating (moving in the direction of the arrow). The three main components of the lateral line system are indicated. Afferent neurons (yellow) innervate neuromasts (red circles, only one depicted) on the trunk of the fish. Efferent neurons (blue) also innervate the posterior lateral line. (**B**, **C**) Average projections of the MON (B) and a NM (C) of a larva expressing the glutamate sensor iGluSnFR under transcriptional control of the SILL promoter (Tg[Sill::Gal4, UAS::iGluSnFR]), leading to expression exclusively in lateral line afferent neurons. (**D**) shows the pipette used for stimulating the NM and the pipette used to record the motor neuron activity. (**E**) From the motor nerve activity (middle trace) we could infer the fictive swimming behavior. The top trace depicts the rolling average spike rate of the motor neuron (100 ms time bin). Fictive swimming could be induced by projecting a moving grating (bottom row) onto the larva.

We used 6-10 dpf zebrafish larvae, which transgenically expressed the glutamate sensor iGluSnFR exclusively in lateral line afferent neurons (Tg[Sill2, UAS::iGluSnFR], (Pujol-Martí & López-Schier 2013; Marvin et al 2013)) (Fig. 4.2 A - C), which allowed us to monitor the synaptic activity in the MON, constituting the output of the lateral line system. To stimulate the neuromast, we applied positive and negative pressure steps through a narrow pipette (Fig. 4.2 A and D and see material and methods) that was oriented along the anterior-posterior axis of the larvae, the direction of neuromast

sensitivity, and also putative direction of stimulation during swimming. Simultaneously, we performed extracellular recordings of the motor nerve activity to monitor the fictive locomotor activity of the paralyzed larvae (Masino & Fetcho 2005). The OMR is a visually induced stabilization behavior that compensates for perceived backward displacement. By applying a moving grating in the tail to head direction, we took advantage of this innate behavior to induce fictive swimming (Fig. 4.2 E).

Together, this provides optical access to the output of the lateral line system and electrophysiological access to the (fictive) motor behavior. At the same time we can directly control the mechanical stimulus at the NM while inducing fictive swimming with a visual stimulus.

Some Synapses in the MON are Suppressed by Fictive Locomotion

To what extent do efferent signals induced by locomotion modulate the encoding of mechanical information in the lateral line system of the larval zebrafish? To address this we stimulated a NM of the posterior lateral line with six blocks of positive and negative pressure steps that deflected the cupula towards the tail and towards the head, respectively. Every second block of mechanical stimulation (10-20 s, 30-40 s and 50-60 s, Fig. 4.3 C & E) was superimposed with a drifting grating to induce fictive locomotion. Simultaneously, we measured the glutamate release of individual synapses in the MON. The responses of two representative synapses from the posterior part of the MON are compared in Figure 4.3 A-F (the blue and red-shaded areas represent mechanical stimulation periods that did or did not coincide with fictive locomotion, respectively). Both synapses showed fluctuations in baseline glutamate release but consistently responded to posterior deflections of the cupula, although with a relatively high degree of variability in response amplitude. While the synapse in Fig. 4.3 C was unaffected by simultaneous motor nerve activity, the synapse in Fig. 4.3 E was strongly suppressed by fictive swimming. In this synapse the average magnitude of glutamate release was reduced by 42% ($P<0.005$, Mann-Whitney U-test). A synapse was labeled as suppressed when the amplitude of the mechanically induced response was significantly different (using a Mann-Whitney U-test) in the presence and absence of fictive swimming. In the three out of eight synapses in which this was the case, the average suppressive effect was 47%, but ranged from 27% to 58% (Fig. 4.3 G). We cannot tell if the suppressive effect in the remaining five synapses was too small to be detected or simply not present.

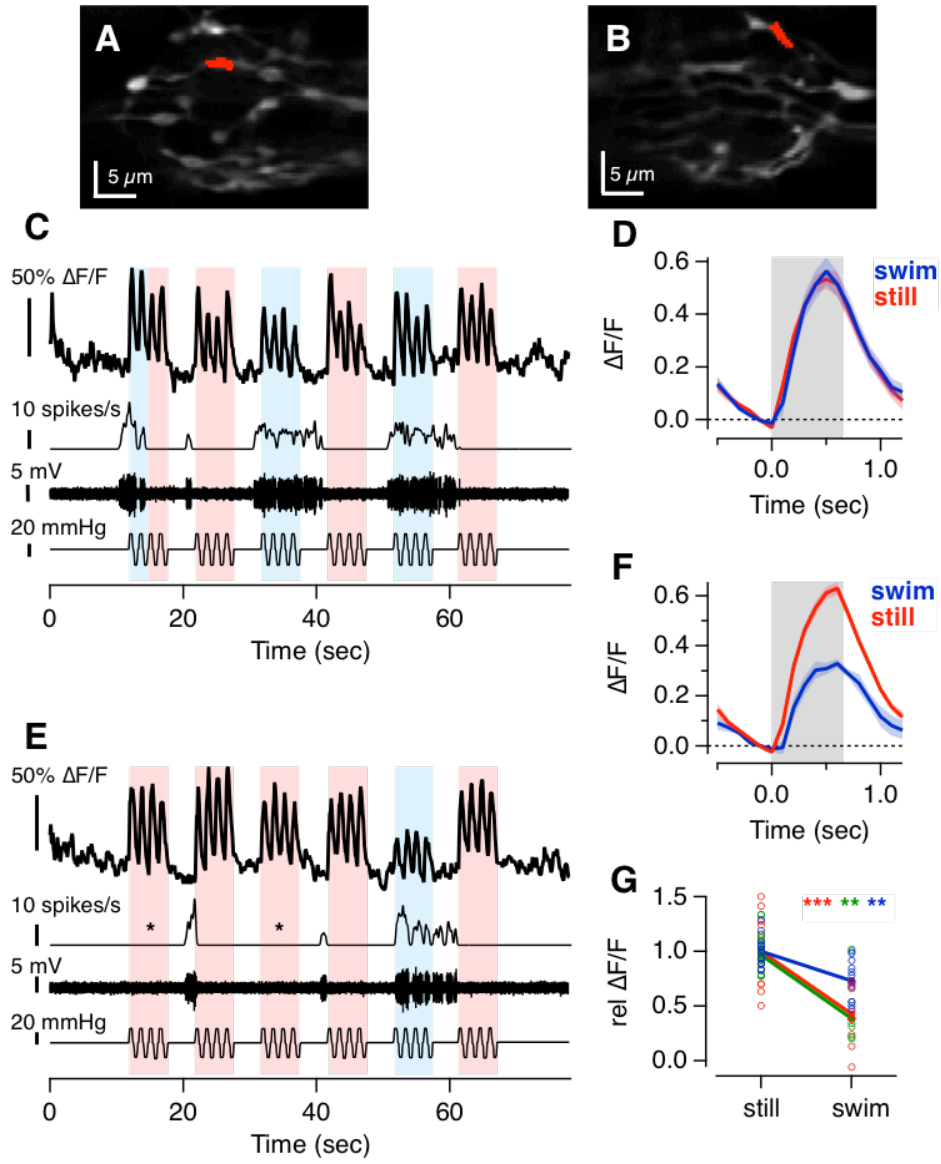

Figure 4.3. The Mechanically Induced Output of a Subset of Lateral Line Afferent Neurons is Suppressed during Fictive Swimming

(**A** and **B**) Average projections of synapses in the posterior part of the MON. Highlighted in (A) is the synapse whose response is depicted in (C) and highlighted in (B) is the synapse whose response is depicted in (E). (**C** and **E**) Two representative examples of afferent synapses in the MON. The bottom trace represents the mechanical stimulation of the NM (positive pressure deflects the cupula towards the tail and negative pressure towards the head, respectively). The middle two traces depict the raw motor signal and average spike rate, respectively, and the top trace shows the synaptic activity of the synapse. Blue-shaded areas indicate periods in which mechanical stimulation coincided with fictive swimming and red-shaded areas indicate periods in which it did not. The first third and fifth mechanical stimulation period always overlapped with the presentation of a moving grating. (**C**) The activity of this synapse was not affected by fictive locomotion. This is quantified in (**D**), which depicts the mean responses of this synapse in the presence and absence of fictive locomotion. (**E**) Example of a synapse whose response to mechanical stimulation was suppressed when it coincided with fictive locomotion. Asterisks indicate periods in which visual stimulation failed to induce locomotion. (**F**) The peak amplitude was reduced by 42% during fictive locomotion ($P<0.005$, Mann-Whitney U-test). (**G**) The normalized mechanically induced glutamate release of three hindbrain synapses in a 'fictive still' (left) and 'fictive swimming' (right) condition, respectively. Open circles represent the response to individual stimulations and filled circles their average (*** $P<0.0001$, ** $P<0.001$, Mann-Whitney U-test). (Shaded areas in (D) and (F) represent the SEM).

Interestingly, the baseline glutamate release of afferent neurons in the absence of visual stimulation was also suppressed during fictive swimming (Fig. 4.4 B). This baseline signal corresponds to a spontaneous firing rate between 10 and 50 Hz (Trapani & Nicolson 2011; Levi et al 2014; Lv et al 2016) and although relative noisy was consistently lower during motor neuron activity. The temporal profile of the suppression closely mimicked that of the motor neuron firing rate, with every swimming episode leading to a transient decrease in glutamate release (Fig. 4.4 C).

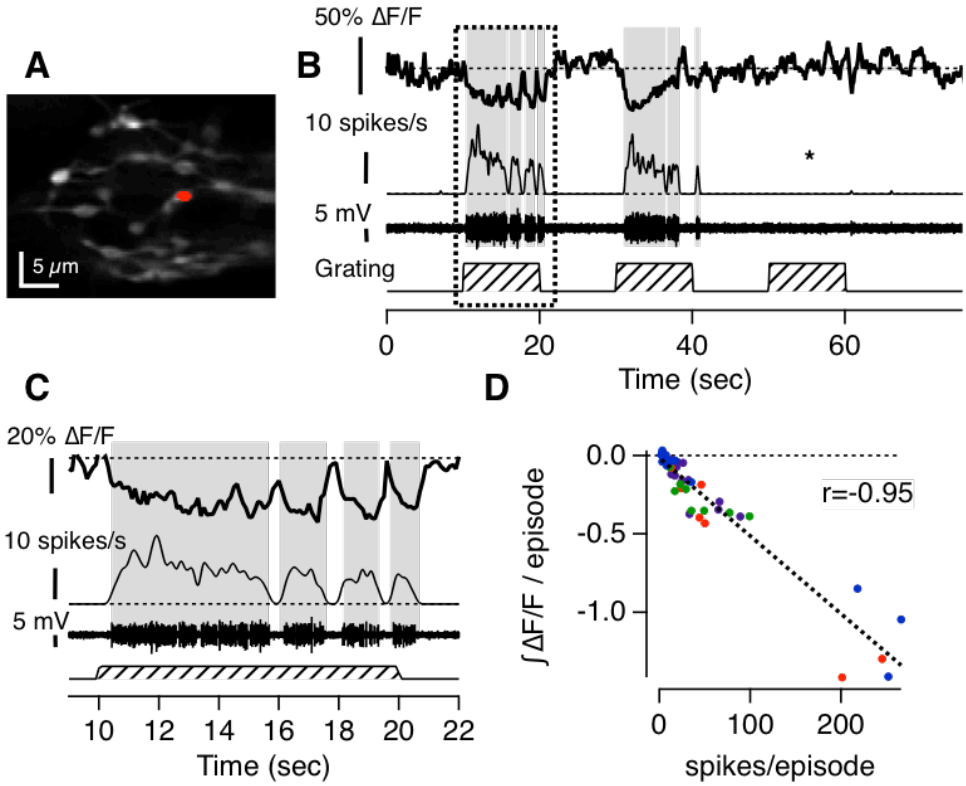

Figure 4.4. Spontaneous Activity of Afferent Neurons is Suppressed during Fictive Swimming
(**A**) An average projection of the posterior arm of the MON, highlighting the synapse whose response is depicted in (B). (**B**) An example of a synapse, whose baseline glutamate release, in the absence of a mechanical stimulus, was suppressed by fictive locomotion (grey-shaded area). The absence of suppression during the third presentation of a visual grating (*****) indicated that visual information itself had no immediate effect on the encoding of mechanical information. (**C**) Magnification of the dashed box in (B) reveals that each individual swim-burst leads to a transient suppression of the glutamate release. (**D**) The number of spikes in the motor neuron during a swim-bout (episode) and the integral of the suppressive effect in the hindbrain synapse is tightly correlated (r=-0.95, n=49 bouts from 4 synapses).

Suppression was quantified as the negative integral of the iGluSnFR signal from baseline during a swim episode, which linearly increased with the number of spikes fired by the motor neuron in each episode (Fig. 4.4 D). This strong correlation

suggests that the source of the inhibition is indeed the motor system and therefore constitutes an efference copy or corollary discharge signal. Consistently, the visual stimulation by itself, without inducing a motor response did not have any noticeable, direct effects on the mechanosensory output in the MON. This held true in the presence and in the absence of mechanical stimulation (asterisks in Fig. 4.3 E and Fig. 4.4 B) and hence rules out the possibility of visually induced inhibition of mechanical information (Tricas & Highstein 1990; Mu et al 2012) while strengthening the notion of a feed-forward efference copy signal.

Taken together, the majority of synapses in the MON was not responding to mechanical stimulation, most likely because they belonged to afferent neurons that were not mechanically stimulated. They were also not suppressed during fictive locomotion. However, in a subset of synapses fictive locomotion resulted in a profound decrease of both spontaneous and mechanically induced glutamate release at the level of the MON, consistent with the presence of an efference copy signal. Unfortunately, the precise number of synapses in the MON could not be counted as we were relying on stimulus or locomotion triggered responses to identify individual synapses in the absence of a synaptic marker.

Efferent Synapses Convey a Quantitative Prediction of Locomotor Activity

Where this integration of sensory and motor signals takes place remains unanswered. The MON itself is a good candidate, as it belongs to the so-called cerebellum-like structures, which share a common cytoarchitecture and are involved in the adaptive filtering of putatively self-generated sensory inputs (for example in weakly electric fish) (reviewed by: Bell et al 2008). More likely, the inhibitory effect occurs directly in the NMs, where efferent neurons terminate (Metcalfe et al 1985) and motor related activity has been shown to occur in other species (Russell 1971), but not zebrafish.

We sought to identify the source of the efferent inhibition of lateral line afferent neurons. Because we did not have specific genetic access to these neurons (but see: Higashijima et al 2000) we took advantage of the pan-neuronal *HuC* (or *elevl3*) promoter (Park et al 2000) to drive expression of the calcium indicator GCaMP6f (Tg[HuC::GCaMP6f]) in all neurons, including lateral line afferents and efferents (Faucherre et al 2010) (but fortunately not hair cells, Fig. 4.5 A and B).

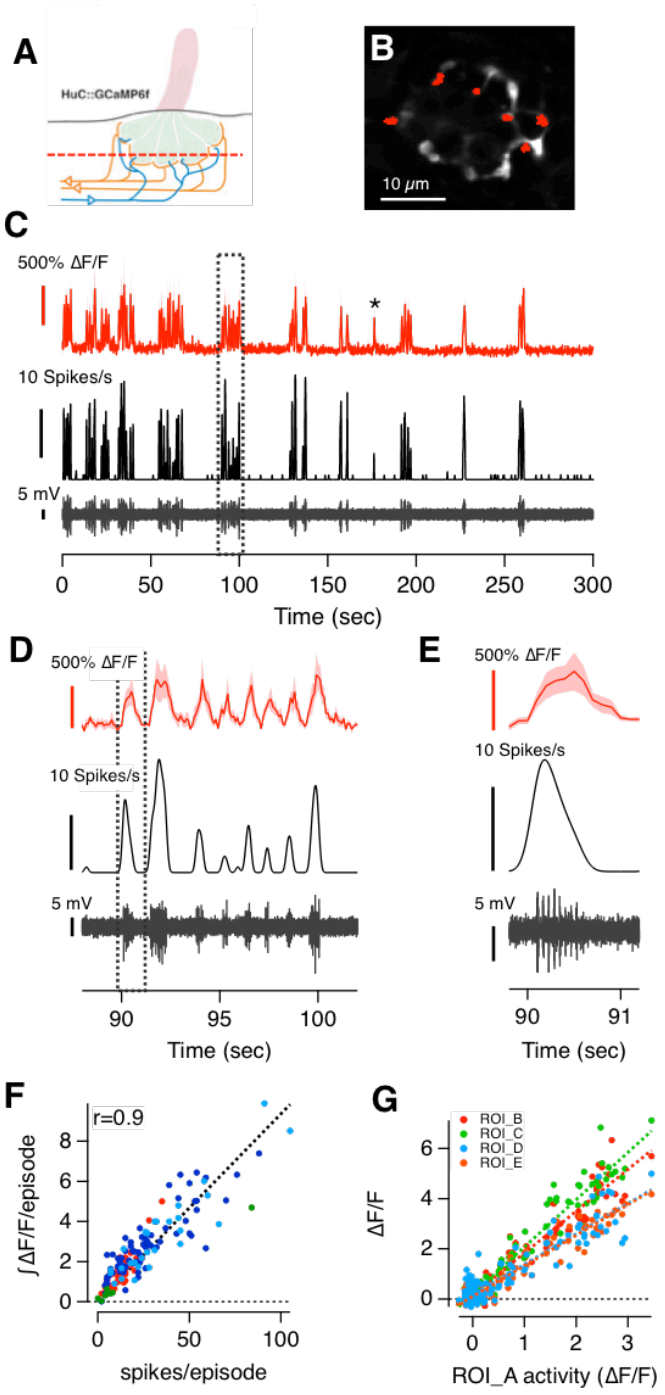

Figure 4.5. Activity of Efferent Synapses in the Neuromast strongly Correlates with Motor Neuron Activity

(**A**) Schematic of a NM, highlighting the afferent and efferent synapses that are labelled by the HuC::GCaMP6f line. (**B**) Average projection of a NM in a HuC::GCaMP6f larva (cross section roughly corresponds to the red-dashed line in (A). (**C**) Top trace depicts the activity of the synapses in (B) over a five-minute period without visual or mechanical stimulation. The bottom traces depict the raw motor activity and the spike rate, respectively. The asterisk indicates a signal in the NM-synapses that correlates to only six spikes in the motor nerve. (**D** and **E**) depict magnified views of the dashed areas in C and D, respectively, and show that the correlation holds up to the level of individual swim-bouts or episodes (red-shaded area represents the SEM). →

Morphologically, efferent synapses can be distinguished from afferent varicosities because they appear smaller and rounder (Nagiel et al 2008). Indeed, in 70% of the 21 responding NM we observed small 'blob-like' synapses (Fig. 4.5 B) that fired spontaneously in a burst-like fashion over time periods of several minutes (Fig. 4.5 C top trace). Furthermore, the activity was present in the absence of mechanical stimulation, suggesting it occurred in efferent fibers, transmitting non-sensory information. Simultaneous motor nerve recordings revealed that activity in efferent fibers is strongly correlated with the spike rate of the motor nerve (Fig. 4.5 C). This correlation persisted to the level of individual swim episodes (Fig. 4.5 D-E). Analogous to the motor related inhibitory effect in the MON (Fig. 4.4 D), the integral of the synaptic calcium-influx in efferent synapses in the NM increased linearly with the number of spikes that the motor neuron fired in one burst (Fig. 4.5 F). As few as six spikes in the motor neuron resulted in a strong fluorescent signal in the NM (asterisk in Fig. 4.5 C), suggesting that the efference copy signal is indeed very reliable. We furthermore observed that whenever present, there were multiple of these synapses (on average 5 ± 0.7 in a single section through a NM) and their activity was almost perfectly synchronous (Fig. 4.5 G).

In summary, we observed synapses in lateral line NM which matched previous morphological descriptions of efferent synapses and whose activity was highly correlated with the firing rate of ipsilateral motor neurons in a fictive swimming preparation. The strong correlation suggests that they transmit an extremely reliable efference copy signal. It is thus very likely that the motor related suppression of afferent neurons in the MON is at least partly a result of these synapses acting on the first sensory synapse of the lateral line in zebrafish.

(**F**) The number of spikes/episode and the integral of the fluorescent signal during that episode were strongly correlated (r=0.9, n=155 episodes from 4 NMs). (**G**) Plotting the activity of four synapses (B-E) as a function of the activity of a fifth synapse A (all from within the same neuromast, not the one depicted in (B)) reveals a linear relationship (R>0.9) between them, indicating a high degree of synchronicity (activity was down-sampled for illustration purposes).

In a Subset of NM the Postsynaptic Calcium Influx in Afferent Neurons is Suppressed by Efferent Activity

Besides the presence of an exact efference copy signal in NMs, it has recently been shown that hair cells in the lateral line express the α9-nicotinic acetylcholine receptor (nAChR) subunit (Erickson & Nicolson 2015); suggesting that also in larval zebrafish, acetylcholine (ACh) released from efferents may directly affect hair cells. To test this idea functionally, we therefore asked whether the inhibitory effect that we observed in the MON was already present at the level of the NM. Using the HuC::GCaMP6f line, we could observe mechanically induced calcium influx in the postsynaptic varicosities of afferent neurons (Fig. 4.6 A and B), identified by their sensitivity to posterior and anterior deflections of the cupula, respectively (Fig. 4.6 C). This allowed us to ask whether or not calcium influx directly postsynaptic to hair cells is affected by efferent activity.

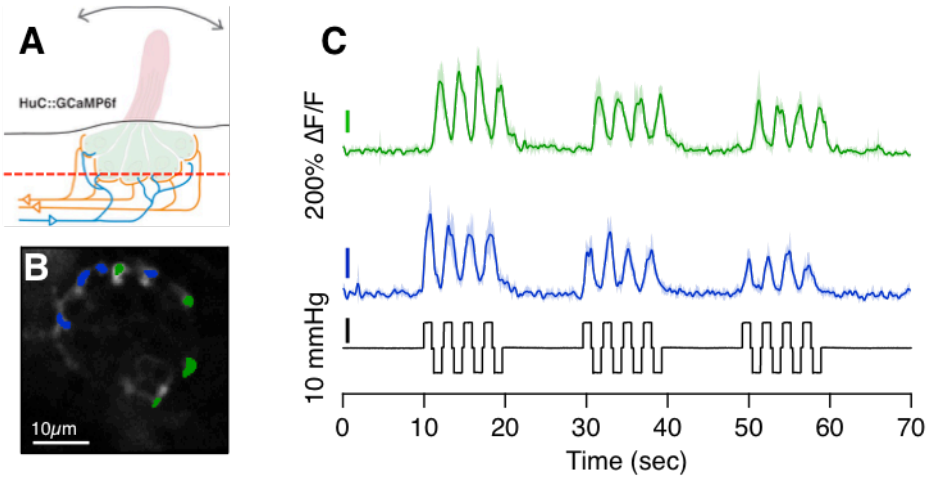

Figure 4.6. Mechanically Induced Calcium Signals in the Postsynaptic Varicosities of Afferent Neurons
(**A**) The HuC::GCamP6f line also faithfully reported the mechanically induced calcium influx in the varicosities of the afferent neurons, postsynaptic to hair cells. (**B**) An average projection of a NM, highlighting varicosities belonging to two afferents with opposing directional sensitivity. (**C**) The signals from the respective ROIs in (B). Blue ROIs are sensitive to posterior and green ROIs to anterior deflections of the cupula, respectively.

Of the 21 afferent neurons that responded to mechanical stimulation and could be imaged simultaneously with spontaneously occurring efferent activity, three (14%) were significantly suppressed whenever the efferent neuron was firing. Figure 4.7 B is a cross-section of a NM that was innervated by (at least) two afferent neurons sensitive to posterior (red) and anterior (green) deflections of the cupula as well as an

efferent neuron (blue). The average response of these three neurons is depicted in Fig. 4.7 C. The same stimulus, consisting of positive and negative pressure steps of increasing magnitude (bottom row), was repeated three times. The characteristic bursting activity of the efferent neuron occurred spontaneously, and independent of mechanical stimulation.

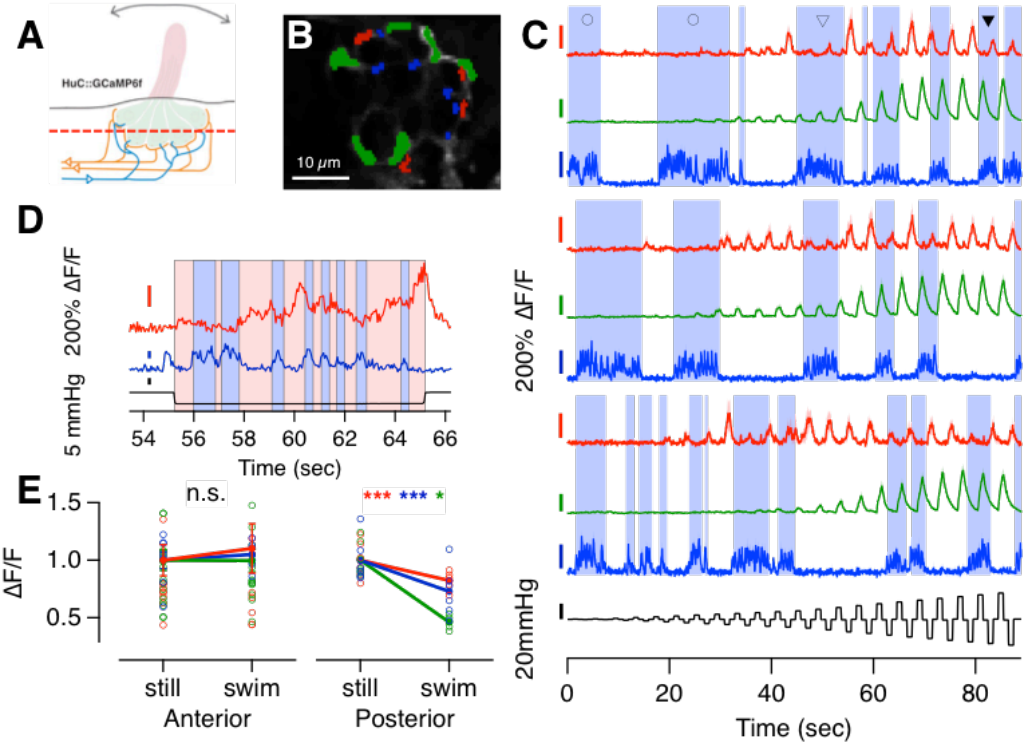

Figure 4.7. Calcium Influx in a Subset of Peripheral Afferent Dendrites is Suppressed by Efferent Activity

(**A**) In 3 out of 21 (14%) afferent neurons we observed a reduction of mechanically induced, post-synaptic calcium-influx in the afferent neuron that correlated with efferent activity. (**B**) Three classes of synapses: efferent synapses (blue), and afferent synapses sensitive to anterior (green), and posterior (red) deflections of the cupula were imaged simultaneously. (**C**) Three repeats of the same stimulus in the same NM (color code as in B). Periods of efferent activity (fictive swimming behavior) are shaded in blue. Responses of the anterior-sensitive afferent neuron (green) are unaffected by the efferent activity, whereas responses of the posterior-sensitive afferent (red) are suppressed during efferent activity. We quantified the suppressive effect by averaging the last five (saturating) responses and compared the ones that coincided with efferent activity with the ones that did not. (**D**) An example of a 10 second posterior deflection period, during which the efferent neuron (blue) fired spontaneously. Responses of the afferent neurons (red) increased only in the absence (red-shaded area) and leveled off in the presence (blue-shaded area) of efferent activity. (**E**) Summary of the data from the three NM in which suppression was observed. In all cases, the anterior responding afferents were not significantly affected by efferent activity (normalized to 'still'), whereas the posterior responding afferents in the same NM were significantly suppressed. (Different colors indicate data from the three different NMs, open circles are individual responses and full circles are averages of each afferent. Error bars represent the SEM, *** $P<0.0001$, * $P<0.01$, Mann-Whitney U-test.)

Mechanically induced responses by the posterior-sensitive afferent neuron (red) were markedly attenuated when the stimulus coincided with activity of the efferent neuron (blue-shaded area). While responses to weak pressure steps were almost completely suppressed (open arrow head in Fig. 4.7 C), responses to stronger pressure steps were only partially attenuated (filled arrow head in Fig. 4.7 C). In contrast, the anterior-sensitive afferent neuron (green) followed the stimulus with increasing calcium responses – unaffected by the presence or absence of efferent activity. We quantified the suppressive effect by comparing the average peak amplitude of the last five saturating pressure steps in the presence or absence of efferent activity, and found an average decrease by 33% (n=3) (Fig. 4.7 E, right panel) (*** $P<0.0001$, * $P<0.01$, Mann-Whitney U-test).

An unexpected but striking observation that is worth mentioning (despite the small n-number), is that every synapse, in the MON as well as the NM, that was affected by fictive swimming, was sensitive to cupula deflections in the posterior direction. Presumably, it might be these afferent neurons that would be stimulated the strongest during an actual swimming bout (see discussion). Although previous studies have suggested that efferent innervation was not selective for a specific direction of deflection (Russell 1968; Faucherre et al 2009), these studies have not distinguished between different types of efferent neurons (for example dopaminergic ones, cf. Toro et al 2015).

The suppressive effect in the NM appeared to be rectified in the sense that afferent baseline activity was not decreased by efferent activity (open circles in Fig. 4.7 C). This is in contrast to the suppression observed in the MON, where spontaneous glutamate release was inhibited by individual (fictive) swim episodes. The most likely explanation for this discrepancy is the non-linearity of the calcium reporter GCaMP6f, which prevents it from being able to detect small changes in calcium concentration at low baseline concentrations. The temporal component of the inhibitory effect could be revealed during prolonged stimulus durations, however (Fig. 4.7 D). The postsynaptic calcium concentration in the afferent neuron increased in the absence and leveled off (or decreased) in the presence of efferent activity (red and blue-shaded area, respectively).

Taken together, in a small fraction of afferent neurons, the presence of an efference copy signal in the NM resulted in a strong attenuation of mechanically induced calcium influx in postsynaptic varicosities. This effect was exclusively observed in afferent neurons sensitive to cupula deflections in the posterior direction

(despite the small n-number). These results confirm that in zebrafish larvae, as in other aquatic species (Flock & Russell 1973; Chagnaud et al 2015), motor related efferent inhibition indeed takes place at the first sensory synapse. The proposed mechanism of inhibition is via α9/α10 nAChR and calcium-activated potassium (SK2) channels, which lead to hyperpolarization of the hair cell (Oliver et al 2000; Glowatzki 2000). This makes our findings somewhat unexpected, as all experiments were performed in the presence of α-Bungarotoxin (α-BTX) as a paralysis agent. α-BTX is a very potent antagonist of nAChR, including the hair cell specific α9/α10-nAChR (Verbitsky et al 2000). The question whether the inhibitory effect is mediated by a different mechanism or whether the α9/α10 retained a certain activity despite paralyzing amounts of α-BTX, remains unanswered at this stage and requires further experimentation.

Discussion

Here we show that the encoding of mechanical information from the posterior lateral line of larval zebrafish is suppressed during fictive swimming. Mechanically induced glutamate release by primary afferent neurons in the MON gets suppressed by 47% and suppression of spontaneous release linearly depends on the number of spikes fired in the motor nerve. The activity of efferent synapses innervating the NM also strongly correlates with motor neuron activity and in 14% of the cases, their firing coincides with a reduction of postsynaptic Ca^{2+}-influx in the afferent neurons. The inhibitory effect of efferent neurons was found exclusively in afferent neurons encoding posterior cupula deflections (towards the tail) (Fig. 4.8).

Pharmacological Source of Inhibition

A recent study, employing a semi-isolated, in-vitro preparation of xenopus larvae reported a significant reduction of firing rate in 67% of afferent neurons during motor nerve activity, which had an average magnitude of 40% (Chagnaud et al 2015), consistent with our findings. This is particularly interesting because the experiments in the above-mentioned study were conducted in the absence of α-BTX. Although there is good evidence that the efferent inhibition of hair cells is mediated via nicotinic AChR, which are blocked by α-BTX (Verbitsky et al 2000; Glowatzki 2000; Dawkins et al 2005), the present results open the possibility that additional mechanisms might be at work in the zebrafish lateral line system. Such mechanisms may include a postsynaptic effect, potentially mediated by muscarinic AChR, which are not affected by α-BTX (Dawkins et al 2005; Pérez et al 2009; Maison et al 2010; Jordan et al 2013;

Sienknecht et al 2014; Mathews et al 2017). However, muscarinic postsynaptic effects were recently shown to be excitatory and significantly slower (Holt et al 2017). Furthermore, it has previously been suggested that efferent neurons in the lateral line form synapses exclusively with hair cells and not with afferents (as opposed to the vestibular system, where they innervate both) (Flock & Russell 1976a), making this proposition rather unlikely. Another possibility to explain the observed inhibitory effects despite the presence of α-BTX is that its antagonistic effect is more transient in α9/α10 subunits in comparison to the muscle-specific subunits (Albuquerque et al 2009). An elegant approach to circumvent the pharmacological interference with the cholinergic system is the use of a paralyzed 'realxed' mutant (Granato et al 1996; Böhm et al 2016). These experiments remain to be conducted, but we would predict that both the number of afferents affected as well as the amplitude of inhibition would be increased.

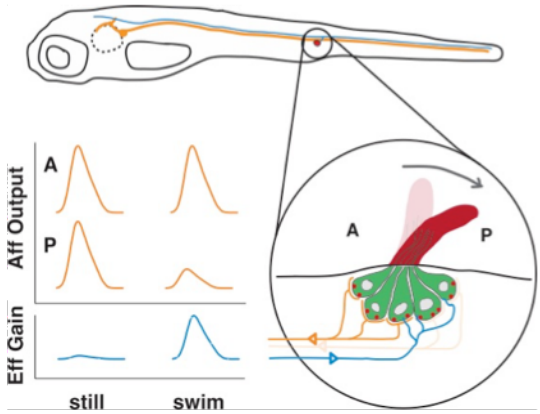

Figure 4.8. Selective Suppression of Lateral Line Information
During a swimming bout, efferent neurons transmit a copy of the motor signal (efference copy) to the neuromast, which leads to a temporally precise and direction-selective suppression of mechanical information. The fact that afferent neurons sensitive to posterior deflections of the cupula get suppressed, and not the anterior sensitive ones, might indicate that this population of hair cells and afferents are activated more strongly by locomotion induced (re-afferent) stimuli. This would indicate that the efferent neurons in the zebrafish lateral line system indeed have a twofold role, to suppress an innate reflex behavior and to enhance the sensitivity to ex-afferent stimuli.

Content of the Efferent Signal

Efferent neurons signal locomotor activity irrespective of whether it was induced by stimulation or occurred spontaneously. This is consistent with a recent study that showed that the activity of efferent neurons derives from central pattern generator activity in the rostral spinal cord (Chagnaud et al 2015). As far as it could be resolved with the GCaMP6f, the correlation between motor neurons and lateral line efferents is maintained until the level of individual swim episodes, not further. During such a swim

episode, the motor nerve of the right and the left side of the larvae are oscillating with a phase offset of 180° (Masino & Fetcho 2005), which leads to the undulatory motion of the trunk. This means that the lateral line is not inhibited during a certain phase of the swim episode but rather during the entire time of locomotion. It would also imply that the activity of the left and right efferent neurons should not differ during a symmetrical (forward) swim stroke, but this remains to be tested.

The result that only afferent neurons that encode tail-wards motion of the cupula are affected by locomotion induced efferent inhibition is unexpected. Previous studies have suggested that efferent neurons innervate neuromast hair cells unspecifically. To our knowledge, however, this is based entirely on anatomical data (Metcalfe et al 1985; Nagiel et al 2008; Faucherre et al 2009). It is therefore conceivable that functional synapses are indeed only formed onto hair cells (or afferents) that detect posterior deflections, or that only hair cells sensitive to posterior deflection express the α9/α10 nAChR. This specific wiring (or expression) would, for example, retain the ability of the system to detect ex-afferent stimuli during swimming via the unaffected anterior afferent (Feitl et al 2010).

An important bit of information to better understand this observation is what kind of neuronal response active locomotion *would* induce in the lateral line system of larval zebrafish. In larger animals it was merely shown *that* the lateral line gets activated during active locomotion (Palmer et al 2005; Ayali et al 2009). The filter properties of the viscous boundary layer and its interaction with the cupula, which define the relationship between external, freestream flow and hair bundle deflection have been described and modeled for a stationary fish (van Netten & McHenry 2014). Additionally, the flow patterns around larvae during undulatory swimming have been measured using particle image velocimetry and computationally modeled (Müller et al 2008; Li et al 2012). Although these models might provide clues about the exact nature of the cupula deflection (and subsequent hair cell activity), it would be preferable to empirically test it.

Nonetheless, the efferent information in the lateral line system of larval zebrafish appears to encode a predictive signal of the expected self-induced mechanical information, which serves at least three distinct purposes. First, it prevents the animal from getting stuck in a reflex-loop by suppressing the otherwise reflex-inducing sensory signal during active locomotion. Secondly, because of the selective suppression of only half the hair cells, the system retains a certain sensitivity, which facilitates the detection of ex-afferent information, even during active locomotion. And

thirdly, it protects the sensory system from overstimulation and from adaptation (depression) induced by strong stimuli, which would otherwise decrease the sensitivity to subsequent potentially weaker external stimuli.

The Reciprocal Influence of Sensory and Motor System

Our understanding of the sensory motor transformations in zebrafish larvae has significantly advanced in the last decade, although almost exclusively in the visual system (Semmelhack et al 2014; Portugues et al 2014; Kubo et al 2014; Bianco & Engert 2015; Temizer et al 2015; Barker & Baier 2015; Dunn et al 2016a). In contrast, how the motor system influences the encoding sensory information has only recently been rediscovered, most prominently in drosophila and mice. Efference copy signals in the drosophila visual system have been shown to directly inhibit the perception of self-induced turns (Kim et al 2015; Kim et al 2017). Similarly, abundant projections from the motor cortex to the visual cortex in mouse result in mismatch signals between sensory input and motor system derived predictions of the sensory input (Keller et al 2012; Zmarz & Keller 2016; Leinweber et al 2017). Furthermore, information about locomotion has been demonstrated to be linearly integrated with visual information to better estimate running speed (Saleem et al 2013). In contrast to these model organisms, little work has been done in zebrafish larvae, which is somewhat surprising given its popularity in the systems neuroscience community. The finding that also in zebrafish, locomotion strongly influences the processing of sensory information in the periphery has strong implications for the investigation of sensory representation in higher brain areas. Our understanding of the reciprocal influence of the sensory and motor system will strongly benefit from more sophisticated imaging techniques such as whole brain imaging using single plane illumination microscopy (SPIM) and clever experimental paradigms such as closed looped (virtual reality) systems (Ahrens et al 2012; Ahrens et al 2013; Vladimirov et al 2014).

Experimental Procedures

Animals

Transgenic zebrafish (Danio *rerio*) were kept under standard conditions (Brand et al 2002) and as described previously (chapter 3). All experimental procedures were in accordance with the UK Animal Act 1986 and were approved by the Home Office and the University of Sussex Ethical Committee. In short, larvae were maintained in E2

medium and after 24 hours post fertilization (hpf) 1-phenyl2-thiourea (pTU) was added (final concentration of 0.2mM) to prevent pigmentation. The following transgenic lines were used: Tg[HuC::GCaMP6f], which expresses the calcium indicator GCaMP6f (Chen et al 2013) in all neurons (except hair cells) and the Tg[Sill2, UAS::iGluSnFR], which drives expression of the glutamate indicator iGluSnFR exclusively in lateral line afferent neurons (Pujol-Martí et al 2012; Marvin et al 2013). The former line allowed to measure the postsynaptic calcium influx in the neuromasts and the latter allowed to measure the glutamatergic output of the afferent in the hindbrain. All lines were maintained in a nacre mutant background (Lister et al 1999), which was particularly important for imaging synaptic activity in the hindbrain.

In Vivo Two-photon Imaging

Sample preparation and imaging were performed as described earlier (chapter 3). In short, larval zebrafish between 6 and 10 days post fertilization (dpf) were mounted sideways and without the use of agarose to allow mechanical access to posterior lateral line neuromasts. To that end, larvae were placed into pits carved out of a thin layer of PDMS (Sylgard184, Dow Crowning) and held down by the strings of a nylon harp. 0.25mM alpha-Bungarotoxin (αBTX) (Tocris) was injected directly into the heart to paralyze the larvae. Mounting and paralysis were performed in the presence of 0.016% tricaine (MS-222) in E2, which was thoroughly washed out before the experiment. Imaging was performed on a two-photon microscope, custom built around a mode-locked Titanium-sapphire laser (Chameleon 2, Coherent), as described previously (chapter 2). The sample was excited at 915-940 nm and emitted light was collected through a water immersion objective (Olympus, 40x LUMIPlanF, NA: 0.8), as well as through a substage oil condenser (Olympus, U-AAC, NA 1.4) and filtered with 525/70 nm (and 530/60 nm) bandpass emission filters before being detected by two photomultiplier tubes (PMTs, Hamamatsu). The software Scanimage 3.8 (Vidrio technologies) was used to control the scanning parameters, image acquisition and synchronization with the mechanical and visual stimulation. Movies were acquired at 10-50 Hz, at spatial resolutions between 256x50 pixels to 128x20 pixels and saved as tiff stacks. Imaging was restricted to parallel neuromasts with an axis of sensitivity parallel to the anterior posterior axis of the fish.

Mechanical Stimulation

Mechanical stimulation of the cupula was performed as previously reported (chapter 3). Briefly, positive and negative pressure steps were applied through a narrow borosilicate pipette (~30 µm tip diameter) that was positioned approximately 100 µm away from the neuromast and approximately 20 µm above the body surface of the fish. The tip of the pipette was bent to facilitate stimulation parallel to the body and easy access. Pressure steps were controlled by a high-speed pressure clamp (HSPC-1, ALA scientific), connected to two pumps (KNF Inc.) that supplied positive and negative pressures. MafPC (courtesy of M. A. Xu-Friedman), running in Igor Pro (WaveMetrics) controlled the pressure steps and also triggered image acquisition in ScanImage via a TTL pulse.

Visual Stimulation

To induce fictive swimming, we projected a moving grating in the tail to head direction directly onto the larvae. This sufficed to engage the Optomotor response and induce fictive locomotion. The grating consisted of 12 mm wide bars at 100% contrast that moved at 5 mm/sec, and was projected from a microprojector (Pico PK320, Optoma) from which the blue and green LED channels were removed to yield a red-only image. Intensity of the red light was adjusted to prevent bleed-through to the imaging PMTs. In between grating presentations, a uniform average intensity screen was projected onto the larvae. The projector was controlled by the PsychoPy toolbox running in Python and synchronized to the mechanical stimulation and imaging software via a TTL pulse.

Motor nerve recordings

Motor nerve recordings were performed as described by (Masino & Fetcho 2005) with minor modifications. The recording electrode was pulled from borosilicate glass (GC150T-10, Harvard Apparatus) to have a tip diameter of approximately 30 µm and was fire polished to smooth the edges. It was filled with extracellular recording solution (concentrations in mM: 134 NaCl, 2.9 KCl, 1.2 MgCl2, 2.1 CaCl2, 10 HEPES buffer, adjusted to pH 7.8 with NaOH). Pressure in the pipette was manually adjusted with a plastic syringe and monitored with a pressure-meter. Using a micromanipulator, larvae were approached dorsally at an angle of approximately 45° and perpendicular to the longitudinal body axis (Fig. 4.2 A), while very slight positive pressure was applied. The tip was positioned above the myotomal cleft between segments 8-14.

Upon contacting the skin, slight negative pressure (30-60 mmHg) was applied to produce a tight seal. The extracellular voltage was measured in current-clamp mode using a BVC-700A (Dagan, USA). The signal was filtered (Brownlee model 440, Neurophase) with high pass and low pass cut off frequency of 300 Hz and 1 kHz, respectively (and to additionally reduce noise a notch filter at 50 Hz). Usually, spontaneous bursts of motor nerve activity could be observed after 10-15 minutes. The signal was recorded at a sample rate of 5 kHz using mafPC (courtesy of M. A. Xu-Friedman).

Analysis

Images were analyzed in Igor Pro. Small drifts in the x/y dimension were registered, using the SARFIA toolbox (Dorostkar et al 2010). Images with large drifts, including potential z-drifts were discarded. Regions of Interest (ROIs) were determined using a custom written procedure (described in chapter 3) that was identifying pixels with the highest correlation value (to neighboring pixels). Background fluorescence was subtracted. Baseline fluorescence (F) was defined as the average fluorescence preceding the first stimulation interval; and the ratio of change in fluorescence (ΔF) was calculated relative to that value (ΔF/F) and used for further analysis. For presentation purposes contrast in images was adjusted and traces were smoothed. The motor nerve recordings were further digitally filtered (300 Hz high-pass 1kHz low-pass and 50 Hz notch). Spikes were extracted using a custom written procedure that applied a simple threshold to the filtered signal and detected when it was crossed by the signal. Spike rate was calculated as the rolling average over a 100 ms time window.

Chapter 5

General Discussion

The work presented in this thesis touches upon several aspects of lateral line function, ranging from the transfer characteristics of the hair cells themselves to the effects of locomotion on sensory encoding. Many interesting questions could not be addressed within the scope of this project. Below, I will summarize the findings and elaborate on potential future questions.

New Tools to Study the Encoding of Mechanical Information in the Lateral Line

The initial aim of this thesis was to establish the necessary tools required to study the encoding of mechanical information in the lateral line organ of zebrafish larvae by imaging genetically encoded reporters of neuronal activity (**Chapter 2**). This approach is experiencing growing interest from researchers investigating the physiology and genetics of hair cells (Zhang et al 2016; Sebe et al 2017; Sheets et al 2017) because the ever-improving neuronal activity indicators and relatively easy-to-use imaging systems provide a cheap and fast alternative (and complement) to existing electrophysiological approaches that have been used to asses hair cell function (Trapani & Nicolson 2010). Since recently, forward genetic screens are potentially superseded by the CRISPR-Cas9 system (Hwang et al 2013) which allows site-specific mutagenesis of genes potentially involved in the transmission of mechanical information. Further, imaging techniques can be relatively easily implemented in high throughput screens, for example for agents that protect from antibiotic induced hair cell death (Thomas et al 2015).

To that end we established and tested a number of different transgenic zebrafish lines with different combinations of promoters and functional reporter proteins (GCaMPs and iGluSnFR) that can be used to monitor the physiology of hair cells as well as the output of the afferent neurons in the hindbrain (Table 2.2 & Fig. 2.7). Additionally, we described a simple mounting technique and an all-optical method to reliably measure the angular deflection of the cupula that can be easily implemented in the sample preparation and used on any fluorescent imaging system (Fig. 2.2). To our knowledge, these efforts have lead to the first direct recordings of hair cell glutamate release using iGluSnFR and to the first measurements of mechanically induced synaptic activity in the hindbrain of zebrafish larvae.

However, the list of reporters that were not tested is long and new ones are constantly being added. Of particular interest are voltage indicators (Jin et al 2012; St-Pierre et al 2014; Storace et al 2016) and red-shifted calcium indicators (Akerboom et al 2013). The latter has the advantage that it could be used together with green

indicators to simultaneously image either different cellular processes, for instance calcium influx and glutamate release, or the same process in different cells, such as hair cells and afferent neurons. The red-shifted calcium indicator RGECO was successfully used in hair cells using single-photon microscopy (Zhang et al 2016; Sheets et al 2017). However, we did not manage to establish it for two-photon microscopy. This could be partly explained by red indicators being more susceptible to photo bleaching than green ones, which becomes potentiated under a two-photon excitation. However, this is very unfortunate because two-photon microscopy allows for the simultaneous excitation of multiple indicators, and would therefore be ideal for multi-color imaging. As demonstrated in this thesis, new tools permit to ask new questions.

Transmission of Mechanical Information by Lateral Line Hair Cells

The second aim of the thesis was to employ the tools established in chapter 2 to characterize the transformation of cupula deflection to hair cell glutamate release. During the last half-century a large body of work has elucidated the fundamental principles of mechanoelectrical transduction (MET) (reviewed by: Hudspeth 2014; Fettiplace & Kim 2014; Fettiplace 2017) and exocytosis (reviewed by: Nouvian et al 2006; Wichmann & Moser 2015; Nicolson 2015) in a variety of different hair cell types. Classically, mechanoelectrical transduction and exocytosis at the ribbon synapse were investigated separately, under different experimental conditions. The transduction process was generally assayed by recording the MET current, or the receptor potential while deflecting the hair bundle. On the other hand, the process of exocytosis was investigated by artificially depolarizing the hair cell while measuring either the change in membrane capacitance or excitatory postsynaptic currents in the afferent bouton. The approach presented here has several advantages over these more traditional ones. Firstly, it is possible to monitor the activity of different hair cells simultaneously. This not only decreases the experimental time, but also allows to directly compare the activity of neighboring hair cells. Secondly, the sensory transduction process is monitored *in vivo* in the intact structure, which means that hair cells are embedded in their natural physiological and anatomical context. This also means that the stimulus is filtered by the mechanical properties of the cupula and boundary layer in much the same way as it would be in the natural environment of the fish. Thirdly, it was possible to measure the hair cell output – glutamate release – without interfering with the electrical properties of the cell. When measuring the

transducer current or capacitance of the cell, the membrane potential is experimentally controlled, which not only decouples these processes but also masks a potential source of heterogeneity that might play a functional role. In contrast, in the present approach hair bundle deflection is experimentally induced and exocytosis is observed, revealing these two fundamental processes acting *in concert*.

These measurements revealed several basic properties that contribute to the signaling of mechanical information of the lateral line system (**Chapter 3**). We found that the transformation of cupula deflection to glutamate release within a single neuromast is shaped by a heterogeneous population of hair cells. They varied in sensitivity, working range, relative set point and adaptive properties. While some hair cells saturated within cupula deflections of just 1°, others had working ranges of up to 10° (Fig. 3.2). While some hair cells had a dynamic range that spanned both sides of the resting position and therefore encoded cupula deflections in their preferred as well as the opposite direction, others rectified completely. Heterogeneity was also present in their temporal properties, while some cells adapted completely during a 5 s stimulation, others maintained strong tonic vesicle release or even sensitized during sustained stimulation, with time constants of several seconds (Fig 3.6 & 7). Additionally we observed a strong and reliable response to the return to rest from negative deflections. Functional heterogeneity as a strategy to extend the dynamic range of a sensory system can be implemented on different levels.

It has been proposed that variability in cupula morphology introduces heterogeneity in the filter properties among different neuromasts of the lateral line (Van Trump & McHenry 2008) and thereby extending the dynamic range of the system as a whole. Our data suggests that within a single neuromast physiological heterogeneity of hair cells increases the dynamic range of stimuli that can be encoded by a single neuromast. On yet another level, functional heterogeneity was demonstrated to occur between synaptic ribbons within inner ear hair cells of the mammalian cochlear (Ohn et al 2016). It would be interesting to test if the same holds true in lateral line hair cells.

We could only speculate about the relative contribution of the transduction and exocytosis process to this heterogeneity. It might be possible to address this question by employing genetically encoded voltage sensors (Jin et al 2012; St-Pierre et al 2014; Storace et al 2016). This would allow monitoring the membrane potential while deflecting the cupula and should reveal the extent to which the transduction current contributes to the variability in terms of half angle and set point as well as adaptation. It was shown that the biophysical properties of lateral line hair cells depend on their

maturity (Olt et al 2014) and we proposed it as a potential source of the observed heterogeneity. It would be interesting to test this by chemically ablating hair cells of the lateral line and monitoring their functional properties during the process of regeneration.

The approach presented in chapters 2 and 3 bears the potential to address other key properties of hair cells. For instance, it is well known that ribbon-type synapses in the retina and hair cells possess the ability to synchronize vesicle release, resulting in monophasic postsynaptic currents with varying amplitude, a phenomenon called multivesicular release (MVR) (Glowatzki & Fuchs 2002). In auditory hair cells MVR has been suggested to enhance the hair cell's ability to phase lock to sinusoidal stimuli (Li et al 2014) but little is known about the role of MVR in lateral line hair cells. Is MVR present in lateral line hair cells? Are stronger cupula deflections more likely to trigger multivesicular events or more single events? How many vesicles are released per degree cupula deflection? How does the signal adapt, by releasing less multivesicular events or fewer vesicles in general? Can a single multivesicular event trigger postsynaptic activity?

Under certain experimental circumstances, most likely to do with the expression level of the iGluSnFR, it was possible to observe glutamate release in the form of distinct, separable 'spikes' or events, most likely corresponding to the fusion of individual vesicles. These indeed appeared to vary in magnitude and encode stimulus strength in the frequency domain. However, it was not possible to reproducibly generate these kinds of signals so they were not included in this thesis. Recently, new variants of the glutamate reporter iGluSnFR with improved brightness and an extended dynamic range were reported (Marvin et al 2017). Using these, it might become possible to resolve the release of single vesicles and address the role of MVR in the encoding of cupula deflections in lateral line hair cells, which would help to better understand this phenomenon in general.

Quantifying the relationship of cupula deflection and glutamate release using a square wave stimulus was only the first step towards understanding the transfer characteristics of lateral line hair cells and already revealed a large degree of heterogeneity. The major disadvantage of using this stimulus is that each stimulus step contains all frequencies. Therefore, this analysis should be extended into the frequency domain, by testing the system using single frequency sine waves. This would permit the construction of the physiological transfer function of a neuromast hair cell, the mathematical definition of its input-output relationship (van Netten &

McHenry 2014) and would nicely complement our understanding of the mechanical filter properties of the cupula (McHenry et al 2008; Van Trump & McHenry 2008; Windsor & McHenry 2009; van Netten & McHenry 2014) as well as frequency response measurement of the afferent neuron (Levi et al 2014).

Central Processing of Lateral Line Information

It was shown that in the medial octavolateralis nucleus (MON) central projections of lateral line afferents are somatotopically organized in respect to the position of the neuromasts they innervate (Alexandre & Ghysen 1999; Pujol-Martí et al 2010). It has further been shown that afferent neurons strictly innervate hair cells with the same functional polarity (Nagiel et al 2008). Thus, the population of afferent neurons in the posterior lateral line represents any flow around the animal as a projection onto the four cardinal axes: anterior, posterior, dorsal and ventral. However, how (or whether at all) these channels are spatially organized in the hindbrain, or synapse onto specific second-order neurons remains to be tested. Although the question was not directly addressed in this thesis, the tools to do so are at hand. Preliminary data suggested that afferent synapses sensitive to opposite cupula deflections could be found in close proximity, suggesting that they are least not coarsely segregated.

By embedding the head of larvae right side up and leaving the tail free, it is possible to image both sides of the MON simultaneously while stimulating the posterior lateral line. This allows to ask questions about the central representation of more complex stimuli such as vibrating spheres, which have been used in larger fish (Chagnaud et al 2007). It has been proposed that afferents coarsely fall into two categories, those who innervate the Mauthner neurons and those who do not (Pujol-Martí et al 2012). These afferents were suggested to be activated by different stimuli and trigger separate behaviors. With the tools at hand, the (mechano-) sensory-motor transformations that are responsible for initiating different lateral line triggered behaviors, such as rheotaxis or predator avoidance (Olszewski et al 2012; Stewart et al 2013; Olive et al 2016; Troconis et al 2017; Oteiza et al 2017), could be addressed. The circuit mechanisms could be studied much in the same way as they have been in the visual system for some years; by population imaging of neuronal activity in the hindbrain, monitoring (fictive) locomotor output and using optogenetics and two-photon laser ablation to interrogate the circuit (e.g. Semmelhack et al 2014; Bianco & Engert 2015; Barker & Baier 2015; Orger 2016; Koyama et al 2016).

Efferent Modulation – Efference Copy

The third aim of the thesis was to use the tools established in previous chapters to study the effects of efferent modulation of mechanical information. Efferent modulation of hair cells and their afferents has been investigated for as long as hair cells themselves and led to a good understanding of the basic mechanisms; however efferent neurons are functionally and physiologically diverse (reviewed by: Ryugo et al 2011; Sienknecht et al 2014; Mathews et al 2017). Since they were first described in larval zebrafish, more than 30 years ago (Metcalfe et al 1985) our understanding of mechanosensory efferents has barely improved (but see: Bricaud et al 2001; Sapède et al 2005; Suli et al 2006). Still, very little is known about their function and how they contribute to sensory encoding. This is particularly surprising when compared to the progress that has been made in the same time period for other sensory modalities as well as the motor system (for example: Orger et al 2000; Orger et al 2008; Bianco et al 2012; Robles et al 2014; Kubo et al 2014; Orger 2016; Schoppik et al 2017). However, this appears to be changing at the moment (Toro et al 2015; Reinig et al 2017; Knafo et al 2017).

Using the tools that were established in chapter 2, we were able to measure mechanically induced glutamate release of afferent neurons in the MON in the hindbrain, in vivo. Employing electrophysiological recordings of the motor nerve activity and visual stimulation, we could record and induce fictive locomotion while mechanically stimulating individual neuromasts and measuring the synaptic output of their afferent neurons. This approach has the advantage that experiments are performed in vivo, in the awake but paralyzed animal, which means that efferent neurons are activated endogenously, by presynaptic neurons, and that they convey the same signal in amplitude and frequency as they would in the natural environment. Furthermore, it is possible to simultaneously observe the responses of a large number of afferent synapses, from different neurons and innervating different populations of hair cells.

The experiments presented in **chapter 4** revealed a profound reduction of mechanically induced and spontaneous glutamate release of afferent neurons in the MON during fictive swimming. Furthermore, the activity of efferent synapses, which strongly correlated with motor neuron activity, could be observed in neuromasts. Activity of these efferent synapses lead to a significant decrease of mechanically

induced calcium influx in postsynaptic varicosities of afferent neurons. Strikingly, and in contrast to previous anatomical descriptions, the inhibitory effect was only observed in afferent neurons that were sensitive to posterior deflections of the cupula. We hypothesized that this might constitute a mechanism to specifically suppress self-induced sensory information in one afferent channel while maintaining sensitivity in the other. These data have to be interpreted with caution, as all experiments were conducted in larvae that were paralyzed by injecting α-BTX, a potent antagonist to nicotinic acetylcholine receptors that mediate muscle contraction. However, α-BTX also acts as an antagonist to the hair cell specific α9/α10 nicotinic acetylcholine receptor subunits that are likely to mediate the suppressive effect (Verbitsky et al 2000; Glowatzki 2000; Dawkins et al 2005). Somewhat counterintuitive, the suppressive effect was never observed when measuring the glutamate release by hair cells (chapter 3). Assuming that efferent inhibition indeed takes place at the level of the hair cell, then sustained stimuli as used for the adaptation experiments should be modulated similarly as observed for the postsynaptic calcium influx (Fig. 4.7 D), however this has never been observed.

Although other toxins have been reported to be more specific to the muscle type nicotinic subunits, such as α-Conotixin-M1 and G1 (Lebbe et al 2014), the most elegant approach to circumvent this problem would be to not use pharmacological means at all. Potentially this could be achieved by using a paralyzed mutant zebrafish line (Granato et al 1996; Böhm et al 2016). In the absence of αBTX, it would be possible to confirm the identity of the efferent receptor using pharmacological tools. Since stronger inhibitory effects would be expected, it should be possible to ascertain the directionally selective inhibition. These findings highlight the importance of using in vivo paradigms to understand sensory encoding and the necessity to understand peripheral modulation of sensory systems to interpret their central representation.

The ideal experimental system to test the neural basis for behavior and the interdependence of the sensory and motor system would be the behaving animal. Besides not interfering with any aspect of the sensory system, this would most importantly preserve the sensory motor contingencies. Thus, the physical context that the animal is embedded in, which leads to a permanent feedback loop between the motor system, the environment and the sensory system would remain intact. And such experiments are indeed feasible by physically moving the stage to compensate for the animal's motion while simultaneously imaging neuronal activity of the whole brain (Kim et al 2017). A much easier alternative to this, however, are virtual-reality

systems, which have successfully been used to study adaptive swimming behaviors (Ahrens et al 2012; Ahrens et al 2013). In the context of the lateral line, such an approach would be more challenging, as it would be necessary to experimentally apply the appropriate sensory consequences of self-induced locomotion. If possible, however, it would allow to ask, for example how much information the central nervous system receives form the lateral line system during locomotion while the efferent system is intact.

Taken together, initial efforts (chapter 2) to establish functional imaging in the lateral line of larval zebrafish could be employed to study the basic physiological properties of hair cells (chapter 3), underlining the importance of functional heterogeneity in sensory systems and to measure motor related efferent signals as well as their effect on afferent signaling (chapter 4), pointing towards the selective suppression of self-induced re-afferent information in the hindbrain.

References

Ahrens, M.B., Huang, K.H., Narayan, S., Mensh, B.D. & Engert, F., 2013, Two-photon calcium imaging during fictive navigation in virtual environments, *Frontiers in Neural Circuits*, 7, p. 104.

Ahrens, M.B., Li, J.M., Orger, M.B., Robson, D.N., Schier, A.F., Engert, F. & Portugues, R., 2012, Brain-wide neuronal dynamics during motor adaptation in zebrafish, *Nature*, 485(7399), pp. 471-7.

Ahrens, M.B., Orger, M.B., Robson, D.N., Li, J.M. & Keller, P.J., 2013, Whole-brain functional imaging at cellular resolution using light-sheet microscopy, *Nature methods*, 10(5), pp. 413-20.

Akerboom, J., Carreras Calderón, N., Tian, L., Wabnig, S., Prigge, M., Tolö, J., Gordus, A., Orger, M.B., Severi, K.E., Macklin, J.J., Patel, R., Pulver, S.R., Wardill, T.J., Fischer, E., Schüler, C., Chen, T.W., Sarkisyan, K.S., Marvin, J.S., Bargmann, C.I., Kim, D.S., Kügler, S., Lagnado, L., Hegemann, P., Gottschalk, A., Schreiter, E.R. & Looger, L.L., 2013, Genetically encoded calcium indicators for multi-color neural activity imaging and combination with optogenetics, *Frontiers in Molecular Neuroscience*, 6, p. 2.

Albuquerque, E.X., Pereira, E.F., Alkondon, M. & Rogers, S.W., 2009, Mammalian nicotinic acetylcholine receptors: from structure to function, *Physiological Reviews*, 89(1), pp. 73-120.

Alexandre, D. & Ghysen, A., 1999, Somatotopy of the lateral line projection in larval zebrafish, *Proceedings of the National Academy of Sciences USA* 96(13), pp. 7558-62.

Assad, J.A. & Corey, D.P., 1992, An active motor model for adaptation by vertebrate hair cells, *The Journal of Neuroscience*, 12(9), pp. 3291-309.

Assad, J.A., Hacohen, N. & Corey, D.P., 1989, Voltage dependence of adaptation and active bundle movement in bullfrog saccular hair cells, *Proceedings of the National Academy of Sciences USA*, 86(8), pp. 2918-22.

Ayali, A., Gelman, S., Tytell, E.D. & Cohen, A.H., 2009, Lateral-line activity during undulatory body motions suggests a feedback link in closed-loop control of sea lamprey swimming, *Canadian Journal of Zoology*, 87(8), pp. 671-83.

Baker, E.R., Zwart, R., Sher, E. & Millar, N.S., 2004, Pharmacological properties of alpha 9 alpha 10 nicotinic acetylcholine receptors revealed by heterologous expression of subunit chimeras, *Molecular Pharmacology*, 65(2), pp. 453-60.

Barker, A.J. & Baier, H., 2015, Sensorimotor decision making in the zebrafish tectum, *Current Biology*, 25(21), pp. 2804-14.

Bell, C.C., Han, V. & Sawtell, N.B., 2008, Cerebellum-like structures and their implications for cerebellar function, *Annual Review of Neuroscience*, 31, pp. 1-24.

Beurg, M., Evans, M.G., Hackney, C.M. & Fettiplace, R., 2006, A large-conductance calcium-selective mechanotransducer channel in mammalian cochlear hair cells, *The Journal of Neuroscience,* 26(43), pp. 10992-1000.

Beurg, M., Fettiplace, R., Nam, J.H. & Ricci, A.J., 2009, Localization of inner hair cell mechanotransducer channels using high-speed calcium imaging, *Nature Neuroscience*, 12(5), pp. 553-8.

Beurg, M., Goldring, A.C., Ricci, A.J. & Fettiplace, R., 2016, Development and localization of reverse-polarity mechanotransducer channels in cochlear hair cells, *Proceedings of the National Academy of Sciences USA*, 113(24), pp. 6767-72.

Beurg, M., Michalski, N., Safieddine, S., Bouleau, Y., Schneggenburger, R., Chapman, E.R., Petit, C. & Dulon, D., 2010, Control of exocytosis by synaptotagmins and otoferlin in auditory hair cells, *The Journal of neuroscience*, 30(40), pp. 13281-90.

Beutner, D., Voets, T., Neher, E. & Moser, T., 2001, Calcium dependence of exocytosis and endocytosis at the cochlear inner hair cell afferent synapse, *Neuron*, 29(3), pp. 681-90.

Bianco, I.H. & Engert, F., 2015, Visuomotor transformations underlying hunting behavior in zebrafish, *Current Biology*, 25(7), pp. 831-46.

Bianco, I.H., Kampff, A.R. & Engert, F., 2011, Prey capture behavior evoked by simple visual stimuli in larval zebrafish, *Frontiers in Systems Neuroscience*, 5, p. 101.

Bianco, I.H., Ma, L.H., Schoppik, D., Robson, D.N., Orger, M.B., Beck, J.C., Li, J.M., Schier, A.F., Engert, F. & Baker, R., 2012, The tangential nucleus controls a gravito-inertial vestibulo-ocular reflex, *Current Biology*, 22(14), pp. 1285-95.

Borghuis, B.G., Marvin, J.S., Looger, L.L. & Demb, J.B., 2013, Two-photon imaging of nonlinear glutamate release dynamics at bipolar cell synapses in the mouse retina, *The Journal of Neuroscience,* 33(27), pp. 10972-85.

Bortolozzi, M., Lelli, A. & Mammano, F., 2008, Calcium microdomains at presynaptic active zones of vertebrate hair cells unmasked by stochastic deconvolution, *Cell Calcium*, 44(2), pp. 158-68.

Böhm, U.L., Prendergast, A., Djenoune, L., Nunes Figueiredo, S., Gomez, J., Stokes, C., Kaiser, S., Suster, M., Kawakami, K., Charpentier, M., Concordet, J.P., Rio, J.P., Del Bene, F. & Wyart, C., 2016, CSF-contacting neurons regulate locomotion by relaying mechanical stimuli to spinal circuits, *Nature Communication*, 7, p. 10866.

Brand, A.H. & Perrimon, N., 1993, Targeted gene expression as a means of altering cell fates and generating dominant phenotypes, *Development*, 118(2), pp. 401-15.

Brand, M., Granato, M. & Nüsslein-Volhard, C. 2002, Keeping and raising zebrafish, in *Zebrafish: A Practical Approach,* Oxford University Press: Oxford, UK, pp. 7-37.

Brandt, A., Khimich, D. & Moser, T., 2005, Few CaV1.3 channels regulate the exocytosis of a synaptic vesicle at the hair cell ribbon synapse, *The Journal of Neuroscience*, 25(50), pp. 11577-85.

Bricaud, O., Chaar, V., Dambly-Chaudière, C. & Ghysen, A., 2001, Early efferent innervation of the zebrafish lateral line, *Journal of Comparative Neurology*, 434(3), pp. 253-61.

Brockerhoff, S.E., Hurley, J.B., Janssen-Bienhold, U., Neuhauss, S.C., Driever, W. & Dowling, J.E., 1995, A behavioral screen for isolating zebrafish mutants with visual system defects, *Proceedings of the National Academy of Sciences USA*, 92(23), pp. 10545-9.

Burgess, H.A. & Granato, M., 2007, Sensorimotor gating in larval zebrafish, *The Journal of Neuroscience*, 27(18), pp. 4984-94.

Burighel, P., Caicci, F. & Manni, L., 2011, Hair cells in non-vertebrate models: lower chordates and molluscs, *Hearing Research*, 273(1-2), pp. 14-24.

Butler, J.M. & Maruska, K.P., 2016, The Mechanosensory Lateral Line System Mediates Activation of Socially-Relevant Brain Regions during Territorial Interactions, *Frontiers in Behavioral Neuroscience*, 10, p. 93.

Butts, D.A. & Goldman, M.S., 2006, Tuning curves, neuronal variability, and sensory coding, *PLoS Biology*, 4(4), p. e92.

Castellano-Muñoz, M. & Ricci, A.J., 2014, Role of intracellular calcium stores in hair-cell ribbon synapse, *Frontiers in Cellular Neuroscience*, 8, p. 162.

Chagnaud, B.P., Banchi, R., Simmers, J. & Straka, H., 2015, Spinal corollary discharge modulates motion sensing during vertebrate locomotion, *Nature Communication*, 6, p. 7982.

Chagnaud, B.P., Hofmann, M.H. & Mogdans, J., 2007, Responses to dipole stimuli of anterior lateral line nerve fibres in goldfish, Carassius auratus, under still and running water conditions, *Journal of Comparative Physiology A*, 193(2), pp. 249-63.

Chen, T.W., Wardill, T.J., Sun, Y., Pulver, S.R., Renninger, S.L., Baohan, A., Schreiter, E.R., Kerr, R.A., Orger, M.B., Jayaraman, V., Looger, L.L., Svoboda, K. & Kim, D.S., 2013, Ultrasensitive fluorescent proteins for imaging neuronal activity, *Nature*, 499(7458), pp. 295-300.

Chen, X. & Engert, F., 2014, Navigational strategies underlying phototaxis in larval zebrafish, *Frontiers in Systems Neuroscience*, 8, p. 39.

Coombs, S., Bleckmann, H., Fay, R.R. & Popper, A.N., 2014, *The lateral line system,* Springer,.
Corey, D.P. & Holt, J.R., 2016, Are TMCs the Mechanotransduction Channels of Vertebrate Hair Cells? *The Journal of Neuroscience*, 36(43), pp. 10921-6.

Corey, D.P. & Hudspeth, A.J., 1979, Response latency of vertebrate hair cells, *Biophysical Journal*, 26(3), pp. 499-506.

Corey, D.P. & Hudspeth, A.J., 1983, Kinetics of the receptor current in bullfrog saccular hair cells, *The Journal of Neuroscience*, 3(5), pp. 962-76.

Corns, L.F., Johnson, S.L., Kros, C.J. & Marcotti, W., 2014, Calcium entry into stereocilia drives adaptation of the mechanoelectrical transducer current of mammalian cochlear hair cells, *Proceedings of the National Academy of Sciences USA*, 111(41), pp. 14918-23.

Crawford, A.C., Evans, M.G. & Fettiplace, R., 1989, Activation and adaptation of transducer currents in turtle hair cells, *The Journal of Physiology*, 419, pp. 405-34.

Dana, H., Mohar, B., Sun, Y., Narayan, S., Gordus, A., Hasseman, J.P., Tsegaye, G., Holt, G.T., Hu, A., Walpita, D., Patel, R., Macklin, J.J., Bargmann, C.I., Ahrens, M.B., Schreiter, E.R., Jayaraman, V., Looger, L.L., Svoboda, K. & Kim, D.S., 2016, Sensitive red protein calcium indicators for imaging neural activity, *eLife*, 5.

Dawkins, R., Keller, S.L. & Sewell, W.F., 2005, Pharmacology of acetylcholine-mediated cell signaling in the lateral line organ following efferent stimulation, *Journal of Neurophysiology*, 93(5), pp. 2541-51.

Dayan, P. & Abbott, L.F., 2001, *Theoretical neuroscience,* Cambridge, MA: MIT Press,.
Denk, W., Strickler, J.H. & Webb, W.W., 1990, Two-photon laser scanning fluorescence microscopy, *Science*, 248(4951), pp. 73-6.

Dick, O., Hack, I., Altrock, W.D., Garner, C.C., Gundelfinger, E.D. & Brandstätter, J.H., 2001, Localization of the presynaptic cytomatrix protein Piccolo at ribbon and conventional synapses in the rat retina: comparison with Bassoon, *Journal of Comparative Neurology*, 439(2), pp. 224-34.

Dijkgraaf, S., 1963, The functioning and significance of the lateral-line organs, *Biological Reviews, Cambridge Philosophical Society*, 38, pp. 51-105.

Dinklo, T., Meulenberg, C.J. & van Netten, S.M., 2007, Frequency-dependent properties of a fluid jet stimulus: calibration, modeling, and application to cochlear hair cell bundles, Journal of the Association for Research in Otolaryngology, 8(2), pp. 167-82.

Dorostkar, M.M., Dreosti, E., Odermatt, B. & Lagnado, L., 2010, Computational processing of optical measurements of neuronal and synaptic activity in networks, *Journal of Neuroscience Methods*, 188(1), pp. 141-50.

Dreosti, E., Odermatt, B., Dorostkar, M.M. & Lagnado, L., 2009, A genetically encoded reporter of synaptic activity in vivo, *Nature methods*, 6(12), pp. 883-9.

Drobizhev, M., Makarov, N.S., Tillo, S.E., Hughes, T.E. & Rebane, A., 2011, Two-photon absorption properties of fluorescent proteins, *Nature methods*, 8(5), pp. 393-9.

Dulon, D., Safieddine, S., Jones, S.M. & Petit, C., 2009, Otoferlin is critical for a highly sensitive and linear calcium-dependent exocytosis at vestibular hair cell ribbon synapses, *The Journal of Neuroscience*, 29(34), pp. 10474-87.

Dunn, T.W., Gebhardt, C., Naumann, E.A., Riegler, C., Ahrens, M.B., Engert, F. & Del Bene, F., 2016a, Neural Circuits Underlying Visually Evoked Escapes in Larval Zebrafish, *Neuron*, 89(3), pp. 613-28.

Dunn, T.W., Mu, Y., Narayan, S., Randlett, O., Naumann, E.A., Yang, C.-T., Schier, A.F., Freeman, J., Engert, F. & Ahrens, M.B., 2016b, Brain-wide mapping of neural activity controlling zebrafish exploratory locomotion, *eLife*, 5, p. e12741.

Eatock, R.A., 2000, Adaptation in hair cells, *Annual Review of Neuroscience*, 23, pp. 285-314.

Eatock, R.A., Corey, D.P. & Hudspeth, A.J., 1987, Adaptation of mechanoelectrical transduction in hair cells of the bullfrog's sacculus, *The Journal of neuroscience*, 7(9), pp. 2821-36.

Eggermann, E., Bucurenciu, I., Goswami, S.P. & Jonas, P., 2012, Nanodomain coupling between Ca^{2+} channels and sensors of exocytosis at fast mammalian synapses, *Nature Reviews Neuroscience*, 13(1), pp. 7-21.

Elgoyhen, A.B., Johnson, D.S., Boulter, J., Vetter, D.E. & Heinemann, S., 1994, Alpha 9: an acetylcholine receptor with novel pharmacological properties expressed in rat cochlear hair cells, *Cell*, 79(4), pp. 705-15.

Erickson, T. & Nicolson, T., 2015, Identification of sensory hair-cell transcripts by thiouracil-tagging in zebrafish, *BMC Genomics*, 16, p. 842.

Erickson, T., Morgan, C.P., Olt, J., Hardy, K., Busch-Nentwich, E., Maeda, R., Clemens, R., Krey, J.F., Nechiporuk, A., Barr-Gillespie, P.G., Marcotti, W. & Nicolson, T., 2017, Integration of Tmc1/2 into the mechanotransduction complex in zebrafish hair cells is regulated by Transmembrane O-methyltransferase (Tomt), *eLife*, 6.

Fame, R.M., Brajon, C. & Ghysen, A., 2006, Second-order projection from the posterior lateral line in the early zebrafish brain, *Neural Development*, 1, p. 4.

Faucherre, A., Baudoin, J.P., Pujol-Martí, J. & López-Schier, H., 2010, Multispectral four-dimensional imaging reveals that evoked activity modulates peripheral arborization and the selection of plane-polarized targets by sensory neurons, *Development*, 137(10), pp. 1635-43.

Faucherre, A., Pujol-Martí, J., Kawakami, K. & López-Schier, H., 2009, Afferent neurons of the zebrafish lateral line are strict selectors of hair-cell orientation, *PloS one*, 4(2), p. e4477.

Feitl, K.E., Ngo, V. & McHenry, M.J., 2010, Are fish less responsive to a flow stimulus when swimming? *Journal of Experimental Biology*, 213(Pt 18), pp. 3131-7.

Fettiplace, R., 2017, Hair Cell Transduction, Tuning, and Synaptic Transmission in the Mammalian Cochlea, *Comprehensive Physiology*, 7(4), pp. 1197-227.

Fettiplace, R. & Kim, K.X., 2014, The physiology of mechanoelectrical transduction channels in hearing, *Physiological Reviews*, 94(3), pp. 951-86.

Fettiplace, R. & Ricci, A.J., 2003, Adaptation in auditory hair cells, *Current Opinion in Neurobiology*, 13(4), pp. 446-51.

Flock, A. & Cheung, H.C., 1977, Actin filaments in sensory hairs of inner ear receptor cells, *The Journal of Cell Biology*, 75(2 Pt 1), pp. 339-43.

Flock, A. & Lam, D.M., 1974, Neurotransmitter synthesis in inner ear and lateral line sense organs, *Nature*, 249(453), pp. 142-4.

Flock, A. & Russell, I., 1976a, Inhibition by efferent nerve fibres: action on hair cells and afferent synaptic transmission in the lateral line canal organ of the burbot Lota lota, *The Journal of Physiology*, 257(1), pp. 45-62.

Flock, A. & Russell, I., 1976b, Inhibition by efferent nerve fibres: action on hair cells and afferent synaptic transmission in the lateral line canal organ of the burbot Lota lota, *The Journal of Physiology*, 257(1), pp. 45-62.

Flock, A. & Russell, I.J., 1973, The post-synaptic action of efferent fibres in the lateral line organ of the burbot Lota lota, *The Journal of Physiology*, 235(3), pp. 591-605.

Flock, Å. & Wersäll, J., 1962, A study of the orientation of the sensory hairs of the receptor cells in the lateral line organ of fish, with special reference to the function of the receptors, *The Journal of Cell Biology*, 15, pp. 19-27.

Flock, Å., Kimura, R., Lundquist, P.G. & Wersäll, J., 1962, Morphological Basis of Directional Sensitivity of the Outer Hair Cells in the Organ of Corti, *The Journal of the Acoustical Society of America*, 34(1351).

Franke, K., Berens, P., Schubert, T., Bethge, M., Euler, T. & Baden, T., 2017, Inhibition decorrelates visual feature representations in the inner retina, *Nature*, 542(7642), pp. 439-44.

Friedrich, R.W., Jacobson, G.A. & Zhu, P., 2010, Circuit neuroscience in zebrafish, *Current biology*, 20(8), pp. R371-81.

Fritzsch, B. & Straka, H., 2014, Evolution of vertebrate mechanosensory hair cells and inner ears: toward identifying stimuli that select mutation driven altered morphologies, *Journal of Comparative Physiology A*, 200(1), pp. 5-18.

Fuchs, P.A., 2014, A 'calcium capacitor' shapes cholinergic inhibition of cochlear hair cells, *The Journal of Physiology*, 592(16), pp. 3393-401.

Furness, D. & Hackney, C. 2006, The Structure and Composition of the Stereociliary Bundle of Vertebrate Hair Cells, in *Vertebrate Hair Cells,* pp. 95-153.

Gale, J.E., Marcotti, W., Kennedy, H.J., Kros, C.J. & Richardson, G.P., 2001, FM1-43 dye behaves as a permeant blocker of the hair-cell mechanotransducer channel, *The Journal of Neuroscience*, 21(18), pp. 7013-25.

Ghysen, A. & Dambly-Chaudière, C., 2004, Development of the zebrafish lateral line, *Current Opinion in Neurobiology*, 14(1), pp. 67-73.

Ghysen, A. & Dambly-Chaudière, C., 2007, The lateral line microcosmos, *Genes Development*, 21(17), pp. 2118-30.

Glowatzki, E., 2000, Cholinergic Synaptic Inhibition of Inner Hair Cells in the Neonatal Mammalian Cochlea, *Science*, 288(5475), pp. 2366-8.

Glowatzki, E. & Fuchs, P.A., 2002, Transmitter release at the hair cell ribbon synapse, *Nature Neuroscience*, 5(2), pp. 147-54.

Goodyear, R.J. & Richardson, G.P., 2003, A novel antigen sensitive to calcium chelation that is associated with the tip links and kinocilial links of sensory hair bundles, *The Journal of Neuroscience*, 23(12), pp. 4878-87.

Goodyear, R.J., Marcotti, W., Kros, C.J. & Richardson, G.P., 2005, Development and properties of stereociliary link types in hair cells of the mouse cochlea, *Journal of Comparative Neurology*, 485(1), pp. 75-85.

Goutman, J.D., 2017, Mechanisms of synaptic depression at the hair cell ribbon synapse that support auditory nerve function, *Proceedings of the National Academy of Sciences USA*, 114(36), pp. 9719-24.

Goutman, J.D. & Glowatzki, E., 2007, Time course and calcium dependence of transmitter release at a single ribbon synapse, *Proceedings of the National Academy of Sciences USA*, 104(41), pp. 16341-6.

Granato, M., van Eeden, F.J., Schach, U., Trowe, T., Brand, M., Furutani-Seiki, M., Haffter, P., Hammerschmidt, M., Heisenberg, C.P., Jiang, Y.J., Kane, D.A., Kelsh, R.N., Mullins, M.C., Odenthal, J. & Nüsslein-Volhard, C., 1996, Genes controlling and mediating locomotion behavior of the zebrafish embryo and larva, *Development*, 123, pp. 399-413.

Grant, L., Yi, E. & Glowatzki, E., 2010, Two modes of release shape the postsynaptic response at the inner hair cell ribbon synapse, *The Journal of Neuroscience*, 30(12), pp. 4210-20.

Graydon, C.W., Manor, U. & Kindt, K.S., 2017, In Vivo Ribbon Mobility and Turnover of Ribeye at Zebrafish Hair Cell Synapses, *Scientific Reports*, 7(1), p. 7467.

Hacohen, N., Assad, J.A., Smith, W.J. & Corey, D.P., 1989, Regulation of tension on hair-cell transduction channels: displacement and calcium dependence, *The Journal of Neuroscience*, 9(11), pp. 3988-97.

Haehnel, M., Taguchi, M. & Liao, J.C., 2012, Heterogeneity and dynamics of lateral line afferent innervation during development in zebrafish (Danio rerio), *Journal of Comparative Neurology*, 520(7), pp. 1376-86.

Haehnel-Taguchi, M., Akanyeti, O. & Liao, J.C., 2014, Afferent and motoneuron activity in response to single neuromast stimulation in the posterior lateral line of larval zebrafish, *Journal of Neurophysiology*, 112(6), pp. 1329-39.

Higashijima, S.-I., Hotta, Y. & Okamoto, H., 2000, Visualization of cranial motor neurons in live transgenic zebrafish expressing green fluorescent protein under the control of the islet-1 promoter/enhancer, *The Journal of Neuroscience*, 20(1), pp. 206-18.

Hirono, M., Denis, C.S., Richardson, G.P. & Gillespie, P.G., 2004, Hair cells require phosphatidylinositol 4,5-bisphosphate for mechanical transduction and adaptation, *Neuron*, 44(2), pp. 309-20.

Holt, J.C., Jordan, P.M., Lysakowski, A., Shah, A., Barsz, K. & Contini, D., 2017, Muscarinic Acetylcholine Receptors and M-Currents Underlie Efferent-Mediated Slow Excitation in Calyx-Bearing Vestibular Afferents, *The Journal of Neuroscience*, 37(7), pp. 1873-87.

Holt, J.C., Kewin, K., Jordan, P.M., Cameron, P., Klapczynski, M., McIntosh, J.M., Crooks, P.A., Dwoskin, L.P. & Lysakowski, A., 2015, Pharmacologically distinct nicotinic acetylcholine receptors drive efferent-mediated excitation in calyx-bearing vestibular afferents, *The Journal of Neuroscience*, 35(8), pp. 3625-43.

Holt, J.C., Lysakowski, A. & Goldberg, J.M., 2006, Mechanisms of efferent-mediated responses in the turtle posterior crista, *The Journal of Neuroscience,* 26(51), pp. 13180-93.

Holt, J.R. & Corey, D.P., 2000, Two mechanisms for transducer adaptation in vertebrate hair cells, *Proceedings of the National Academy of Sciences USA*, 97(22), pp. 11730-5.

Holt, J.R. & Eatock, R.A., 1995, Inwardly rectifying currents of saccular hair cells from the leopard frog, *Journal of Neurophysiology*, 73(4), pp. 1484-502.

Holt, J.R., Corey, D.P. & Eatock, R.A., 1997, Mechanoelectrical transduction and adaptation in hair cells of the mouse utricle, a low-frequency vestibular organ, *The Journal of Neuroscience*, 17(22), pp. 8739-48.

Holt, J.R., Gillespie, S.K., Provance, D.W., Shah, K., Shokat, K.M., Corey, D.P., Mercer, J.A. & Gillespie, P.G., 2002, A chemical-genetic strategy implicates myosin-1c in adaptation by hair cells, *Cell*, 108(3), pp. 371-81.

Holton, T. & Hudspeth, A.J., 1986, The transduction channel of hair cells from the bull-frog characterized by noise analysis, *The Journal of Physiology*, 375, pp. 195-227.

Howard, J. & Hudspeth, A.J., 1987, Mechanical relaxation of the hair bundle mediates adaptation in mechanoelectrical transduction by the bullfrog's saccular hair cell, *Proceedings of the National Academy of Sciences USA*, 84(9), pp. 3064-8.

Howard, J. & Hudspeth, A.J., 1988, Compliance of the hair bundle associated with gating of mechanoelectrical transduction channels in the bullfrog's saccular hair cell, *Neuron*, 1(3), pp. 189-99.

Hudspeth, A.J., 1982, Extracellular current flow and the site of transduction by vertebrate hair cells, *The Journal of Neuroscience*, 2(1), pp. 1-10.

Hudspeth, A.J., 1989, How the ear's works work, *Nature*, 341(6241), pp. 397-404.

Hudspeth, A.J., 2014, Integrating the active process of hair cells with cochlear function, *Nature Reviews Neuroscience*, 15(9), pp. 600-14.

Hung, I.C., Cherng, B.W., Hsu, W.M. & Lee, S.J., 2013, Calnexin is required for zebrafish posterior lateral line development, *The International journal of developmental biology*, 57(5), pp. 427-38.

Hwang, W.Y., Fu, Y., Reyon, D., Maeder, M.L., Tsai, S.Q., Sander, J.D., Peterson, R.T., Yeh, J.R. & Joung, J.K., 2013, Efficient genome editing in zebrafish using a CRISPR-Cas system, *Nature Biotechnology*, 31(3), pp. 227-9.

Jin, L., Han, Z., Platisa, J., Wooltorton, J.R., Cohen, L.B. & Pieribone, V.A., 2012, Single action potentials and subthreshold electrical events imaged in neurons with a fluorescent protein voltage probe, *Neuron*, 75(5), pp. 779-85.

Johnson, S.L. & Marcotti, W., 2008, Biophysical properties of CaV1.3 calcium channels in gerbil inner hair cells, *The Journal of Physiology*, 586(4), pp. 1029-42.

Johnson, S.L., Marcotti, W. & Kros, C.J., 2005, Increase in efficiency and reduction in Ca2+ dependence of exocytosis during development of mouse inner hair cells, *The Journal of Physiology*, 563(Pt 1), pp. 177-91.

Jordan, P.M., Parks, X.X., Contini, D. & Holt, J.C., 2013, A review of synaptic mechanisms of vestibular efferent signaling in turtles: extrapolation to efferent actions in mammals, *Journal of Vestibular Research*, 23(3), pp. 161-75.

Karavitaki, K.D. & Corey, D.P., 2010, Sliding adhesion confers coherent motion to hair cell stereocilia and parallel gating to transduction channels, *The Journal of Neuroscience,* 30(27), pp. 9051-63.

Kastner, D.B. & Baccus, S.A., 2011, Coordinated dynamic encoding in the retina using opposing forms of plasticity, *Nature Neuroscience*, 14(10), pp. 1317-22.

Kastner, D.B. & Baccus, S.A., 2013, Spatial segregation of adaptation and predictive sensitization in retinal ganglion cells, *Neuron*, 79(3), pp. 541-54.

Kazmierczak, P., Sakaguchi, H., Tokita, J., Wilson-Kubalek, E.M., Milligan, R.A., Müller, U. & Kachar, B., 2007, Cadherin 23 and protocadherin 15 interact to form tip-link filaments in sensory hair cells, *Nature*, 449(7158), pp. 87-91.

Keen, E.C. & Hudspeth, A.J., 2006, Transfer characteristics of the hair cell's afferent synapse, *Proceedings of the National Academy of Sciences USA*, 103(14), pp. 5537-42.

Keller, G.B., Bonhoeffer, T. & Hübener, M., 2012, Sensorimotor mismatch signals in primary visual cortex of the behaving mouse, *Neuron*, 74(5), pp. 809-15.

Keller, P.J. & Ahrens, M.B., 2015, Visualizing whole-brain activity and development at the single-cell level using light-sheet microscopy, *Neuron*, 85(3), pp. 462-83.

Kennedy, H.J., Evans, M.G., Crawford, A.C. & Fettiplace, R., 2003, Fast adaptation of mechanoelectrical transducer channels in mammalian cochlear hair cells, *Nature Neuroscience*, 6(8), pp. 832-6.

Khimich, D., Nouvian, R., Pujol, R., Tom Dieck, S., Egner, A., Gundelfinger, E.D. & Moser, T., 2005, Hair cell synaptic ribbons are essential for synchronous auditory signalling, *Nature*, 434(7035), pp. 889-94.

Kim, A.J., Fenk, L.M., Lyu, C. & Maimon, G., 2017, Quantitative Predictions Orchestrate Visual Signaling in Drosophila, *Cell*, 168(1-2), pp. 280-294.

Kim, A.J., Fitzgerald, J.K. & Maimon, G., 2015, Cellular evidence for efference copy in Drosophila visuomotor processing, *Nature Neuroscience*, 18(9), pp. 1247-55.

Kim, D.H., Kim, J., Marques, J.C., Grama, A., Hildebrand, D.G.C., Gu, W., Li, J.M. & Robson, D.N., 2017, Pan-neuronal calcium imaging with cellular resolution in freely swimming zebrafish, *Nature Methods*, 14(11), pp. 1107-14.

Kimmel, C.B., Ballard, W.W., Kimmel, S.R., Ullmann, B. & Schilling, T.F., 1995, Stages of embryonic development of the zebrafish, *Developmental Dynamics*, 203(3), pp. 253-310.

Kindt, K.S., Finch, G. & Nicolson, T., 2012, Kinocilia mediate mechanosensitivity in developing zebrafish hair cells, *Developmental Cell*, 23(2), pp. 329-41.

Kirkwood, N.K., O'Reilly, M., Derudas, M., Kenyon, E.J., Huckvale, R., van Netten, S.M., Ward, S.E., Richardson, G.P. & Kros, C.J., 2017, d-Tubocurarine and Berbamine: Alkaloids That Are Permeant Blockers of the Hair Cell's Mechano-Electrical Transducer Channel and Protect from Aminoglycoside Toxicity, *Frontiers in Cellular Neuroscience*, 11, p. 262.

Kitajiri, S., Sakamoto, T., Belyantseva, I.A., Goodyear, R.J., Stepanyan, R., Fujiwara, I., Bird, J.E., Riazuddin, S., Riazuddin, S., Ahmed, Z.M., Hinshaw, J.E., Sellers, J., Bartles, J.R., Hammer, J.A., Richardson, G.P., Griffith, A.J., Frolenkov, G.I. & Friedman, T.B., 2010, Actin-bundling protein TRIOBP forms resilient rootlets of hair cell stereocilia essential for hearing, *Cell*, 141(5), pp. 786-98.

Knafo, S., Fidelin, K., Prendergast, A., Tseng, P.B., Parrin, A., Dickey, C., Böhm, U.L., Figueiredo, S.N., Thouvenin, O., Pascal-Moussellard, H. & Wyart, C., 2017, Mechanosensory neurons control the timing of spinal microcircuit selection during locomotion, *eLife*, 6.

Kong, J.H., Adelman, J.P. & Fuchs, P.A., 2008, Expression of the SK2 calcium-activated potassium channel is required for cholinergic function in mouse cochlear hair cells, *The Journal of Physiology*, 586(Pt 22), pp. 5471-85.

Korn, H. & Faber, D.S., 2005, The Mauthner cell half a century later: a neurobiological model for decision-making? *Neuron*, 47(1), pp. 13-28.

Koyama, M., Minale, F., Shum, J., Nishimura, N., Schaffer, C.B. & Fetcho, J.R., 2016, A circuit motif in the zebrafish hindbrain for a two alternative behavioral choice to turn left or right, *eLife*, 5.

Kozlov, A.S., Risler, T. & Hudspeth, A.J., 2007, Coherent motion of stereocilia assures the concerted gating of hair-cell transduction channels, *Nature Neuroscience*, 10(1), pp. 87-92.

Köppl, C. 2011, Evolution of the octavolateral efferent system, in *Auditory and vestibular efferents,* Springer, pp. 217-59.

Kros, C.J., Marcotti, W., van Netten, S.M., Self, T.J., Libby, R.T., Brown, S.D., Richardson, G.P. & Steel, K.P., 2002a, Reduced climbing and increased slipping adaptation in cochlear hair cells of mice with Myo7a mutations, *Nature Neuroscience*, 5(1), pp. 41-7.

Kros, C.J., Rüsch, A. & Richardson, G.P., 1992, Mechano-electrical transducer currents in hair cells of the cultured neonatal mouse cochlea, *Proceedings of the Royal Society B*, 249(1325), pp. 185-93.

Kruger, M., Boney, R., Ordoobadi, A.J., Sommers, T.F., Trapani, J.G. & Coffin, A.B., 2016, Natural Bizbenzoquinoline Derivatives Protect Zebrafish Lateral Line Sensory Hair Cells from Aminoglycoside Toxicity, *Frontiers in Cellular Neuroscience*, 10, p. 83.

Kubo, F., Hablitzel, B., Dal Maschio, M., Driever, W., Baier, H. & Arrenberg, A.B., 2014, Functional architecture of an optic flow-responsive area that drives horizontal eye movements in zebrafish, *Neuron*, 81(6), pp. 1344-59.

Lagnado, L. & Schmitz, F., 2015, Ribbon Synapses and Visual Processing in the Retina, *Annual Review of Vision Science*, 1, pp. 235-62.

Lebbe, E.K., Peigneur, S., Wijesekara, I. & Tytgat, J., 2014, Conotoxins targeting nicotinic acetylcholine receptors: an overview, *Marine Drugs*, 12(5), pp. 2970-3004.

Leinweber, M., Ward, D.R., Sobczak, J.M., Attinger, A. & Keller, G.B., 2017, A Sensorimotor Circuit in Mouse Cortex for Visual Flow Predictions, *Neuron*, 95(6), pp. 1420-1432.e5.

Levi, R., Akanyeti, O., Ballo, A. & Liao, J.C., 2014, Frequency response properties of primary afferent neurons in the posterior lateral line system of larval zebrafish, *Journal of Neurophysiology*, pp. jn.00414.2014.

Li, G., Müller, U.K., van Leeuwen, J.L. & Liu, H., 2012, Body dynamics and hydrodynamics of swimming fish larvae: a computational study, *Journal of Experimental Biology*, 215(Pt 22), pp. 4015-33.

Li, G.L., Cho, S. & von Gersdorff, H., 2014, Phase-locking precision is enhanced by multiquantal release at an auditory hair cell ribbon synapse, *Neuron*, 83(6), pp. 1404-17.

Li, G.L., Keen, E., Andor-Ardó, D., Hudspeth, A.J. & von Gersdorff, H., 2009, The unitary event underlying multiquantal EPSCs at a hair cell's ribbon synapse, *The Journal of neuroscience*, 29(23), pp. 7558-68.

Liao, J.C., 2010, Organization and physiology of posterior lateral line afferent neurons in larval zebrafish, *Biological Letters*, 6(3), pp. 402-5.

Liao, J.C. 2014, Functional architecture of lateral line afferent neurons in larval zebrafish, in *Flow Sensing in Air and Water,* Springer, pp. 319-32.

Liao, J.C. & Haehnel, M., 2012, Physiology of afferent neurons in larval zebrafish provides a functional framework for lateral line somatotopy, *Journal of Neurophysiology*, 107(10), pp. 2615-23.

Lister, J.A., Robertson, C.P., Lepage, T., Johnson, S.L. & Raible, D.W., 1999, nacre encodes a zebrafish microphthalmia-related protein that regulates neural-crest-derived pigment cell fate, *Development*, 126(17), pp. 3757-67.

López-Schier, H. & Hudspeth, A.J., 2006, A two-step mechanism underlies the planar polarization of regenerating sensory hair cells, *Proceedings of the National Academy of Sciences USA*, 103(49), pp. 18615-20.

López-Schier, H., Starr, C.J., Kappler, J.A., Kollmar, R. & Hudspeth, A.J., 2004, Directional cell migration establishes the axes of planar polarity in the posterior lateral-line organ of the zebrafish, *Developmental Cell*, 7(3), pp. 401-12.

Lumpkin, E.A. & Hudspeth, A.J., 1995, Detection of Ca2+ entry through mechanosensitive channels localizes the site of mechanoelectrical transduction in hair cells, *Proceedings of the National Academy of Sciences USA*, 92(22), pp. 10297-301.

Lumpkin, E.A. & Hudspeth, A.J., 1998, Regulation of free Ca2+ concentration in hair-cell stereocilia, *The Journal of Neuroscience*, 18(16), pp. 6300-18.

Lv, C., Stewart, W.J., Akanyeti, O., Frederick, C., Zhu, J., Santos-Sacchi, J., Sheets, L., Liao, J.C. & Zenisek, D., 2016, Synaptic Ribbons Require Ribeye for Electron Density, Proper Synaptic Localization, and Recruitment of Calcium Channels, Cell Reports 15(12) pp. 2784-95

Maeda, R., Pacentine, I.V., Erickson, T. & Nicolson, T., 2017, Functional Analysis of the Transmembrane and Cytoplasmic Domains of Pcdh15a in Zebrafish Hair Cells, *The Journal of Neuroscience*, 37(12), pp. 3231-45.

Maison, S.F., Liu, X.P., Vetter, D.E., Eatock, R.A., Nathanson, N.M., Wess, J. & Liberman, M.C., 2010, Muscarinic signaling in the cochlea: presynaptic and postsynaptic effects on efferent feedback and afferent excitability, *The Journal of Neuroscience,* 30(19), pp. 6751-62.

Marcotti, W. & Masetto, S., 2010, Hair Cells, *Encyclopedia of Life Sciences*.

Markin, V.S. & Hudspeth, A.J., 1995, Gating-spring models of mechanoelectrical transduction by hair cells of the internal ear, *Annual review of Biophysics and Biomolecular Structure*, 24, pp. 59-83.

Marvin, J.S., Borghuis, B.G., Tian, L., Cichon, J., Harnett, M.T., Akerboom, J., Gordus, A., Renninger, S.L., Chen, T.W., Bargmann, C.I., Orger, M.B., Schreiter, E.R., Demb, J.B., Gan, W.B., Hires, S.A. & Looger, L.L., 2013, An optimized fluorescent probe for visualizing glutamate neurotransmission, *Nature Methods*, 10(2), pp. 162-70.

Marvin, J.S., Scholl, B., Wilson, D.E., Podgorski, K., Kazemipour, A., Mueller, J.A., Schoch-McGovern, S., Wang, S.S.-H., Quiroz, F.J.U., Rebola, N., Bao, H., Little, J.P., Tkachuk, A.N., Hantman, A.W., Chapman, E.R., Dietrich, D., DiGregorio, D.A., Fitzpatrick, D. & Looger, L.L., 2017, Stability, affinity and chromatic variants of the glutamate sensor iGluSnFR, *bioRxiv*, p. 235176.

Masino, M.A. & Fetcho, J.R., 2005, Fictive swimming motor patterns in wild type and mutant larval zebrafish, *Journal of Neurophysiology*, 93(6), pp. 3177-88.

Masland, R.H., 2012, The neuronal organization of the retina, *Neuron*, 76(2), pp. 266-80.

Mathews, M.A., Camp, A.J. & Murray, A.J., 2017, Reviewing the Role of the Efferent Vestibular System in Motor and Vestibular Circuits, *Frontiers in Physiology*, 8, p. 552.

Matthews, G. & Fuchs, P., 2010, The diverse roles of ribbon synapses in sensory neurotransmission, *Nature Reviews Neuroscience*, 11(12), pp. 812-22.

McDermott, B.M., Asai, Y., Baucom, J.M., Jani, S.D., Castellanos, Y., Gomez, G., McClintock, J.M., Starr, C.J. & Hudspeth, A.J., 2010, Transgenic labeling of hair cells in the zebrafish acousticolateralis system, *Gene Expression Patterns*, 10(2-3), pp. 113-8.

McHenry, M.J. & van Netten, S.M., 2007, The flexural stiffness of superficial neuromasts in the zebrafish (Danio rerio) lateral line, *Journal of Experimental Biology*, 210(Pt 23), pp. 4244-53.

McHenry, M.J., Feitl, K.E., Strother, J.A. & Van Trump, W.J., 2009, Larval zebrafish rapidly sense the water flow of a predator's strike, *Biology Letters*, 5(4), pp. 477-9.

McHenry, M.J., Strother, J.A. & van Netten, S.M., 2008, Mechanical filtering by the boundary layer and fluid-structure interaction in the superficial neuromast of the fish lateral line system, *Journal of Comparative Physiology A*, 194(9), pp. 795-810.

Metcalfe, W.K., Kimmel, C.B. & Schabtach, E., 1985, Anatomy of the posterior lateral line system in young larvae of the zebrafish, *Journal of Comparative Neurology*, 233(3), pp. 377-89.

Monesson-Olson, B.D., Browning-Kamins, J., Aziz-Bose, R., Kreines, F. & Trapani, J.G., 2014, Optical stimulation of zebrafish hair cells expressing channelrhodopsin-2, *PloS one*, 9(5), p. e96641.

Moorman, S.J., 2001, Development of sensory systems in zebrafish (Danio rerio), *ILAR Journal*, 42(4), pp. 292-8.

Mu, Y., Li, X.Q., Zhang, B. & Du, J.L., 2012, Visual input modulates audiomotor function via hypothalamic dopaminergic neurons through a cooperative mechanism, *Neuron*, 75(4), pp. 688-99.

Müller, U.K., van den Boogaart, J.G. & van Leeuwen, J.L., 2008, Flow patterns of larval fish: undulatory swimming in the intermediate flow regime, *Journal of Experimental Biology*, 211(Pt 2), pp. 196-205.

Nagiel, A., Andor-Ardó, D. & Hudspeth, A.J., 2008, Specificity of afferent synapses onto plane-polarized hair cells in the posterior lateral line of the zebrafish, *The Journal of Neuroscience*, 28(34), pp. 8442-53.

Nam, J.H., Peng, A.W. & Ricci, A.J., 2015, Underestimated Sensitivity of Mammalian Cochlear Hair Cells Due to Splay between Stereociliary Columns, *Biophysical Journal*, 108(11), pp. 2633-47.

Nayak, G.D., Ratnayaka, H.S., Goodyear, R.J. & Richardson, G.P., 2007, Development of the hair bundle and mechanotransduction, *The International Journal of Developmental Biology*, 51(6-7), pp. 597-608.

Nicolson, T., 2005, The genetics of hearing and balance in zebrafish, *Annual Reviews Genetics*, 39, pp. 9-22.

Nicolson, T. 2012, The Hair Cell Synapse, in *Synaptic Mechanisms in the Auditory System,* pp. 43-60.

Nicolson, T., 2015, Ribbon synapses in zebrafish hair cells, *Hearing Research*, 330(Pt B), pp. 170-7.

Nicolson, T., Rüsch, A., Friedrich, R.W., Granato, M., Ruppersberg, J.P. & Nüsslein-Volhard, C., 1998, Genetic analysis of vertebrate sensory hair cell mechanosensation: the zebrafish circler mutants, *Neuron*, 20(2), pp. 271-83.

Nikolaev, A., Leung, K.M., Odermatt, B. & Lagnado, L., 2013, Synaptic mechanisms of adaptation and sensitization in the retina, *Nature Neuroscience*, 16(7), pp. 934-41.

Nouvian, R., Beutner, D., Parsons, T.D. & Moser, T., 2006, Structure and function of the hair cell ribbon synapse, *Journal of Membrane Biology*, 209(2-3), pp. 153-65.

Nouvian, R., Neef, J., Bulankina, A.V., Reisinger, E., Pangršič, T., Frank, T., Sikorra, S., Brose, N., Binz, T. & Moser, T., 2011, Exocytosis at the hair cell ribbon synapse apparently operates without neuronal SNARE proteins, *Nature Neuroscience*, 14(4), pp. 411-3.

Obholzer, N., Wolfson, S., Trapani, J.G., Mo, W., Nechiporuk, A., Busch-Nentwich, E., Seiler, C., Sidi, S., Söllner, C., Duncan, R.N., Boehland, A. & Nicolson, T., 2008, Vesicular glutamate transporter 3 is required for synaptic transmission in zebrafish hair cells, *The Journal of Neuroscience*, 28(9), pp. 2110-8.

Odermatt, B., Nikolaev, A. & Lagnado, L., 2012, Encoding of luminance and contrast by linear and nonlinear synapses in the retina, *Neuron*, 73(4), pp. 758-73.

Ohmori, H., 1985, Mechano-electrical transduction currents in isolated vestibular hair cells of the chick, *The Journal of Physiology*, 359, pp. 189-217.

Ohn, T.L., Rutherford, M.A., Jing, Z., Jung, S., Duque-Afonso, C.J., Hoch, G., Picher, M.M., Scharinger, A., Strenzke, N. & Moser, T., 2016, Hair cells use active zones with different voltage dependence of Ca2+ influx to decompose sounds into complementary neural codes, *Proceedings of the National Academy of Sciences USA*, 113(32), pp. E4716-25.

Olive, R., Wolf, S., Dubreuil, A., Bormuth, V., Debrégeas, G. & Candelier, R., 2016, Rheotaxis of Larval Zebrafish: Behavioral Study of a Multi-Sensory Process, *Frontiers in Systems Neuroscience*, 10, p. 14.

Oliver, D., Klöcker, N., Schuck, J., Baukrowitz, T., Ruppersberg, J.P. & Fakler, B., 2000, Gating of Ca2+-activated K+ channels controls fast inhibitory synaptic transmission at auditory outer hair cells, *Neuron*, 26(3), pp. 595-601.

Olszewski, J., Haehnel, M., Taguchi, M. & Liao, J.C., 2012, Zebrafish larvae exhibit rheotaxis and can escape a continuous suction source using their lateral line, *PloS one*, 7(5), p. e36661.

Olt, J., Allen, C.E. & Marcotti, W., 2016, In vivo physiological recording from the lateral line of juvenile zebrafish, *The Journal of Physiology*, 594(19), pp. 5427-38.

Olt, J., Johnson, S.L. & Marcotti, W., 2014, In vivo and in vitro biophysical properties of hair cells from the lateral line and inner ear of developing and adult zebrafish, *The Journal of Physiology*, 592(Pt 10), pp. 2041-58.

Olt, J., Ordoobadi, A.J., Marcotti, W. & Trapani, J.G., 2016, Physiological recordings from the zebrafish lateral line, *Methods Cell Biology*, 133, pp. 253-79.

Orger, M.B., 2016, The Cellular Organization of Zebrafish Visuomotor Circuits, *Current Biology*, 26(9), pp. R377-85.

Orger, M.B., Kampff, A.R., Severi, K.E., Bollmann, J.H. & Engert, F., 2008, Control of visually guided behavior by distinct populations of spinal projection neurons, *Nature Neuroscience*, 11(3), pp. 327-33.

Orger, M.B., Smear, M.C., Anstis, S.M. & Baier, H., 2000, Perception of Fourier and non-Fourier motion by larval zebrafish, *Nature Neuroscience*, 3(11), pp. 1128-33.

Oteiza, P., Odstrcil, I., Lauder, G., Portugues, R. & Engert, F., 2017, A novel mechanism for mechanosensory-based rheotaxis in larval zebrafish, *Nature*, 547, pp. 445-448.

Ou, H.C., Santos, F., Raible, D.W., Simon, J.A. & Rubel, E.W., 2010, Drug screening for hearing loss: using the zebrafish lateral line to screen for drugs that prevent and cause hearing loss, *Drug Discovery Today*, 15(7-8), pp. 265-71.

Palmer, L.M. & Mensinger, A.F., 2004, Effect of the anesthetic tricaine (MS-222) on nerve activity in the anterior lateral line of the oyster toadfish, Opsanus tau, *Journal of Neurophysiology*, 92(2), pp. 1034-41.

Palmer, L.M., Deffenbaugh, M. & Mensinger, A.F., 2005, Sensitivity of the anterior lateral line to natural stimuli in the oyster toadfish, Opsanus tau (Linnaeus), *Journal of Experimental Biology*, 208(Pt 18), pp. 3441-50.

Pangrsic, T., Lasarow, L., Reuter, K., Takago, H., Schwander, M., Riedel, D., Frank, T., Tarantino, L.M., Bailey, J.S., Strenzke, N., Brose, N., Müller, U., Reisinger, E. & Moser, T., 2010, Hearing requires otoferlin-dependent efficient replenishment of synaptic vesicles in hair cells, *Nature Neuroscience*, 13(7), pp. 869-76.

Park, H.C., Kim, C.H., Bae, Y.K., Yeo, S.Y., Kim, S.H., Hong, S.K., Shin, J., Yoo, K.W., Hibi, M., Hirano, T., Miki, N., Chitnis, A.B. & Huh, T.L., 2000, Analysis of upstream elements in the HuC promoter leads to the establishment of transgenic zebrafish with fluorescent neurons, *Developmental Biology*, 227(2), pp. 279-93.

Peng, A.W., Salles, F.T., Pan, B. & Ricci, A.J., 2011, Integrating the biophysical and molecular mechanisms of auditory hair cell mechanotransduction, *Nature Communication*, 2, p. 523.

Pérez, C., Limón, A., Vega, R. & Soto, E., 2009, The muscarinic inhibition of the potassium M-current modulates the action-potential discharge in the vestibular primary-afferent neurons of the rat, *Neuroscience*, 158(4), pp. 1662-74.

Pickles, J.O., Comis, S.D. & Osborne, M.P., 1984, Cross-links between stereocilia in the guinea pig organ of Corti, and their possible relation to sensory transduction, *Hearing Research*, 15(2), pp. 103-12.

Pirih, P., Sendin, G.C. & van Netten, S.S. 2014, Techniques for Studying Neuromast Function in Zebrafish, in *Flow Sensing in Air and Water,* Springer, berlin, Heidelberg, .

Platzer, J., Engel, J., Schrott-Fischer, A., Stephan, K., Bova, S., Chen, H., Zheng, H. & Striessnig, J., 2000, Congenital deafness and sinoatrial node dysfunction in mice lacking class D L-type Ca2+ channels, *Cell*, 102(1), pp. 89-97.

Portugues, R., Feierstein, C.E., Engert, F. & Orger, M.B., 2014, Whole-brain activity maps reveal stereotyped, distributed networks for visuomotor behavior, *Neuron*, 81(6), pp. 1328-43.

Pujol-Martí, J. & López-Schier, H., 2013, Developmental and architectural principles of the lateral-line neural map, *Frontiers Neural Circuits*, 7, p. 47.

Pujol-Martí, J., Baudoin, J.P., Faucherre, A., Kawakami, K. & López-Schier, H., 2010, Progressive neurogenesis defines lateralis somatotopy, *Developmental Dynamics*, 239(7), pp. 1919-30.

Pujol-Martí, J., Zecca, A., Baudoin, J.P., Faucherre, A., Asakawa, K., Kawakami, K. & López-Schier, H., 2012, Neuronal birth order identifies a dimorphic sensorineural map, *The Journal of Neuroscience*, 32(9), pp. 2976-87.

Rabbitt, R.D., Boyle, R., Holstein, G.R. & Highstein, S.M., 2005, Hair-cell versus afferent adaptation in the semicircular canals, *Journal of Neurophysiology*, 93(1), pp. 424-36.

Raible, D.W. & Kruse, G.J., 2000, Organization of the lateral line system in embryonic zebrafish, *The Journal of Comparative Neurology*, 421(2), pp. 189-98.

Reinig, S., Driever, W. & Arrenberg, A.B., 2017, The Descending Diencephalic Dopamine System Is Tuned to Sensory Stimuli, *Current Biology, 27(3), pp. 318-333*.

Ricci, A.J. & Kachar, B. 2007, Hair Cell Mechanotransduction: The Dynamic Interplay Between Structure and Function, in *Current Topics in Membranes,* Elsevier, pp. 339-74.

Ricci, A.J., Bai, J.P., Song, L., Lv, C., Zenisek, D. & Santos-Sacchi, J., 2013, Patch-clamp recordings from lateral line neuromast hair cells of the living zebrafish, *The Journal of Neuroscience*, 33(7), pp. 3131-4.

Roberts, B.L. & Russell, I.J., 1972, The activity of lateral-line efferent neurones in stationary and swimming dogfish, *Journal of Experimental Biology*, 57(2), pp. 435-48.

Robles, E., Laurell, E. & Baier, H., 2014, The retinal projectome reveals brain-area-specific visual representations generated by ganglion cell diversity, *Current Biology*, 24(18), pp. 2085-96.

Roeser, T. & Baier, H., 2003, Visuomotor behaviors in larval zebrafish after GFP-guided laser ablation of the optic tectum, *The Journal of Neuroscience*, 23(9), pp. 3726-34.

Rose, T., Goltstein, P.M., Portugues, R. & Griesbeck, O., 2014, Putting a finishing touch on GECIs, *Frontiers in Molecular Neuroscience*, 7, p. 88.

Roux, I., Safieddine, S., Nouvian, R., Grati, M., Simmler, M.C., Bahloul, A., Perfettini, I., Le Gall, M., Rostaing, P., Hamard, G., Triller, A., Avan, P., Moser, T. & Petit, C., 2006, Otoferlin, defective in a human deafness form, is essential for exocytosis at the auditory ribbon synapse, *Cell*, 127(2), pp. 277-89.

Russell, I.J., 1968, Influence of Efferent Fibres on a Receptor, *Nature*, 219, pp. 177-8.

Russell, I.J., 1971, The role of the lateral-line efferent system in Xenopus laevis, *Journal of Experimental Biology*, 54(3), pp. 621-41.

Ryugo, D.K., Fay, R.R. & Popper, A.N., 2011, *Auditory and vestibular efferents,* Springer,.

Saleem, A.B., Ayaz, A., Jeffery, K.J., Harris, K.D. & Carandini, M., 2013, Integration of visual motion and locomotion in mouse visual cortex, *Nature Neuroscience*, 16(12), pp. 1864-9.

Sankrithi, N.S. & O'Malley, D.M., 2010, Activation of a multisensory, multifunctional nucleus in the zebrafish midbrain during diverse locomotor behaviors, *Neuroscience*, 166(3), pp. 970-93.

Sapède, D., Rossel, M., Dambly-Chaudière, C. & Ghysen, A., 2005, Role of SDF1 chemokine in the development of lateral line efferent and facial motor neurons, *Proceedings of the National Academy of Sciences USA*, 102(5), pp. 1714-8.

Sarrazin, A.F., Nuñez, V.A., Sapède, D., Tassin, V., Dambly-Chaudière, C. & Ghysen, A., 2010, Origin and early development of the posterior lateral line system of zebrafish, *The Journal of Neuroscience*, 30(24), pp. 8234-44.

Sarrazin, A.F., Villablanca, E.J., Nuñez, V.A., Sandoval, P.C., Ghysen, A. & Allende, M.L., 2006, Proneural gene requirement for hair cell differentiation in the zebrafish lateral line, *Developmental Biology*, 295(2), pp. 534-45.

Schindelin, J., Arganda-Carreras, I., Frise, E., Kaynig, V., Longair, M., Pietzsch, T., Preibisch, S., Rueden, C., Saalfeld, S., Schmid, B., Tinevez, J.Y., White, D.J., Hartenstein, V., Eliceiri, K., Tomancak, P. & Cardona, A., 2012, Fiji: an open-source platform for biological-image analysis, *Nature Methods*, 9(7), pp. 676-82.

Schmitz, F., Königstorfer, A. & Südhof, T.C., 2000, RIBEYE, a component of synaptic ribbons: a protein's journey through evolution provides insight into synaptic ribbon function, *Neuron*, 28(3), pp. 857-72.

Schnee, M.E., Lawton, D.M., Furness, D.N., Benke, T.A. & Ricci, A.J., 2005, Auditory hair cell-afferent fiber synapses are specialized to operate at their best frequencies, *Neuron*, 47(2), pp. 243-54.

Schnee, M.E., Santos-Sacchi, J., Castellano-Muñoz, M., Kong, J.H. & Ricci, A.J., 2011, Calcium-dependent synaptic vesicle trafficking underlies indefatigable release at the hair cell afferent fiber synapse, *Neuron*, 70(2), pp. 326-38.

Schoppik, D., Bianco, I.H., Prober, D.A., Douglass, A.D., Robson, D.N., Li, J.M.B., Greenwood, J.S.F., Soucy, E., Engert, F. & Schier, A.F., 2017, Gaze-Stabilizing Central Vestibular Neurons Project Asymmetrically to Extraocular Motoneuron Pools, *The Journal of Neuroscience*, 37(47), pp. 11353-65.

Sebe, J.Y., Cho, S., Sheets, L., Rutherford, M.A., von Gersdorff, H. & Raible, D.W., 2017, Ca(2+)-Permeable AMPARs Mediate Glutamatergic Transmission and Excitotoxic Damage at the Hair Cell Ribbon Synapse, *The Journal of Neuroscience*, 37(25), pp. 6162-75.

Semmelhack, J.L., Donovan, J.C., Thiele, T.R., Kuehn, E., Laurell, E. & Baier, H., 2014, A dedicated visual pathway for prey detection in larval zebrafish, *eLife*, 3.

Severi, K.E., Portugues, R., Marques, J.C., O'Malley, D.M., Orger, M.B. & Engert, F., 2014, Neural control and modulation of swimming speed in the larval zebrafish, *Neuron*, 83(3), pp. 692-707.

Sheets, L., He, X.J., Olt, J., Schreck, M., Petralia, R.S., Wang, Y.X., Zhang, Q., Beirl, A., Nicolson, T., Marcotti, W., Trapani, J.G. & Kindt, K.S., 2017, Enlargement of Ribbons in Zebrafish Hair Cells Increases Calcium Currents But Disrupts Afferent Spontaneous Activity and Timing of Stimulus Onset, *The Journal of Neuroscience*, 37(26), pp. 6299-313.

Sheets, L., Kindt, K.S. & Nicolson, T., 2012, Presynaptic CaV1.3 channels regulate synaptic ribbon size and are required for synaptic maintenance in sensory hair cells, *The Journal of Neuroscience*, 32(48), pp. 17273-86.

Sheets, L., Trapani, J.G., Mo, W., Obholzer, N. & Nicolson, T., 2011, Ribeye is required for presynaptic Ca(V)1.3a channel localization and afferent innervation of sensory hair cells, *Development*, 138(7), pp. 1309-19.

Shepherd, G.M. & Corey, D.P., 1994, The extent of adaptation in bullfrog saccular hair cells, *The Journal of Neuroscience*, 14(10), pp. 6217-29.

Shin, J.B., Krey, J.F., Hassan, A., Metlagel, Z., Tauscher, A.N., Pagana, J.M., Sherman, N.E., Jeffery, E.D., Spinelli, K.J., Zhao, H., Wilmarth, P.A., Choi, D., David, L.L., Auer, M. & Barr-Gillespie, P.G., 2013, Molecular architecture of the chick vestibular hair bundle, *Nature Neuroscience*, 16(3), pp. 365-74.

Sidi, S., Busch-Nentwich, E., Friedrich, R., Schoenberger, U. & Nicolson, T., 2004, gemini encodes a zebrafish L-type calcium channel that localizes at sensory hair cell ribbon synapses, *The Journal of Neuroscience*, 24(17), pp. 4213-23.

Sienknecht, U.J., Köppl, C. & Fritzsch, B., 2014, Evolution and development of hair cell polarity and efferent function in the inner ear, *Brain, Behavior and Evolution*, 83(2), pp. 150-61.

Spassova, M., Eisen, M.D., Saunders, J.C. & Parsons, T.D., 2001, Chick cochlear hair cell exocytosis mediated by dihydropyridine-sensitive calcium channels, *The Journal of Physiology*, 535(Pt 3), pp. 689-96.

Spoon, C. & Grant, W., 2011, Biomechanics of hair cell kinocilia: experimental measurement of kinocilium shaft stiffness and base rotational stiffness with Euler-Bernoulli and Timoshenko beam analysis, *Journal of Experimental Biology*, 214(Pt 5), pp. 862-70.

Stauffer, E.A. & Holt, J.R., 2007, Sensory transduction and adaptation in inner and outer hair cells of the mouse auditory system, *Journal of Neurophysiology*, 98(6), pp. 3360-9.

Stauffer, E.A., Scarborough, J.D., Hirono, M., Miller, E.D., Shah, K., Mercer, J.A., Holt, J.R. & Gillespie, P.G., 2005, Fast adaptation in vestibular hair cells requires myosin-1c activity, *Neuron*, 47(4), pp. 541-53.

Stewart, W.J., Cardenas, G.S. & McHenry, M.J., 2013, Zebrafish larvae evade predators by sensing water flow, *Journal of Experimental Biology*, 216(Pt 3), pp. 388-98.

Storace, D., Sepehri Rad, M., Kang, B., Cohen, L.B., Hughes, T. & Baker, B.J., 2016, Toward Better Genetically Encoded Sensors of Membrane Potential, *Trends in Neuroscience*, 39(5), pp. 277-89.

St-Pierre, F., Marshall, J.D., Yang, Y., Gong, Y., Schnitzer, M.J. & Lin, M.Z., 2014, High-fidelity optical reporting of neuronal electrical activity with an ultrafast fluorescent voltage sensor, *Nature Neuroscience*, 17(6), pp. 884-9.

Striessnig, J., Bolz, H.J. & Koschak, A., 2010, Channelopathies in Cav1.1, Cav1.3, and Cav1.4 voltage-gated L-type Ca2+ channels, *European Journal of Physiology*, 460(2), pp. 361-74.

Suli, A., Guler, A.D., Raible, D.W. & Kimelman, D., 2014, A targeted gene expression system using the tryptophan repressor in zebrafish shows no silencing in subsequent generations, *Development*, 141(5), pp. 1167-74.

Suli, A., Mortimer, N., Shepherd, I. & Chien, C.B., 2006, Netrin/DCC signaling controls contralateral dendrites of octavolateralis efferent neurons, *The Journal of Neuroscience*, 26(51), pp. 13328-37.

Suli, A., Watson, G.M., Rubel, E.W. & Raible, D.W., 2012, Rheotaxis in larval zebrafish is mediated by lateral line mechanosensory hair cells, *PloS one*, 7(2), p. e29727.

Temizer, I., Donovan, J.C., Baier, H. & Semmelhack, J.L., 2015, A Visual Pathway for Looming-Evoked Escape in Larval Zebrafish, *Current Biology*, 25(14), pp. 1823-34.

Thiele, T.R., Donovan, J.C. & Baier, H., 2014, Descending control of swim posture by a midbrain nucleus in zebrafish, *Neuron*, 83(3), pp. 679-91.

Thomas, A.J., Wu, P., Raible, D.W., Rubel, E.W., Simon, J.A. & Ou, H.C., 2015, Identification of small molecule inhibitors of cisplatin-induced hair cell death: results of a 10,000 compound screen in the zebrafish lateral line, *Otology & Neurotology*, 36(3), pp. 519-25.

Thompson, A.W., Vanwalleghem, G.C., Heap, L.A. & Scott, E.K., 2016, Functional Profiles of Visual-, Auditory-, and Water Flow-Responsive Neurons in the Zebrafish Tectum, *Current Biology*, 26(6), pp. 743-54.

Tilney, L.G., Derosier, D.J. & Mulroy, M.J., 1980, The organization of actin filaments in the stereocilia of cochlear hair cells, *The Journal of Cell Biology*, 86(1), pp. 244-59.

Toro, C., Trapani, J.G., Pacentine, I., Maeda, R., Sheets, L., Mo, W. & Nicolson, T., 2015, Dopamine Modulates the Activity of Sensory Hair Cells, *The Journal of Neuroscience*, 35(50), pp. 16494-503.

Trapani, J.G. & Nicolson, T., 2010, Physiological recordings from zebrafish lateral-line hair cells and afferent neurons, *Methods Cell Biology*, 100, pp. 219-31.

Trapani, J.G. & Nicolson, T., 2011, Mechanism of spontaneous activity in afferent neurons of the zebrafish lateral-line organ, *The Journal of Neuroscience*, 31(5), pp. 1614-23.

Trapani, J.G., Obholzer, N., Mo, W., Brockerhoff, S.E. & Nicolson, T., 2009, Synaptojanin1 is required for temporal fidelity of synaptic transmission in hair cells, *PLoS Genetics*, 5(5), p. e1000480.

Tricas, T.C. & Highstein, S.M., 1990, Visually mediated inhibition of lateral line primary afferent activity by the octavolateralis efferent system during predation in the free-swimming toadfish, Opsanus tau, *Experimental Brain Research*, 83(1), pp. 233-6.

Troconis, E.L., Ordoobadi, A.J., Sommers, T.F., Aziz-Bose, R., Carter, A.R. & Trapani, J.G., 2017, Intensity-dependent timing and precision of startle response latency in larval zebrafish, *The Journal of Physiology*, 595(1), pp. 265-82.

van Netten, S. & McHenry, M.J. 2014, The Biophysics of the Fish Lateral Line, in S Coombs (ed), *The Lateral Line System,* .

van Netten, S.M., 2006, Hydrodynamic detection by cupulae in a lateral line canal: functional relations between physics and physiology, *Biological Cybernetics*, 94(1), pp. 67-85.

Van Trump, W.J. & McHenry, M.J., 2008, The morphology and mechanical sensitivity of lateral line receptors in zebrafish larvae (Danio rerio), *Journal of Experimental Biology*, 211(Pt 13), pp. 2105-15.

Verbitsky, M., Rothlin, C.V., Katz, E. & Elgoyhen, A.B., 2000, Mixed nicotinic-muscarinic properties of the alpha9 nicotinic cholinergic receptor, *Neuropharmacology*, 39(13), pp. 2515-24.

Vladimirov, N., Mu, Y., Kawashima, T., Bennett, D.V., Yang, C.T., Looger, L.L., Keller, P.J., Freeman, J. & Ahrens, M.B., 2014, Light-sheet functional imaging in fictively behaving zebrafish, *Nature Methods*, 11(9), pp. 883-4.

Voigt, R., Carton, A.G. & Montgomery, J.C., 2000, Responses of anterior lateral line afferent neurones to water flow, *Journal of Experimental Biology*, 203(Pt 16), pp. 2495-502.

Vollrath, M.A. & Eatock, R.A., 2003, Time course and extent of mechanotransducer adaptation in mouse utricular hair cells: comparison with frog saccular hair cells, *Journal of Neurophysiology*, 90(4), pp. 2676-89.

von Holst, E. & Mittelstaedt, H., 1950, Das reafferenzprinzip, *Naturwissenschaften*, 37(20), pp. 464-76.

Wang, W.C. & McLean, D.L., 2014, Selective responses to tonic descending commands by temporal summation in a spinal motor pool, *Neuron*, 83(3), pp. 708-21.

Wark, B., Lundstrom, B.N. & Fairhall, A., 2007, Sensory adaptation, *Current opinion in Neurobiology*, 17(4), pp. 423-9.

Weisz, C.J., Lehar, M., Hiel, H., Glowatzki, E. & Fuchs, P.A., 2012, Synaptic transfer from outer hair cells to type II afferent fibers in the rat cochlea, *The Journal of Neuroscience*, 32(28), pp. 9528-36.

Wichmann, C. & Moser, T., 2015, Relating structure and function of inner hair cell ribbon synapses, *Cell and Tissue Research*, 361(1), pp. 95-114.

Windsor, S.P. & McHenry, M.J., 2009, The influence of viscous hydrodynamics on the fish lateral-line system, *Integrated Computational Biology*, 49(6), pp. 691-701.

Wong, A.B., Rutherford, M.A., Gabrielaitis, M., Pangrsic, T., Göttfert, F., Frank, T., Michanski, S., Hell, S., Wolf, F., Wichmann, C. & Moser, T., 2014, Developmental refinement of hair cell synapses tightens the coupling of Ca2+ influx to exocytosis, *EMBO Journal*, 33(3), pp. 247-64.

Wu, Y.C., Ricci, A.J. & Fettiplace, R., 1999, Two components of transducer adaptation in auditory hair cells, *Journal of Neurophysiology*, 82(5), pp. 2171-81.

Wu, Z. & Müller, U., 2016, Molecular Identity of the Mechanotransduction Channel in Hair Cells: Not Quiet There Yet, *The Journal of Neuroscience*, 36(43), pp. 10927-34.

Xiao, T., Roeser, T., Staub, W. & Baier, H., 2005, A GFP-based genetic screen reveals mutations that disrupt the architecture of the zebrafish retinotectal projection, *Development*, 132(13), pp. 2955-67.

Zenisek, D., Horst, N.K., Merrifield, C., Sterling, P. & Matthews, G., 2004, Visualizing synaptic ribbons in the living cell, *The Journal of Neuroscience*, 24(44), pp. 9752-9.

Zhang, Q.X., He, X.J., Wong, H.C. & Kindt, K.S., 2016, Functional calcium imaging in zebrafish lateral-line hair cells, *Methods Cell Biology*, 133, pp. 229-52.

Zhao, B. & Müller, U., 2015, The elusive mechanotransduction machinery of hair cells, *Current Opinion in Neurobiology*, 34, pp. 172-9.

Zmarz, P. & Keller, G.B., 2016, Mismatch Receptive Fields in Mouse Visual Cortex, *Neuron*, 92(4), pp. 766-72.